Modeling a Run-around Heat and Moisture Exchanger Using Two Counter/Cross Flow Exchangers

A Thesis Submitted to the College of

Graduate Studies and Research

In Partial Fulfillment of the Requirements

For the Degree of Master of Science

In the Department of Mechanical Engineering

University of Saskatchewan

Saskatoon

By

Alireza Vali

Permission to Use

In presenting this thesis in partial fulfilment of the requirements for a Postgraduate degree from the University of Saskatchewan, I agree that the Libraries of this University may make it freely available for inspection. I further agree that permission for copying of this thesis in any manner, in whole or in part, for scholarly purposes may be granted by the professor or professors who supervised my thesis work or, in their absence, by the Head of the Department or the Dean of the College in which my thesis work was done. It is understood that any copying or publication or use of this thesis or parts thereof for financial gain shall not be allowed without my written permission. It is also understood that due recognition shall be given to me and to the University of Saskatchewan in any scholarly use which may be made of any material in my thesis.

Requests for permission to copy or to make other use of material in this thesis in whole or part should be addressed to:

Head of the Department of Mechanical Engineering

University of Saskatchewan

Saskatoon, Saskatchewan (S7N 5A9)

ABSTRACT

In this study, a numerical model is developed for determining coupled heat and moisture transfer in a run-around membrane energy exchanger (RAMEE) using two counter/cross flow exchangers and with a salt solution of $MgCl_2$ as the coupling fluid. The counter/cross flow exchanger is a counter-flow exchanger with cross-flow inlet and outlet headers. The model is two-dimensional, steady-state and based on the physical principles of conservation of momentum, energy, and mass. The finite difference method is used in this model to discretize the governing equations.

The heat transfer model is validated with effectiveness correlations in the literature. It is shown that the difference between the numerical model and correlations is less than ±2% and ±2.5% for heat exchangers and run around heat exchangers (RAHE), respectively. The simultaneous heat and moisture transfer model is validated with data from another model and experiments. The inter-model comparison shows a difference of less than 1%. The experimental validation shows an average discrepancy of 1% to 17% between the experimental and numerical data for overall total effectiveness. At lower NTUs the numerical and experimental results show better agreement (e.g. within 1-4% at NTU=4).

The model for RAHE is used to develop new effectiveness correlations for the geometrically more complex counter/cross flow heat exchangers and RAHE systems. The correlations are developed to predict the response of the exchangers and overall system to the change of different design characteristics as it is determined by the model. Discrepancies between the simulated and correlated results are within ±2% for both the heat exchangers and the RAHE systems.

It is revealed by the model that the overall effectiveness of the counter/cross flow RAMEE depends on the entrance ratio (the ratio of the length of the inlet and

outlet headers to the length of the exchanger, x_i/x_0), aspect ratio (the ratio of the height to the length of the exchanger, y_0/x_0), number of heat transfer units (NTU), heat capacity rate ratio (Cr*), number of mass transfer units (NTU_m), and the mass flow rate ratio of pure salt in desiccant solution to dry air (m*). Beside these dimensionless parameters, the performance of the RAMEE system is affected by the liquid-air flow configuration and the operating inlet temperature and humidity.

This study concludes that the maximum effectiveness of the RAMEE system with two counter/cross flow exchangers occurs when NTU and NTU_m are large (e.g. greater than 10). At any NTU, the overall effectiveness of the RAMEE system increases with Cr* until it reaches a maximum value when $Cr^*=Cr^*_{crit}$. Increasing Cr* above Cr^*_{crit} causes the overall effectiveness to decrease slightly. Therefore, to achieve the maximum overall effectiveness of the system, Cr* must be close to Cr^*_{crit}. Cr^*_{crit} is a function of NTU and operating conditions e.g., with NTU=10, $Cr^*_{crit} \approx 3$ and $Cr^*_{crit} \approx 1.5$ under AHRI summer and winter operating conditions, respectively. The exchangers in the RAMEE system are needed to have a small aspect ratio (e.g. $y_0/x_0<0.2$) and small entrance ratio (e.g. $x_i/x_0<0.1$) to get the maximum overall effectiveness of a RAMEE system using two counter/cross flow exchangers. Such a RAMEE system has a total effectiveness 6% higher and 1.5% lower compared to the same cross-flow and counter-flow RAMEE, respectively (at NTU=10, Cr*≈3, $y_0/x_0=0.2$ and $x_i/x_0=0.1$).

ACKNOWLEDGMENTS

I would like to express my deep appreciation to my supervisors Professor R.W. Besant and Professor C. J. Simonson. Thank you for your help and inspiration throughout this research. It would not be possible to accomplish this work without your support and guidance. I also wish to thank my family for their love and encouragement.

I would like to acknowledge financial support from the Natural Science and Engineering Research Council of Canada (NSERC) and Venmar CES, Saskatoon.

Dedication

I dedicate this thesis to my parents, Bahman and Azar. Thank you very much for your love and support throughout my life.

TABLE OF CONTENTS

LIST OF TABLES

LIST OF FIGURES

NOMENCLATURE

ACRONYMS

AHRI	Air-conditioning Heating and Refrigerating Institute
ANSI	American National Standard Institute
ASHRAE	American Society of Heating, Refrigerating and Air-Conditioning Engineers
HVAC	Heating, Ventilation and Air-Conditioning
LCC	Life-Cycle Cost
LAMEE	Liquid-to-Air Membrane Energy Exchanger
RAHE	Run-Around Heat Exchanger
RAMEE	Run-Around Membrane Energy Exchanger
RAMEETA	Run-Around Membrane Energy Exchanger Testing Apparatus

ENGLISH SYMBOLS

A	ratio of water mass to mass of salt solution (kg/kg)
B	coefficient used for salt solution heat capacity correlation
b	coefficient used for salt solution density correlation
C	heat capacity rate (W/K)
C_{salt}	concentration of salt solution (%)
Cr	heat capacity rate ratio (C_{min}/C_{max})
Cr*	heat capacity rate ratio of salt solution to air (C_{Sol}/C_{Air})
c_p	specific heat capacity [J /(kg.K)]
D	coefficient used for salt solution density correlation
D_h	hydraulic diameter (mm)

d	channel dimension (mm)
E	coefficient used for salt solution heat capacity correlation
f	general function
H	enthalpy (J/kg)
H^*	operating condition factor that represents the ratio of latent to sensible energy differences between the inlets of airstreams
I	ionic strength (mol/kg)
h	convective heat transfer coefficient [W/ (m^2.K)]
K	electrolyte parameter
k	thermal conductivity [W/ (m.K)]
k_m	water vapor permeability of membrane [kg/(m·s)]
Le	Lewis number
M	molecular mass (g/mol)
M_s	molar mass of solvent (g/mol)
m	mass transfer rate (kg/s)
$\dot{m}$	mass flow rate (kg/s)
m*	mass flow rate ratio of pure salt in liquid desiccant to dry air
NTU	number of heat transfer units
NTU_m	number of mass transfer units
Nu	Nusselt number
n	number of liquid (or air) channels
P	pressure (Pa)
Pe	Peclet number
Pr	Prandtl number
p	partial pressure (Pa)

q	energy transfer rate (W)
R	correction parameter
Re	Reynolds number
T	temperature (K)
t	temperature (^{o}C)
U	overall heat transfer coefficient [W /(m^2.K)]
U_m	overall mass transfer coefficient [kg/ (m^2.s)]d
u	bulk mean velocity components (m/s)
V	bulk mean velocity (m/s)
v	bulk mean velocity components (m/s)
W	humidity ratio (kg_w/kg_a)
X	ratio of water mass to mass of pure salt (kg_w/kg_{salt})
x , y , z	coordinates
x_0 , y_0 , z_0	heat exchanger dimensions (mm)
x_i	header dimension (mm)
Z	valency of cation (anion)

GREEK SYMBOLS

α	thermal diffusivity
β	empirical coefficient used for salt solution thermal conductivity correlation
Δ	difference
δ	thickness of the plate
ε	effectiveness
$\bar{\varepsilon}$	average effectiveness

λ	convergence criterion
μ	viscosity (Pa.s)
ν	number of moles of cation (or anion)
ρ	density (kg/m^3)
σ	heat loss/gain ratio which represents heat loss/gain rate relative to energy transfer rate within a exchanger
φ	uncertainty
ψ	stream function

SUBSCRIPTS

A	air
Air	air side
counter	counter-flow heat exchanger
counter/cross	heat exchanger with a combination of cross and counter flow
crit	critical
cross	cross-flow heat exchanger
E	exhaust side
ex	exchanger
in	inlet
L	liquid
l	latent
o	overall
out	outlet
S	supply side
Salt	pure salt

Sol	salt solution
s	sensible
t	total
v	water vapor
w	water
+	positive charge
-	negative charge

CHAPTER 1

Introduction

1.1. Overview

It is important to maintain the indoor environment comfortable and healthy for occupants inside buildings because, on average, people spend more than 90% of their time inside buildings. Therefore, the primary design objective of HVAC engineers is to provide a comfortable and healthy indoor environment for building occupants (ANSI/ASHRAE Standard 55-2004). Human thermal comfort is dependent on the ambient air temperature and humidity ratio, the effective radiation temperature, and the clothing and metabolic rate of the occupants (ASHRAE 2005). Thermal comfort is usually accomplished by cooling and heating to control the temperature and humidity of the supplied air to the indoor space so it remains within a thermal comfort range for the typical occupant. Recent studies showed that occupant productivity (i.e. work output) is affected directly not only by indoor thermal comfort, but also by the indoor air quality. That is, it is important to have a healthy and comfortable indoor environment inside buildings (Abdou and Lorsch 1994, Lagoudi et al. 1996, Fang et al. 2000 and Wargocki et al. 2002). Ventilation air, which replaces the contaminated indoor air with fresh outdoor air that is filtered and less contaminated, is critical in commercial buildings (ASHRAE Standard 62-2001).

Although adding outdoor ventilation air improves the indoor air quality, it increases energy consumption for buildings since outdoor air must be cooled or heated to bring it close to the indoor comfort conditions. According to ASHRAE (2005), about 20% to 40% of the overall energy consumption of air-conditioning systems is consumed for the ventilation air conditioning. In buildings that require 100% outdoor air to meet ventilation standards (e.g. hospitals and some educational

buildings like laboratories) this fraction can be even higher (e.g. 50% to 60%). Increasing the fresh air flow rate also increases HVAC equipment capacities or sizes and building operating costs. Consequently, the minimum outdoor air ventilation rate in buildings has been under discussion for many years.

During the 1970's "energy crisis", the main concern of the HVAC engineers was to reduce the outdoor ventilation air flow to a minimum to reduce energy consumption and operating costs for buildings. As a result, ANSI/ASHRAE Standard 62.1-1981 reduced the previous standard minimum ventilation rate to only 2.5 L/s (5 cfm) per person in office buildings. However, indoor air quality problems associated with an increase in contaminant concentrations (e.g. dust, odors, smoke and bacteria) in indoor air and increased occupant absenteeism were soon observed for many buildings. ASHRAE and HVAC designers realized they had reduced the ventilation air rates too far. As a result, ANSI/ASHRAE Standard 62.1-1989 increased ventilation air flow rates to about four times that recommended in ANSI/ASHRAE Standard 62.1-1981 and recommended 10 L/s (20 cfm) of outdoor ventilation air per person in office buildings.

Based on new research on air quality and concerns about energy costs in the 1990's, a new method was adopted to calculate the minimum outdoor ventilation air in ANSI/ASHRAE Standard 62.1-2004. In this method the minimum ventilation rate is determined based on both the type of building interior and the number of people per unit area. That is, both the building and its occupants are considered to be the primary sources of contaminants. All in all, it is always of interest to have a healthy environment inside buildings while maintaining minimal energy consumption.

1.1.1. Air-to-air heat/energy recovery

A system that can help minimize energy consumption resulting from ventilation air conditioning is an air-to-air energy recovery system (ASHRAE 2005). Air-to-air energy recovery is a method of preconditioning the supply ventilation air by transferring heat and moisture between the supply and exhaust air streams. As a result, less energy will be consumed for the ventilation air handling while the HVAC system provides acceptable quality for indoor air.

Several studies have been done on the economics of energy recovery which include the initial investment and operating costs and savings. These studies have concluded that applying air-to-air heat/energy recovery systems in buildings can reduce the final energy consumption by up to 20% and decrease the capacity of the HVAC equipment (Zhang et al. 2000, Fehrm et al. 2002, Niu and Zhang 2002, Dieckmann et al. 2003 and Fauchoux et al. 2007). Besant and Simonson (2003) presented a design method to determine the capacity and energy use of HVAC equipment with and without an air-to-air heat/energy exchanger. They showed, through a specific example of a typical Chicago office building, that using an air-to-air exchanger could reduce the required capacity of the boiler and chiller by 44% and 52%, respectively and result in an annual energy saving of 64% for the boiler and 31% for the chiller. Indeed, it is cost-effective to use reliable and high performance equipment to recover energy from the exhaust air to precondition the supply ventilation air.

Several types of air-to-air heat/energy recovery devices are commercially available. These exchangers may transfer sensible energy only or both sensible energy and moisture. Exchangers that recover sensible energy only are called sensible energy exchangers or heat recovery ventilators. Devices that transfer both heat and moisture

are known as energy or sometimes enthalpy exchangers or energy recovery ventilators. Due to the importance of indoor humidity and temperature control, an ideal air-to-air exchanger should be able to transfer both heat and moisture between two participating air streams (ASHRAE 2004). In general, an energy recovery system can transfer more energy compared to a heat recovery system which only can transfer sensible energy. The ideal air-to-air exchanger should also have a minimum cross stream air transfer from the exhaust to the fresh supply air to protect the fresh air from cross contamination (ASHRAE 2004 and ANSI/ASHRAE Standard 84-2008).

The selection of the appropriate energy recovery device depends on the application, indoor and outdoor design conditions, yearly weather data and its initial, installation and annual operating costs and savings (Besant and Simonson 2000). Over many decades several types of exchangers have been used to transfer heat and moisture for a variety of air-to-air applications. These include: fixed plate heat exchangers, heat pipe exchangers, air-to-air cross-flow enthalpy or energy exchangers, rotary heat or energy wheels, run-around systems, and twin-tower energy recovery loops. Typical effectivenesses of heat or energy exchangers range from 55% to 80% (ASHRAE 2004). Each of these types of heat/energy recovery systems has its advantages and disadvantages.

A method of classification of the air-to-air energy exchangers is presented in Figure 1.1 (Larson 2006). The air-to-air energy exchangers can be categorized either based on their capability of transferring moisture between two airstreams or based on the flexibility of the system in installing air ducts (i.e. adjacent or separated). This gives four groups of exchangers.

Groups 3 and 4 include energy recovery systems which can transfer both heat and moisture while the systems categorized in groups 1 and 2 are capable of heat

transfer only. Based on this classification, the systems below the horizontal line in Figure 1.1 are energy or enthalpy exchangers and the systems above the horizontal line are sensible heat exchangers or heat recovery systems.

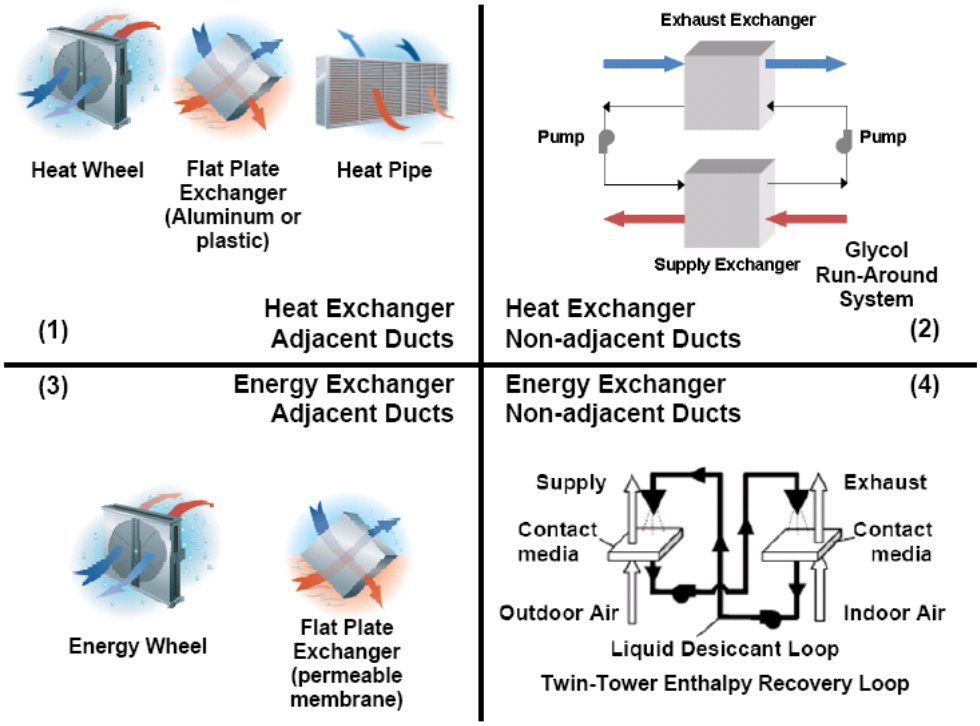

Figure 1.1 *Classification of the air-to-air energy exchangers (Larson 2006).*

The systems on left side of the vertical line in Figure 1.1 require adjacent ducting, which means those systems are restricted to applications where the supply and exhaust ducts are located side-by-side. On the contrary, the systems on the right side provide the flexibility of non-adjacent ducting, and the supply and exhaust air ducts can be located either side-by-side or remotely. As was mentioned before, an ideal exchanger should have minimum cross contamination and air-to-air heat/energy exchangers with remote supply and exhaust air ducts have this advantage. Having the flexibility of non-adjacent ducting also gives the benefit of minimizing the required

ducting and allows application where the supply and exhaust ducts have been already installed far away from each other (i.e. retrofit).

Heat pipes, fixed plate heat exchangers and rotary heat wheels, group 1 in Figure 1.1, only transfer heat and are restricted to adjacent ducts. However, they are very common because of their unique advantages: plate heat exchangers and heat wheels are economical, have low pressure drop and can be easily cleaned and heat pipes can be used where the pressure differences between two airstreams are high (Besant and Simonson 2003).

Run-around heat recovery systems, group 2 in Figure 1.1, are comprised of two liquid-to-air exchangers. The exchangers can be installed side-by-side or separated, but this system only transfers sensible energy between the supply and exhaust air streams using a coupling liquid which is usually aqueous-glycol to prevent freezing.

As illustrated in Figure 1.1 group 3, energy wheels and flat plate exchangers can be used as energy exchangers. An energy wheel coated with a desiccant can transfer both heat and moisture between two air streams (Simonson and Besant 1997a). A flat plate exchanger made of water vapor permeable membrane as the separating plate is also able to transfer heat and moisture between the supply and exhaust air streams (Zhang and Jiang 1999). However, both of these systems are restricted to side-by-side ducting and may cause cross contamination.

According to the criteria presented for an ideal air-to-air exchanger, systems categorized in group 4 in Figure 1.1 have the potential of being ideal systems since they are energy recovery systems and have the flexibility of non-adjacent ducting. The only available system in group 4 is the twin-tower enthalpy recovery loop. The fact that it is an open energy recovery system restricts its application. Moreover, the

direct contact between desiccant and supply air can result in corrosion problems and poor indoor air quality since a small fraction of the desiccant is being transported downstream by the air through the supply ducts. Problems such as the large size of the system, the need to separate the salt solution from the air streams, and a lack of performance information limit the application of this system.

As a result, a practical and effective air-to-air energy recovery system with non-adjacent duct placement is still needed. This led to the development a run-around membrane energy exchanger (RAMEE). In this system, a semi-permeable membrane is applied as the liquid-air separating plates in the exchangers. A coupling liquid (e.g. desiccant solution) which has the ability to absorb and release water vapor from/to air streams is used in a closed loop between the supply and exhaust exchangers to transfer heat and moisture between the air streams. A research project has been started at the University of Saskatchewan (in partnership with Venmar CES Inc.) to investigate the design, performance, limitations, advantages and disadvantages of the RAMEE system. The current study is a part of the RAMEE research project and it is aimed to numerically investigate the use of counter/cross flow exchangers in the RAMEE design to improve its performance.

1.2 Background of RAMEE Project

A run-around energy recovery system, shown in Figure 1.2, can be used to exchange both heat (sensible energy) and water vapor (latent energy). If the exchangers are composed of impermeable plates, the system transfers only heat (i.e. sensible energy) between two air streams and it can be called a Run-Around Heat Exchanger (RAHE). The different aspects of the RAHE design, performance and energy saving were studied for several years (Forsyth and Besant 1988a and 1988b,

Zeng et al. 1992a and 1992b, Bennett et al. 1994a and 1994b, Dhital et al. 1995, Fan et al. 2005)

Like the idea of using a water vapor permeable membrane in the plate enthalpy exchanger (Niu and Zhang 2001, Zhang and Niu 2002), the run-around exchanger can be made from a permeable, micro-porous membrane to transfer both heat and moisture (sensible and latent energies) between the two air streams, which can be referred as Run-Around Membrane Energy Exchanger (RAMEE).

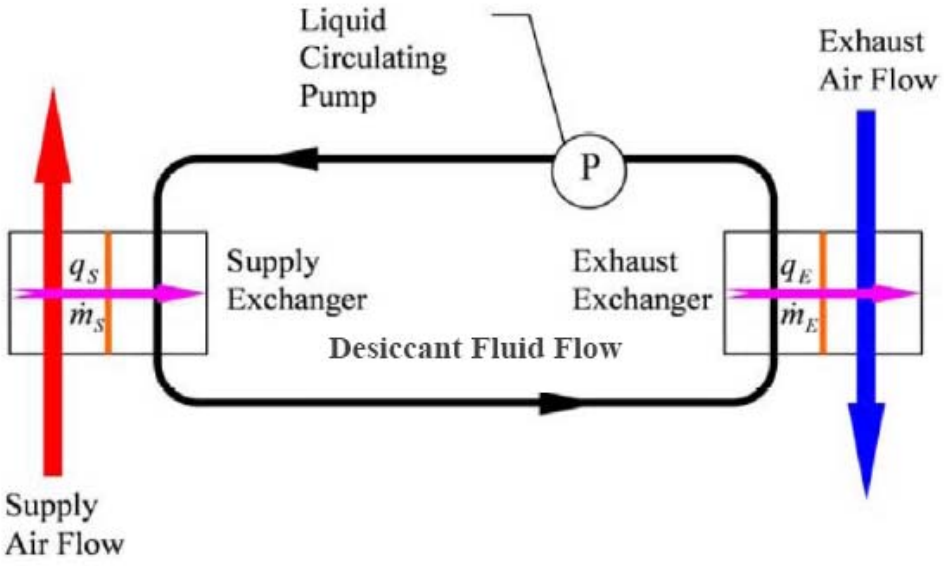

Figure 1.2 *Schematic diagram of a run-around membrane energy exchanger (RAMEE) system.*

The RAMEE system is made of two separate exchangers with a salt solution coupling liquid that is pumped in a closed loop between the exchangers. Each exchanger is constructed with vapor permeable membranes and is called a liquid-to-air membrane energy exchanger (LAMEE). The RAMEE system preconditions the supply air by use of the exhaust air to decrease the energy consumption and HVAC equipment capacity in a building. For example, in the summer when the outdoor air is

warm and humid, the desiccant salt solution gains heat and moisture from the supply air stream in the supply exchanger and releases the heat and moisture to the exhaust air stream in the exhaust exchanger.

Work on the RAMEE project began in 2002 when the first NSERC Collaborative Research and Development (CRD) grant was awarded to Professors Simonson and Besant for partnership research and development with Venmar CES Inc. The research is now in its second NSERC/Venmar CRD grant which started in January 2008.

1.2.1 Numerical Modeling of Fan (2006)

Fan (2006) developed a numerical model for a RAMEE system made of two cross-flow exchangers. Lithium bromide was applied as the coupling liquid salt solution in the model. It was shown by the numerical model that with the appropriate design characteristics (e.g. size and operating conditions) an overall effectiveness of 70% could be accomplished for the RAMEE system employed. However, Fan (2006) did the simulations without using a proper value for the permeability of membranes.

1.2.2 Prototype 1 (Hemingson 2005)

Concurrent with the numerical model development, several prototypes of the RAMEE system were designed, constructed and tested to verify the promising results of the numerical model. The first testing prototype (Hemingson 2005) was built with Tyvek® which is made of a common polymer called high density polyethylene, HDPT, (Larson 2006). In prototype 1 the two cross flow exchangers were coupled using a solution of lithium bromide. This prototype could not be properly tested because the liquid pressure caused excessive deflection of the membranes and the heat exchanger structure. In fact, the deflected membrane blocked a large portion of the

airflow channels. At low liquid pressure and flow rates, air could flow through the membrane and affect the system performance. There was also noticeable liquid leakage through the membrane.

1.2.3 Membrane Research of Larson (2006)

The unsuccessful results from the first prototype experiments which were mostly related to the structural design and poor properties of the membrane material resulted in a search for an appropriate membrane conducted by Larson (2006). His studies included testing and measuring different properties of various semi-permeable membranes. Properties like water vapor permeability, air permeability, liquid water penetration pressure and elastic properties of the membrane were investigated. Eventually, Propore, a two-layer composite material consisting of a proprietary microporous polypropylene membrane, was selected as the best available membrane for the RAMEE prototype because of its water vapor transmission rate and resistance to deflection (Larson et al. 2007, 2008).

1.2.4 Prototype 2 (Erb 2006, 2007)

Erb (2006, 2007) built another RAMEE testing prototype (prototype 2) based on the previous findings. Propore was used as the membrane. To minimize membrane deflection, it was supported by an outer screen that were designed according to the method presented in Larson (2006) and Larson et al. (2007, 2008). In prototype 2, the liquid flow could be either from the top to the bottom or from the bottom to the top of the exchangers in a cross-flow configuration with the air stream. Prototype 2 was tested in the laboratory under conditions similar to the AHRI summer and winter testing conditions (AHRI 2005) and the results were compared with the predicted results from the numerical model of (Seyed Ahmadi 2008, Erb et al. 2009). A quite

good agreement, within 2.2%, between the numerical model and experiments was reported by Erb et al. (2009) for high Cr* (Cr*>15). However, the discrepancies were noticeable (e.g. up to 10%) at lower Cr*, which was speculated to be due to desiccant flow distribution problems at lower Cr* values (i.e. low liquid flow rates).

The overall effectiveness of the RAMEE system must be greater than 50% to meet ASHRAE Standard 90.1 and should be greater than 65% to make it a competitive system for the commercial applications. Even though Fan et al. (2006) found a high (up to 70%) overall effectiveness for the RAMEE system with two cross-flow exchangers, these results were obtained using a membrane with a much higher permeability value than measured by Larson (2006). In order to improve the performance of the RAMEE system for the membranes identified by Larson (2006), it is proposed to modify the exchanger from a cross-flow exchanger to a counter-flow exchanger. The numerical study presented in this thesis, which is part of the RAMEE project, is focused on the system performance when counter/cross flow exchangers are employed instead of cross-flow exchangers to improve the RAMEE performance.

1.3 Counter/Cross Flow Heat and Moisture Exchanger

The performance of the RAMEE system depends heavily on the relative flow configuration of air and desiccant solution in the LAMEEs. Three different flow configurations of liquid and air streams in the LAMEEs are shown in Figure 1.3. In a cross-flow exchanger (Figure 1.3(a)) each fluid flows in a direction perpendicular to the other fluid and in a counter-flow exchanger the two fluids flow along the same axis but in the opposite directions (Figure 1.3(b)). The fact that the effectiveness of a cross-flow LAMEE is lower (up to 15%) than that of a counter-flow LAMEE with the same surface area of the exchangers and the same flow rates, leads designers to

choose the counter-flow exchangers for applications where the effectiveness must be high.

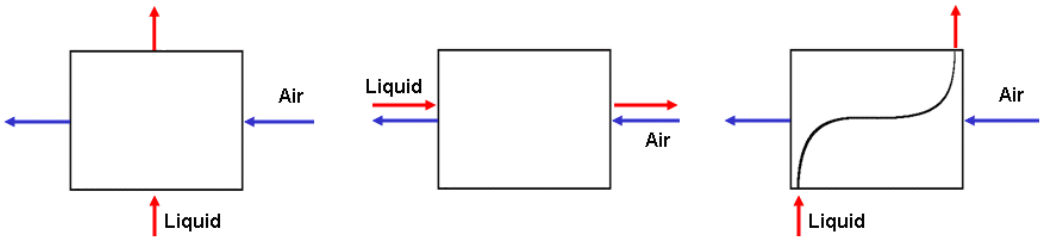

Figure 1.3 *Air and liquid streams configuration in a (a) cross-flow, (b) counter-flow and (c) counter/cross-LAMEE*

Using counter-flow LAMEEs could increase the overall effectiveness of the RAMEE system and eventually lead to a lower life-cycle cost and a shorter payback period compared to a system with cross-flow exchangers. However, a practical difficulty arises in constructing counter-flow LAMEEs in the separation of the two fluids at the ends of the LAMEE. Due to the fact that the counter-flow design (Figure 1.3(b)) needs both the air and liquid headers to be at the same side, it is practically difficult to construct the counter-flow flat plate exchangers in HVAC air ducts. To avoid this problem, cross-flow type inlet and outlet headers are proposed, as shown in Figure 1.3(c). Therefore, the new design is a counter-flow (or nearly counter-flow depending on the aspect ratio) LAMEE with cross-flow inlet and outlet headers or an energy exchanger with a combination of cross and counter-flow (counter/cross flow exchanger). It is expected that this counter/cross flow exchanger will have a better performance compared to the cross-flow exchanger. The RAMEE system with two counter/cross flow exchangers, similar to the one in Figure 1.3(c), is studied in this research.

1.4 Literature Review

1.4.1 Fluid Flow Distribution

Bulk velocities of the air and liquid streams are required to determine the convective heat and mass transfer. Therefore, the continuity and momentum equations are solved at the same time to determine the bulk velocity components of the liquid desiccant in different directions. The momentum equation is very complicated and difficult to solve since Navier-Stokes equations are second-order nonlinear partial differential equations. Some simplifications are adopted to solve the momentum equation under certain circumstances.

For some fluid flows and geometries, the velocity distribution can be determined analytically. One of the most well-known flows is the ideal flow defined as the frictionless and irrotational flow. The velocity distribution of the ideal flow is obtained from solving a second-order Laplace equation for the stream function.

However, real fluid flows are affected by the viscosity of the fluid. A dimensionless criterion which determines the relative importance of inertial and viscous forces is the Reynolds number defined as the ratio of the inertial force to viscous force of the moving fluid. When the viscous forces arising from the shearing motions of the fluid predominate over the inertial forces associated with the acceleration or deceleration of the fluid, the Reynolds number is small and fluid flow is called creeping flow. For an internal flow passing through a channel, the Reynolds number can be calculated using the equation:

$$\mathrm{Re} = \frac{\rho V d}{\mu} \tag{1.1}$$

where ρ is the density, V is the bulk mean velocity, μ is the viscosity of the fluid and d is the hydraulic diameter of the channel through which the fluid flows. Because of

the low velocity of the liquid flow between the membrane surfaces in each LAMEE (e.g. less than 0.1 m/s) and very small channel gap sizes (2 to 3 mm) between membranes, the Reynolds number in the liquid side is very small some distance away from entrance and exit (3 to 5).

Although the solution of the stream function to determine the velocity distribution was primarily restricted to ideal flow, under certain circumstances this method can be used for real flows even though the flow is rotational and controlled by viscosity (Robertson 1965). According to Hele-Shaw experiments (1897-1899), the bulk mean steady flow of a viscous fluid at low Reynolds number between two closely spaced parallel plates can be considered to behave as a plane two-dimensional potential flow for the bulk mean velocity (Robertson 1965). In this method, called the Hele-Shaw analogy, the mean-flow pattern (i.e. the averaged or bulk mean fluid velocity), in the plane of the plates, is determined by calculating the ideal-flow (i.e. potential flow) streamlines. G.G. Stokes (1898) gave a formal mathematical proof of this surprising identity of the streamlines and theoretically justified this analogy (Robertson 1965).

A.D. Moor (1949) showed that the Hele-Shaw analogy could be simply employed. A.D. Moor (1949) developed a fluid flow field mapper based on the Hele-Shaw analogy. The mapper consisted of two parallel plates which were located very close to each other (0.9 mm) and a fluid (e.g. air or water) passed through the channel. The streamlines of the flow around a body were obtained by placing the body in the channel between the two plates and letting colored lines of fluid trace out the streamlines. The fluid flow patterns similar to the ideal-flow streamlines around different body geometries were observed.

The Hele-Shaw analogy is applied in this study to determine the liquid bulk velocity components in a counter/cross flow exchanger. The analytical solutions for potential flow around several geometries such as corners can be found in many fluid mechanics textbooks (e.g. White 2003) and these solutions can be used to validate the model.

1.4.2 Heat Transfer in a Single Heat Exchanger

As mentioned previously, the run-around exchanger is composed of two separate exchangers. Therefore, the study of the run-around system begins with an investigation of the single exchangers. Since the pressure drop across plate heat exchangers can be low and this kind of heat exchanger can be manufactured easily and cost effectively, plate exchangers are very practical in commercial applications.

Many handbooks and textbooks focus on designing and selecting heat exchangers. There are correlations available for predicting the performance of different designs based on the ε-NTU method (ε is the effectiveness and NTU is the number of heat transfer units of the exchanger) (e.g., Kays and London 1984, Incropera and Dewitt 2002, Kuppan 2000). In the ε-NTU method, the steady state sensible effectiveness of an exchanger is calculated as a function of NTU and Cr (the heat capacity ratio). These dimensionless parameters depend on design characteristics such as the size of the exchanger and the mass flow rate of the fluids (Incropera and Dewitt 2002). The fluid flow configuration in the exchanger is another factor in determining the effectiveness.

An analytical model was developed by Luo and Roetzel (1998) to investigate the performance of cross-flow plate heat exchangers. To make the model more accurate, the effects of axial dispersion, flow maldistribution and backmixing were taken into account. The analytical solution of the temperature distribution and sensible

effectiveness showed that the influence of axial dispersion on the sensible effectiveness was only significant when Peclet number is less than 20 (i.e. Pe=Re.Pr). In this study the Peclet number was found to be larger than 50.

Fan et al. (2005) developed a two-dimensional steady state numerical model for the flat-plate cross-flow heat exchangers. The model was validated with the analytical solution and effectiveness correlation for cross-flow heat exchangers. The model showed that the sensible effectiveness increased with NTU and decreased with Cr.

1.4.3 Run-Around Heat Exchangers (RAHE)

Run-around heat exchangers (RAHE) or run-around heat recovery systems can be used in many HVAC applications because of their high reliability and flexibility in the HVAC design and retrofit. They have been the focus for research in recent decades. The initial study of such a system perhaps was done by London and Kays (1951). Their study found the optimum operating condition for the system. It was found that the effectiveness of the system was the highest when the heat capacity rate of the coupling liquid equaled the heat capacity rate of the air (i.e. Cr=1).

Forsyth and Besant (1988a, 1988b) developed a numerical model to investigate the performance and design of a RAHE with two coil heat exchangers using aqueous glycol as a coupling liquid. The analysis focused on the sensitivities of the system to changes in the design variables such as flow rates, dimensions of the system and operating conditions. The results implied that, to reach the maximum overall effectiveness, fully-developed turbulent flow in the coil tubes is essential. The system effectiveness under low liquid flow Reynolds number conditions could drop by up to 50% when a very high concentrated ethylene-glycol was used in the system. These simulated results were compared with the measured data. Although the general

trends of the numerical and experimental results were the same, the simulation and experiment did not show good agreement for a given design used in a university building. Forsyth and Besant (1988a, 1988b) also presented a numerical optimization technique to achieve a better design for the RAHE. They proposed that to obtain optimum design of a complex system with many design parameters, the total life cycle costs should be taken into account rather than only the overall effectiveness. This total system cost (the life-cycle cost of capital, operating and recovery costs and savings) was used to optimize the coil exchanger designs.

Forsyth and Besant (1988a, 1988b) used fluid properties at the mean temperature of the fluid in the model, which could cause errors and be the reason for disagreement between the model and experiments. Zeng et al. (1992a) furthered the research of Forsyth and Besant by studying the effects of temperature dependent properties on the performance of the RAHE. In this numerical model, the coupling fluid properties varied with temperature. They compared the results with variable fluid properties with the results using mean fluid properties. The results showed that when the temperature difference between the inlet supply and exhaust air was large and the Reynolds number was low for the coupling fluid in the coil tubes, temperature dependent properties of the aqueous-glycol coupling fluid needed to be included in the analysis of the RAHE. Using the average properties could lead to errors of up to 25% for the overall effectiveness.

Zeng et al. (1992b) also investigated a two-phase, gas-liquid, coupling fluid in order to improve the performance of the RAHE. The overall effectiveness of a RAHE for both single-phase and two-phase coupling fluids was calculated by the numerical model and then compared with the data measured in a laboratory test facility over a range of operating conditions. There was good agreement between the simulation and

experimental data. Both data sets showed that if the coupling fluid was changed from a pure liquid to two-phase gas-liquid mixture, typically a 20% increase of the overall effectiveness at the same liquid flow rate was obtained.

Because the comparison between the simulated data by Forsyth and Besant (1988a) and measured data was inadequate to validate the computational model, Bennett et al. (1994a, 1994b) improved Forsyth and Besant's (1988a, 1988b) work to validate the model by experimental data. It was believed that the discrepancy was because of different geometry of the coils used in the experiment. The contact resistance between the fins and coil tubes which was not considered in Forsyth and Besant's (1988a) model was also indicated as another potential reason for the discrepancy. Bennett et al. (1994a, 1994b) included the wavy-fin coil geometry and considered the effect of the thermal contact resistance between the fins and coils in their numerical model. They also considered liquid bypass flow and hourly weather data for performing the yearly simulation. The modified model developed by Bennett et al. (1994a, 1994b) was verified using the measured data and the relative difference of this comparison was less than 5%. Using the modified model and optimization techniques presented by Forsyth and Besant (1988b) for a RAHE, a life-cycle cost (LCC) design procedure was developed (Bennett et al. 1994b). The procedure was to improve the performance of the RAHE by optimizing the LCC employing all the design variables and operating conditions. They concluded that the RAHE design for optimal LCC would have a greater cost saving up to 45% and it would increase the overall effectiveness up to 16% compared with the RAHE system designed without considering the system LCC.

Dhital et al. (1995) used the modified model developed by Bennett et al. (1994a). They studied the effect of using a RAHE in a typical large office building

located in several cities for which there was long term weather data available. First, the energy consumption of the building with and without the RAHE was investigated. Second, the building was analyzed with the RAHE using enhanced ventilation but with the same LCC for the office building had without the RAHE system. This later investigation answered the question of what was the maximum ventilation rate that could be achieved using a RAHE system with the same LCC as the building would have if the RAHE was not used in the building. The results indicated that using the RAHE saved significant amount of energy in the buildings, reduced the HVAC system heating and cooling capacity and ultimately improved the LCC of the buildings. Also, the RAHE system could be used to increase the ventilation rate to several times the minimum rate recommended by ANSI/ASHRAE Standard 62-1989 without increasing the energy consumption.

Johnson et al. (1995) presented simulation and optimization procedures based on the techniques developed by Bennett et al (1994a, 1994b) and Forsyth and Besant (1988a, 1988b) for a multiple-coil RAHE. A computer program was developed to simulate any number of supply and exhaust coils. The program was applicable to determine yearly cost and saving and optimize the design based on the life-cycle cost (LCC) of the system. It was found that the performance of an optimized system was almost independent of the number of coils and was substantially better than the design just based on the operating conditions. The LCC analysis showed that the optimized system could save a significant amount of energy and reduce the size of HVAC systems, which finally led to 10%-20% life-cycle cost saving. Variable-speed pumping for heat rate control was simulated and found to be more cost effective than the liquid bypassing control valve investigated by Bennett et al (1994a, 1994b).

Due to the fact that run-around recovery systems with the flat plate heat exchangers may be more cost effective and easier to manufacture compared to those with the coil-type exchangers, the flat plate exchangers were employed in a RAHE system. Fan et al. (2005) presented a mathematical model for a RAHE with two cross-flow flat plate heat exchangers. In the model, a finite difference method was applied to solve the governing equations derived from physical principles. Dimensionless design groups (ε, NTU, Cr) were used to present and interpret the performance of the RAHE. The maximum effectiveness of the RAHE was found when Cr≈1 which was in agreement with Kays and London's (1951) finding. Besides, the numerical model was validated with analytical and empirical correlations and the results showed good agreement.

1.4.4 Energy Recovery Systems

1.4.4.1 Rotating Energy Wheels

As it has been shown in Figure 1.1, there are several kinds of energy recovery systems (i.e. systems that transfer both heat and moisture) available commercially. One of the most common energy recovery devices is the rotating energy wheel which has been of interest over a period of many years. Simonson and Besant (1997a, 1997b) developed and validated a numerical model for coupled heat and mass transfer in energy wheels. Simonson and Besant (1999a, 1999b) derived the dimensionless groups for air-to-air energy wheels. They showed the performance of the energy wheel was a function of the operating temperature and humidity of the participating air streams, number of heat transfer units (NTU), heat capacity rate ratio (Cr*) and moisture capacitance ratio (Crm*) that is analogous to Cr*. Then they used the validated numerical model and the dimensionless groups to develop correlations for

the effectiveness of the energy wheel. The correlations presented by Simonson and Besant (1999b) agreed with the simulation data within ±2.5%.

1.4.4.2 Plate Energy Exchangers

Plate exchangers made from water vapor permeable membranes are the other energy recovery systems studied recently. Zhang and Jiang (1999) simulated heat and mass transfer in a membrane-based plate exchanger. The permeability of the membrane was found to be variable throughout the exchanger due to the moisture transfer. Zhang et al. (2000) studied the possible energy saving by using the membrane-based plate exchanger. They found that up to 18% and 23.5% of energy can be saved when using a plate heat (sensible energy only) exchanger and plate energy (sensible and latent energy) exchanger, respectively.

Niu and Zhang (2001) formulated a numerical model for flat plate air-to-air energy exchangers with a membrane core and investigated the variations of sensible, latent and total effectivenesses with the change of various operating parameters. The model was validated by experimental data for cross-flow enthalpy exchangers. The result showed that due to the change of moisture diffusive resistance of the membrane the latent effectiveness was not only influenced by the membrane material but also by the operating conditions. To consider the effect of the membrane material and the operating conditions on the membrane permeability, a dimensionless factor, the coefficient of moisture diffusive resistance, was defined. It was also revealed that a membrane material with a linear sorption curve had a better performance.

Zhang and Niu (2002) furthered their study by developing correlations for the sensible and latent effectivenesses of the air-to-air enthalpy exchanger. They correlated the sensible effectiveness as a function of the number of heat transfer units, NTU, and the latent effectiveness as a function of the number of mass transfer units,

NTU_m. A comparison between the effectiveness predicted by the correlations and measured in experiments was done to validate the correlations. The average errors between the predicted and experimental results were 7.3% and 8.6% for sensible and latent effectiveness, respectively.

1.4.4.3 Direct Contact or Open Systems

Park et al. (1994) predicted by numerical methods the coupled heat and mass transfer between air and a uniformly distributed falling triethylene glycol solution film in a cross-flow plate gas-liquid exchanger. The results were compared with experiments and a satisfactory agreement was observed. The air stream was in direct contact with the liquid film. A three-dimensional numerical model was developed assuming interfacial equilibrium conditions for the concentration, temperature and pressure in the air and liquid desiccant. The governing equations were solved using a finite difference method. The numerical model gave the three-dimensional temperature and concentration distributions in both the liquid desiccant and air streams, which were used to investigate the performance of the system.

Ali et al. (2003, 2004) studied the heat and mass transfer between air and falling film of solution in parallel, counter, and cross-flow configurations. Their numerical model was developed assuming that the liquid desiccant flow was laminar, fully developed and the Peclet number was large enough to neglect the diffusion in the direction of flow. They added nonoparticle suspensions to the liquid desiccant as solid metal particles had higher thermal conductivity than fluids and enhanced heat and mass transfer within the solid–liquid mixture. Ali et al. (2003) compared two different flow configurations (parallel and counter-flow) and concluded that the parallel flow channel provided better dehumidification and cooling of the air than the counter-flow configuration. They also showed that an increase in the volume fraction

of nanoparticles and dispersion factor resulted in an improvement in the dehumidification and cooling rates of air.

Ali et al. (2004) investigated the enhancement of the heat and mass transfer in the presence of solid metal particles (Cu-ultrafine particles) in the desiccant solution. They modeled the coupled heat and mass transfer of the air in contact with falling solid-liquid mixture in the cross-flow configuration. Ali et al. (2004) verified that a higher volume fraction of Cu-ultrafine particles and thermal dispersion effects provided better dehumidification and air cooling. They performed a parametric study and showed that to enhance dehumidification and cooling for air, the air Reynolds number should be reduced, while the salt solution Reynolds number had a minimal effect. Ali et al. (2004) also concluded that better air dehumidification and cooling could be achieved by increasing the contact surface area and width of the air channels.

Mesquita et al. (2006) developed numerical models for simultaneous heat and mass transfer in parallel-plate internally-cooled liquid-desiccant dehumidifiers. They employed three different approaches to investigate the problem in their numerical models. In all approaches, they assumed fully-developed laminar flow for the liquid desiccant and air streams. The first approach was the most simplified and it was based on heat and mass transfer correlations assuming constant temperature for the liquid desiccant and using bulk mean properties for the air stream. In the second method, the energy and mass balance equations were solved numerically using the finite-difference method. In the second approach it was assumed that the thickness of the liquid desiccant film was constant. A variable film thickness was employed in the third approach to make it more accurate. The variable thickness model (third approach) resulted in close agreement with experimental data for low mass flow rate of liquid desiccant (within 6% difference). However, the discrepancies between the

numerical and experimental results became noticeable for higher liquid desiccant mass flow rates.

Liu et al. (2007) presented a theoretical model to simulate the heat and mass transfer process in a cross-flow dehumidifier/generator using liquid desiccant. In their model, air and liquid desiccant were in direct contact and axial conduction and diffusion were assumed negligible. The predicted results for enthalpy and moisture effectiveness were compared with the experimental findings and the average absolute discrepancies were 7.9% and 8.5%, respectively.

1.4.4.5 Run-Around Membrane Energy Exchanger (RAMEE)

The studies in section 1.4.3 include only sensible heat transfer in run-around systems. However, to achieve an ideal air-to-air energy recovery system, the run-around system must be able to transfer both heat and moisture between the two air streams. Enthalpy, or heat and moisture, plate exchangers are composed of water vapor permeable surfaces which enable the simultaneous heat and moisture transfer between the two fluid streams. The same idea was used to make the run-around energy exchanger which would be capable of transferring both heat and moisture. The difference between these two systems is that the RAMEE system uses a coupling liquid to transfer heat and moisture from one air stream to the other one. However, in the plate enthalpy exchangers the two air streams are separated by a permeable membrane surface and they exchange heat and moisture directly.

Fan et al. (2006) presented an implicit numerical model to study the steady state heat and water vapor transfer in a run-around membrane energy exchanger (RAMEE). The run-around system was made from two identical flat plate cross-flow exchangers, and lithium bromide solution was used as the coupling liquid to exchange heat and moisture between supply and exhaust air streams. A finite difference method

was employed to solve the coupled heat and moisture transfer equations in each exchanger. The results showed the overall effectiveness of the run-around energy recovery system depended on many parameters such as the mass flow rates of fluids, the size of exchangers, and the inlet operating conditions. It was also found that the maximum effectiveness of the RAMEE system at the AHRI summer conditions occurred at approximately $C_{Sol}/C_{Air}=3$ rather than $C_{Sol}/C_{Air}=1$ where the maximum effectiveness of the RAHE happens. According to the results an overall effectiveness of 70% could be achievable if the characteristics of the RAMEE system were chosen correctly (e.g. NTU>10 and $Cr^*\approx3$). However, a very high permeability value was used in the model and the results were not validated by experimental measurements.

Erb (2006, 2007) built and tested a RAMEE system composed of two cross-flow exchangers. The experimental results were compared with the numerical model developed by Fan et al. (2006). For AHRI Summer test conditions (AHRI 2005), the experimental results did not agree well with predicted results from the numerical model. According to the numerical model the effectiveness increased with NTU and the experimental data confirmed that. However, the test results did not show any effectiveness peaking at $Cr^*=3$ (i.e. $C_{Sol}/C_{Air}=3$) which was predicted by the model. The experimental effectiveness increased continuously and then it reached a constant value as Cr* increased. At high Cr* the experimental effectiveness was 5% to 10% lower than numerical predicted values. The discrepancy was believed to be attributed to non-uniform flow distribution of the desiccant which was not considered in the numerical model. For a constant NTU, at lower Cr*, because of the low mass flow rate of desiccant, the liquid desiccant did not flow uniformly through the liquid channels, so the experimental effectiveness was small. As the desiccant flow rate increased, the desiccant flow through the liquid channels became more uniform, and

for a constant NTU, resulted in better agreement between experimental and numerical effectivenesses at higher Cr*.

Erb et al. (2009) compared the experimental data of a cross-flow RAMEE to numerical simulations (Seyed Ahmadi 2008). The experimental data of the RAMEE system were in agreement with the numerical predictions especially at higher Cr*. The effects of different exchanger sizes, liquid and air flow rates, external heat gains/losses and desiccant concentrations on the performance of the system were investigated. It was shown that external heat gain/loss has a large impact on the performance of the RAMEE system. The heat gains/losses could cause different values for effectiveness based on the supply side or the exhaust side of the RAMEE. The transient response of the system (due to both initial start-up and changes in the outdoor air conditions) was studied by Erb et al. (2009). It was revealed that the transient response was sometimes very long due to the thermal and moisture storage capacity of the liquid desiccant. Erb et al. (2009) proposed that to reduce the response time, the desiccant liquid volume in the system should be minimized and initial desiccant concentration should be adjusted according to operating conditions. The desiccant concentration adjustment was proposed to be done by evaporating moisture or adding water when required.

1.5 Objectives

It is the general purpose of this study to investigate the feasibility of using two counter-flow or counter/cross flow exchangers in a run-around heat and moisture recovery system to improve its performance.

The detailed objectives of this research are given below

1. Develop a numerical model for a counter/cross flow plate exchanger to solve the bulk mean flow distribution of the liquid desiccant.

2. Using the bulk mean flow distribution from 1, develop a numerical simulation to study heat and water vapor transfer in a run-around energy recovery system with two counter-flow or two counter/cross flow exchangers.

3. For heat transfer only (i.e. without moisture transfer), validate the accuracy of the model in (2) using the existing validated heat exchanger correlations from the literature. Use this validated model to develop design correlations for counter/cross flow heat exchangers and run-around heat recovery systems with two counter/cross flow exchangers.

4. Validate the numerical model for the RAMEE systems with both heat and mass transfer using (a) the model developed by Seyed Ahmadi (2008) and (b) experimental data presented by Mahmud (2009).

5. Study the performance of the run-around energy recovery system under different operating conditions along with a dimensional analysis. This investigation is aimed to analyze the RAMEE system design characteristics and find an optimized design to determine the best feasible performance of the system.

1.6 Thesis overview

A theoretical/numerical model of a RAMEE system with two counter/cross flow exchangers (objectives 1 and 2) is developed in detail in Chapter 2. The

numerical model is steady state, two-dimensional and is developed based on the physical principles of conservation of momentum, mass and energy. A finite difference method is used to discretize the governing equations. The dimensionless groups used in the study of the RAMEE system are also developed in Chapter 2.

In Chapter 3, the model for the case of only heat transfer (i.e. no moisture transfer) is verified using the available well-known correlations from the literature (objective 3). This verified model is used in Chapter 3 to develop effectiveness correlations for the counter/cross flow heat exchangers and the RAHE system made of two counter/cross flow exchangers. The numerical model and new correlations are applied to show the sensitivity, limitations and accuracy of the correlations.

Verifications of the numerical model for the RAMEE system (i.e. with both heat and mass transfer) is presented in Chapter 4 using experimental and numerical data to satisfy objective 4. For numerical comparison, the predicted effectiveness of the RAMEE system is compared with the numerical results from Seyed Ahmadi (2008). The model validation with experiments is presented for the RAMEE prototype 2 (Erb 2007) consisting of two cross-flow exchangers and prototype 3 (Mahmud 2009) with two counter/cross flow exchangers.

The final objective of this thesis (objective 5) is to study the effects of different design characteristics and operating conditions on the performance of the RAMEE system. The results are presented in Chapter 5 based on the dimensionless groups developed in Chapter 2 to make the results useful for practical applications with the same values for dimensionless variables.

Finally, the conclusions based on the findings in this thesis and the recommendations for future studies to improve the RAMEE system performance are presented in Chapter 6.

Chapter 2

Numerical Model

2.1 Introduction

A run-around membrane energy exchanger (RAMEE) is an energy recovery system that transfers heat and moisture between supply and exhaust air streams by the use of a coupling liquid (Figure 2.1). The RAMEE system is made of two separate liquid-to-air membrane energy exchangers (LAMEE) that transfer heat and moisture between the liquid and air stream. The LAMEEs are coupled in a closed loop and a desiccant salt solution (e.g. $MgCl_2$ solution in this study) is pumped in the loop between the two exchangers.

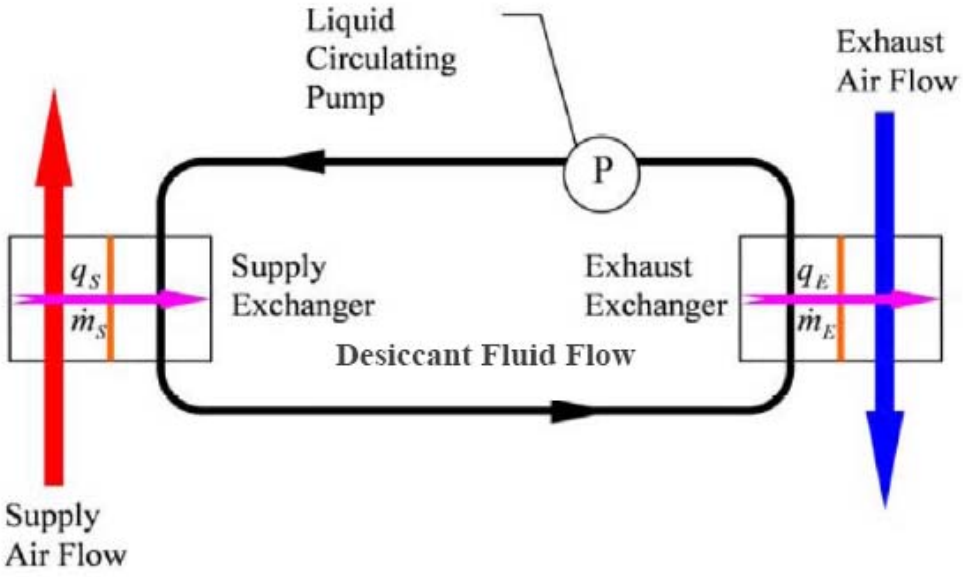

Figure 2.1 *Schematic diagram of a run-around membrane energy exchanger (RAMEE) system consisting of two liquid-to-air membrane energy exchangers (LAMEEs).*

Depending on the operating conditions, the desiccant solution gains heat and moisture from the air stream in one LAMEE and delivers the heat and moisture to the air stream in the other LAMEE. For example, in the summer when the outside

ventilation air (i.e. supply air) is hot and humid, the salt solution obtains energy (heat and moisture) from the supply air stream and transfers this energy to the exhaust air stream.

As discussed in Chapter 1, the cross-flow configuration for each LAMEE is practical for HVAC installations, while the counter-flow configuration would provide the best performance. Therefore, each LAMEE is a combination of cross-flow and counter-flow. The geometry of the counter/cross flow LAMEE and the liquid flow path in the exchanger are shown in Figure 2.2. In this exchanger, liquid enters from the bottom left-hand corner of the exchanger. The bottom header has a length of x_i, which is less than the exchanger length (x_0). That is, the entire bottom side is not open to liquid flow. Liquid leaves the exchanger from the top header, after traveling along a S-shape path line through the exchanger. The top header also has a length of x_i as indicated in Figure 2.2. To avoid a large pressure drop on the air side, the air flows in a straight path directly through the exchanger from right to left in Figure 2.2. The pressure drop on the liquid side is very small so the path line can be more complex then the air side. The result is a composite exchanger with a counter-flow core, but with cross-flow headers.

Using the counter/cross flow configuration makes the model more complicated because the liquid flow is two-dimensional compared to models of cross or counter-flow exchangers where each fluid flow is one-dimensional. It is expected that the performance of the RAMEE system with two counter/cross flow LAMEEs, as those in Figure 2.2, is better than the RAMEE system with two cross-flow LAMEEs because having the counter-flow configuration as a significant part of the exchangers improves the performance.

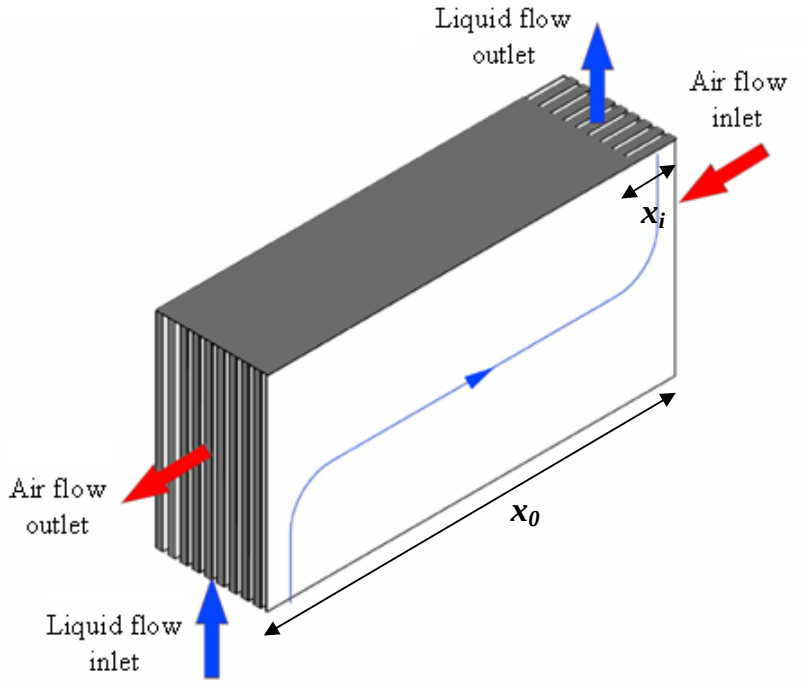

Figure 2.2 *Schematic of a flat-plate counter/cross flow LAMEE showing one streamline for the liquid flow*

The purpose of this chapter is to develop a steady state numerical model for a liquid-to-air membrane energy exchanger (LAMEE) similar to the one shown in Figure 2.2 and a RAMEE system with two counter/cross-LAMEEs as shown in Figure 2.1. Since the model is going to be used to investigate the design and performance of the RAMEE system under different operating conditions, it must be based on accurate physical principles. However, simplifying assumptions which do not affect the accuracy of the model significantly are beneficial to reduce the complexity of the model. The simplifying assumptions, governing equations and boundary conditions applied to develop the numerical model for the RAMEE system are presented in detail in this chapter.

A schematic of a module of the counter/cross flow LAMEE containing a pair of flow channels: one air channel adjacent to one liquid channel is shown in Figure 2.3. The coordinate system employed for the mathematical model and the air and the liquid flow paths are also indicated in Figure 2.3. The separating semi-permeable membrane is Propore which was proposed by Larson 2007. As indicated, the flow configuration used in this model is counter/cross flow. Several of these unit modules are stacked together along the z-direction to form a complete LAMEE similar to that shown in Figure 2.2. In the LAMEE, then each liquid channel is sandwiched between two air channels or vice-versa.

The numerical model solves the fluid streamlines and determines the bulk mean flow distribution in each LAMEE. Then, the fluid mean velocity in each direction will be used to solve the coupled heat and mass transfer equations in the LAMEE. By coupling two LAMEEs in a closed loop the numerical model simulates the RAMEE system.

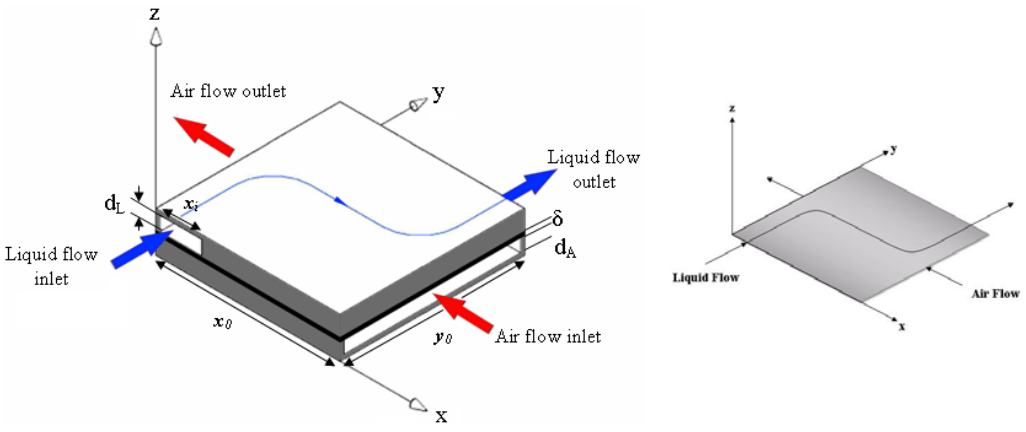

Figure 2.3 *A module of a counter/cross flow LAMEE. The module consists of an air channel, a liquid channel and three separating semi-permeable membrane. The air and liquid paths in the counter/cross flow LAMEE are shown on the coordinate system.*

2.2 Assumptions

The following assumptions are applied to develop the numerical model for the RAMEE system.

1. It is assumed that both the air and liquid flows are laminar, steady and fully developed. The heat and mass transfer is also assumed to be steady and fully developed.

2. The liquid and air flows are independent of heat and moisture transfer.

3. The semi-permeable membrane separating the air and liquid streams in each LAMEE allow the transmission of water vapor, but not liquid water.

4. The heat and mass transport is only normal to each membrane in the z-direction (Figure 2.3). The axial conduction of heat and molecular diffusion of water vapor through the membrane and in fluid streams in the direction parallel to the plates are assumed to be negligible compared to the advection heat and mass transport in the fluid streams and transport normal to the membrane.

5. It is assumed that the heat gain/loss from the phase change of water occurs only in the liquid side.

6. The exchanger flow channels are assumed to be identical. Only one air channel and one liquid channel are simulated in the model for each exchanger. The effect of edge channels without adjacent fluid channel on one side, is neglected.

7. It is assumed that the air and salt solution are well mixed and have uniform properties at the inlets of exchanger.

8. It is assumed that the connecting pipes are perfectly insulated and impermeable, and heat and moisture transfer occurs only between the air and the liquid in the LAMEE.

9. The moisture transfer resistance of the salt solution is negligible and the humidity ratio can be determined from equilibrium relations.

Assumption 1 means that the entrance effects on the fluid flow and heat and mass transfer are neglected. This assumption avoids the use of different properties and governing equations in the entrance region. However, it does not result in a significant inaccuracy in the model because the entrance regions of the air and liquid flows are very small compared to the remaining flow area of the exchanger. Sensitivity studies done by Fan (2006) for the entrance effect in a cross-flow exchanger showed the effect of the entry length is very small (i.e. it causes less than 1% change in the effectiveness) and can be neglected without compromising accuracy. The mean bulk temperature and moisture concentration over the cross section of the channels are used in the model. In reality, the temperature and moisture content in the air and desiccant liquid vary slightly from the edge to the middle (in z-direction) of both the air and liquid channels cross section. This assumption simplifies the model and makes it a two-dimensional problem. As the fluid channels are very narrow in z-direction, any variations of properties in each channel along z-direction can be neglected without a major error in results.

Assumption 2 can be used since both the air and liquid flows are dominated by the pressure difference between the inlet and outlet pressure produced by pumps and fans, so the momentum equations can be decoupled from the heat and moisture transfer equations. Although heat and mass transfer can change the fluid properties

such as density and viscosity which can affect the fluid flow distribution, the changes in fluid properties are very small for the temperature and moisture concentration differences across the exchanger. For example, the density of $MgCl_2$ salt solution, used in this study as a coupling liquid, changes by only 0.08% for each 5^oC temperature variation for an average salt concentration of 32%. The density also changes with salt concentration at temperature of 15^oC by 0.7% for each 1% salt concentration change (Zaytsev and Aseyev 1992). Since the temperature and salt concentration differences across each LAMEE are in the range of 10^oC and 1%, respectively, the effect of property variations is trivial and can be neglected. This assumption allows decoupling the momentum equations from the energy and moisture balance equations. It simplifies the numerical solution and decreases the number of iterations and computation time significantly without a significantly compromising the accuracy.

Assumption 3 is accurate for some commercial semi-permeable membranes such as Propore which is used in this study (Larson 2007).

The reason for applying the fourth assumption, which simplifies the governing equations, is that the membrane thickness is very small compared to its surface area. Therefore, heat and mass transfer is only between the air flow and the liquid flow and in the direction normal to the membrane. (z-direction, see Figure 2.3) and conduction in the membrane in x and y directions is negligible. Justification of assumption 4 can also be found in the literature. Luo and Roetzel (1997) showed that the effect of axial conduction in the fluid stream was negligible in an exchanger with Peclet number (Pe=RePr) greater than 20. In this thesis, the Pe is mostly greater than 20. Fan (2006) also showed that including axial conduction in the fluid streams changed the latent and sensible effectiveness by less than 0.5%.

The fifth assumption that the heat of phase change of water is transferred to or from the liquid desiccant is expected to be very close to reality. Figure 2.4 shows a schematic of a liquid and an air channel separated by a semi-permeable membrane. Heat and mass transfer occurs between two streams in different phases (i.e. gas-liquid). Due to the fact that only water vapor can diffuse through the membrane (Assumption 3) and the membrane holds back liquid water due to the small pores and capillary pressure, the phase change must occur at a gas-liquid interface on the membrane surface in the liquid side.

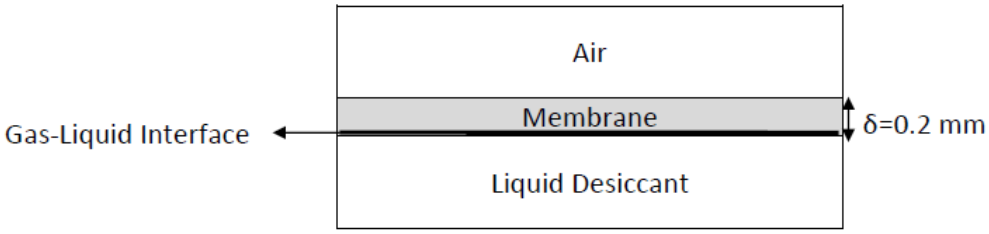

Figure 2.4 *Schematic of two adjacent channels separated by a semi-permeable membrane*

The heat transfer coefficient between the gas-liquid interface and liquid desiccant is:

$$U_L = h_L \tag{2.1}$$

and the heat transfer coefficient between gas-liquid interface and air side is:

$$U_A = \left[\frac{\delta}{k} + \frac{1}{h_A}\right]^{-1} \tag{2.2}$$

where δ is the membrane thickness, k is the thermal conductivity of the membrane, and h_A and h_L are the convective heat transfer coefficients on the air and liquid sides, respectively.

Comparing these two values and considering the fact that the liquid side convective heat transfer coefficient is much greater than the air side convective heat transfer coefficient (an order of 10 times), the phase change heat delivered to the air stream can be neglected.

The model assumes that each air channel in the LAMEE is located between two desiccant liquid channels and each liquid channel is located between two air channels (Assumption 6). However in reality, the air channels at each edge of the LAMEE (in z-direction) will be adjacent to only one liquid channel at the inner side. These air channels are referred as the edge channels. The heat and mass transfer rate between the liquid and air in the edge channels is different because the air stream interacts with only one liquid channel. This means that different governing equations are needed to determine the correct heat and mass transfer in the edge channels. Seyed Ahmadi (2008) presented a sensitivity analysis to investigate the effect of considering the edge effect on the performance of the RAMEE system. He found that steady-state sensible, latent and total effectivnesses of the system using LAMEEs with 10 panels (each panel is comprised of one liquid and one air channel) decreased by 0.6%, 1.1% and 0.9%, respectively, when the effect of edge channels was included in the model. For exchangers with more panels, the effects of the edge channels will be even less. Therefore, the edge effects are neglected in the model developed in this thesis.

Because of the presence of pumps and storage tanks in the desiccant solution loop which will mix the solution in a real system, assumption 7 is reasonable for the model. Assumption 8 means there is no heat and moisture exchange between the ambient air and any component of the RAMEE system. In practice, the insulation is not perfect and some heat transfer between the surroundings and liquid desiccant in pipes, pumps and header is unavoidable. However, the temperature difference of the

liquid desiccant across the connecting pipes, pumps, and headers is small compared to the temperature change across a LAMEE in a well-insulated system. It is thus realistic to assume negligible heat loss/gain from the surrounding air to the RAMEE system because Seyed Ahmadi (2008) showed that the average overall sensible and latent effectivenesses of the RAMEE system were reduced by less than 1% when the heat transfer in piping, storage tank and pumps was 20% of the total heat transfer in each LAMEE (Seyed Ahmadi 2008).

Assumption 9 is valid for low moisture transfer rates and means that the concentration and equilibrium humidity ratio of the salt solution are constant in the z-direction and equal to the bulk mean salt solution concentration.

2.3 Liquid-to-Air Membrane Energy Exchanger (LAMEE)

A run-around membrane energy exchanger (RAMEE) system is made of two liquid-to-air membrane energy exchangers (LAMEE). The heat and moisture transfer between the liquid and air occurs in the two LAMEEs. The phase change of water in the coupling liquid results in a strong coupling of the heat and mass transfer equations, which means that they must be solved simultaneously.

In this section, the governing equations for solving the flow distribution and the coupled heat and moisture transfer in a counter/cross flow LAMEE are presented. The development of the governing equations is contained in Appendix A.

2.3.1 Liquid Desiccant Flow Distribution

In each LAMEE, the liquid flows at a low Re number through the thin liquid channels (e.g. less than 3 mm). This results in a plane two-dimensional flow where the Navier-Stokes equations can be simplified to the second-order Laplace equation

for the stream function (ψ) (Robertson 1965). Therefore, the governing equation to determine the liquid flow pattern using the stream function is,

$$\nabla^2 \psi = 0 \tag{2.3}$$

where ψ is the stream function. The bulk mean velocity components can be determined from the stream function as follows.

In the *x* direction:

$$u = \frac{\partial \psi}{\partial y} \tag{2.4}$$

and in the *y* direction

$$v = -\frac{\partial \psi}{\partial x} \tag{2.5}$$

In these flows, the streamlines are parallel to the direction of bulk flow at every point. In the viscous flow, the pressure gradient is parallel to the streamlines such that the pressure drop across the exchanger is the same for each streamline. Thus, the constant pressure lines are perpendicular to the streamlines.

2.3.2 Coupled Heat and Moisture Transfer Governing Equations

The governing equations for coupled heat and mass transfer are developed from the steady state energy and mass balance equations for the air and liquid sides after employing the simplifying assumptions presented in the preceding section.

Air side

Under steady-state operating conditions, the water vapour flux through the membrane surface is balanced by the mass gain/loss in the air:

$$\frac{2U_m y_0}{\dot{m}_{Air}}\left(W_{Air} - W_{Sol}\right) = -\frac{\partial W_{Air}}{\partial x} \tag{2.6}$$

where y_0 is the height of the LAMEE, W_{Air} is the bulk mean humidity ratio of the air stream.

$$W_{Air} = \frac{\text{Mass of Water}}{\text{Mass of Dry Air}} = f(\phi_{Air}, T_{Air}) \tag{2.7}$$

W_{Air} is a function of relative humidity and the temperature of the air. W_{Sol} is the equilibrium humidity ratio of the salt solution. Even though W_{Sol} is a salt solution property, it actually is the equilibrium humidity ratio for air in contact with the salt solution at the condition of concentration and temperature of the bulk mean flows. In other words, it is the humidity ratio of the air when the air left in contact with the salt solution for a long time in a closed vessel, so the partial pressure of water vapor in the air and the salt solution are equal and there is no net moisture transfer between them at the equilibrium state.

$$W_{Sol} = f(X_{Sol}, T_{Sol}) \tag{2.8}$$

where

$$X_{Sol} = \frac{\text{Mass of } H_2O}{\text{Mass of Salt}} \tag{2.9}$$

The correlation used for calculating the equilibrium humidity ratio of salt solution will be presented in Section 2.5.

In equation (2.6), $\dot{m}_{Air}$ is the mass flow rate of air through a single air channel and U_m is the overall mass transfer coefficient for water vapor mass flux between the air and liquid salt solution. U_m is calculated using the following equation and assumption 9.

$$U_m = \left[\frac{1}{h_{m,Air}} + \frac{\delta}{k_m} \right]^{-1} \tag{2.10}$$

In equation (2.10), $h_{m,Air}$ is the convective mass transfer coefficient of the air stream, δ is the thickness of the membrane which, on average, was measured to be 0.2 mm, and k_m is the permeability of the membrane. The permeability of the membrane (k_m) depends on the material properties such as the size, shape and distribution of the

pores ant the thickness of the membrane. The value used in this study for Propor is $k_m=1.66\times10^{-6}$ kg/(m·s) (Larson 2006).

It is assumed that the phase change energy is only delivered to the liquid desiccant. Therefore, at any point (x, y) in the exchanger, the heat gain/loss in the air is balanced by the heat flux through the membrane surface.

$$\frac{2Uy_0}{C_{Air}}\left(T_{Air}-T_{Sol}\right)=-\frac{\partial T_{Air}}{\partial x} \tag{2.11}$$

where T_{Air} and T_{Sol} are the bulk mean temperatures of the air and liquid salt solution at (x, y), respectively, and C_{Air} is heat capacity rate of the air.

$$C_{Air}=\dot{m}_{Air}\left(C_{pAir}+W_{Air}C_{pv}\right) \tag{2.12}$$

In equation (2.11), U is the overall heat transfer coefficient between the air and salt solution:

$$U=\left[\frac{1}{h_{Sol}}+\frac{\delta}{k}+\frac{1}{h_{Air}}\right]^{-1} \tag{2.13}$$

where h_{Sol} and h_{Air} are the convective heat transfer coefficients of the liquid desiccant flow and the air flow, respectively, and k is the thermal conductivity of the membrane separating the two fluid streams. A value of k= 0.3 W/(m.K) is used in this study, which is close to the value found for Teflon (Incropera and Dewitt 2002).

Convective heat and mass transfer coefficients for fluid streams must be obtained to calculate the overall heat and mass transfer coefficients from equations (2.10) and (2.13). The convective heat transfer coefficient can be determined from empirical correlations presented in the heat transfer text books. For fully-developed laminar flow, the Nusselt number is constant when there is a constant heat flux. The convective heat transfer coefficient for the fully-developed laminar flow between infinite rectangular parallel plates with a uniform heat flux boundary condition can then be obtained from the following equation (Incropera and Dewitt 2002)

$$Nu_D = \frac{hD_h}{k_f} = 8.24 \tag{2.14}$$

where D_h is the hydraulic diameter of the flow channel and k_f is the thermal conductivity of the fluid. For flow between two infinite parallel flat plates, D_h is twice the channel spacing.

To obtain the overall mass transfer coefficient, the convective mass transfer coefficients of the air and the membrane permeability are needed. The convective mass transfer coefficient of the air can be obtained directly from an analogy between the convective heat and the convective mass transfer coefficients (Incropera and Dewitt 2002).

$$\frac{h}{h_m} = \rho c_p Le^{2/3} \tag{2.15}$$

where Le is Lewis number given by the ratio of thermal to mass diffusivities:

$$Le = \frac{\alpha}{D_{AB}} \tag{2.16}$$

Liquid side

To have steady state conditions, at any point (x, y) in the exchanger, the mass gain/loss in the liquid must be balanced by the water vapor flux through the membrane.

$$2U_m(W_{Air} - W_{Sol}) = \rho_{Salt} d_{Sol}(u_{Sol}\frac{\partial X_{Sol}}{\partial x} + v_{Sol}\frac{\partial X_{Sol}}{\partial y}) \tag{2.17}$$

where u_{Sol} and v_{Sol} are the liquid bulk mean velocity components in the x and y directions, respectively, ρ_{Salt} is the density of the pure salt, d_{Sol} is liquid channel size, and X_{Sol} is the ratio of mass of water to mass of salt in the salt solution (equation 2.9).

The energy equation for the liquid side includes the heat flux through the membrane, advection terms and latent energy change associated with the phase

change. Under steady-state operating conditions, the heat flux through the membrane surface is balanced by the net heat gain/loss by the liquid solution and the heat of phase change at any point (x, y) in the exchanger.

$$2U(T_{Air} - T_{Sol}) + 2U_m h_{fg}(W_{Air} - W_{Sol}) = (\rho c_p d)_{Sol}(u_{Sol}\frac{\partial T_{Sol}}{\partial x} + v_{Sol}\frac{\partial T_{Sol}}{\partial y}) \quad (2.18)$$

where $2U_m h_{fg}(W_{Air} - W_{Sol})$ is the heat of phase change, h_{fg} is the heat of vaporization, and c_p is the specific heat capacity of the salt solution. The correlations used to determine the salt solution properties are presented in Appendix B. The design parameters and properties of the LAMEE investigated in this thesis are provided in Table 2.1.

Table 2.1 *Design parameters of the LAMEE*

Name	Symbol	Value
Size of exchanger	$x_0 \times y_0 \times z_0$	$1 \times 0.5 \times 0.073$ m^3
Header length	x_i	0.1 m
Channel thickness, air side	d_A	4.2 mm
Channel Thickness, liquid side	d_L	2.7 mm
Number of air channels	n_A	11
Number of liquid channels	n_L	10
Membrane thickness	δ	0.2 mm
Thermal conductivity of the membrane	k	0.3 W/(m.K)
Moisture conductivity of the membrane	k_m	1.66×10^{-6} kg/(m.s)
Mass flow rate of air (NTU=10, Cr*=3)	$\dot{m}_A$	0.024 kg/s
Mass flow rate of liquid (NTU=10, Cr*=3)	$\dot{m}_L$	0.03 kg/s
Face velocity of air (NTU=10, Cr*=3)		0.55 m/s

2.3.3 Boundary Conditions

The boundary conditions required to solve the governing equations are presented in this section. To solve the flow field, uniform velocity is assumed at the inlet and outlet of each LAMEE and the velocity component in y-direction can be calculated from the liquid mass flow rate.

$$\frac{\partial \psi}{\partial x}\left(0 \le x \le x_i, y = 0\right) = -v_{Sol} = -\frac{\dot{m}_L}{\rho_L x_i d_L} \tag{2.19}$$

$$\frac{\partial \psi}{\partial x}\left(x_0 - x_i \le x \le x_0, y = y_0\right) = -v_{Sol} = -\frac{\dot{m}_L}{\rho_L x_i d_L} \tag{2.20}$$

Because there is no flow through the sidewalls of the exchanger each sidewall is a streamline. Therefore, according to the solid body boundary condition, the stream function is a constant on the walls of the LAMEE (White 2003).

$$\psi(x_i < x \le x_0, y = 0) = \text{const.} \tag{2.21}$$

$$\psi(x = x_0, y) = \text{const.} \tag{2.22}$$

$$\psi(0 \le x < x_0 - x_i, y = y_0) = \text{const.} \tag{2.23}$$

$$\psi(x = 0, y) = \text{const.} \tag{2.24}$$

To solve the coupled heat and mass transfer equations the boundary conditions applied are constant temperature and humidity ratio of the air at the inlet of the exchanger on the air side. The air side inlet is located at $x=x_0$.

$$T_{Air}\left(x = x_0, y\right) = T_{Air,in} \tag{2.25}$$

$$W_{Air}\left(x = x_0, y\right) = W_{Air,in} \tag{2.26}$$

For the liquid side, the temperature and water content of the salt solution are constant at the inlet. Thus, at liquid side inlet ($x \le x_i, y=0$)

$$T_{Sol}\left(0 \le x \le x_i, y = 0\right) = T_{Sol,in} \tag{2.27}$$

$$X_{Sol}\left(0 \le x \le x_i, y = 0\right) = X_{Sol,in} \tag{2.28}$$

The walls of the exchanger are assumed insulated and impermeable. That is, the boundary conditions at the walls are no heat flux and no mass flux. The boundary conditions are summarized as shown in Figure 2.5.

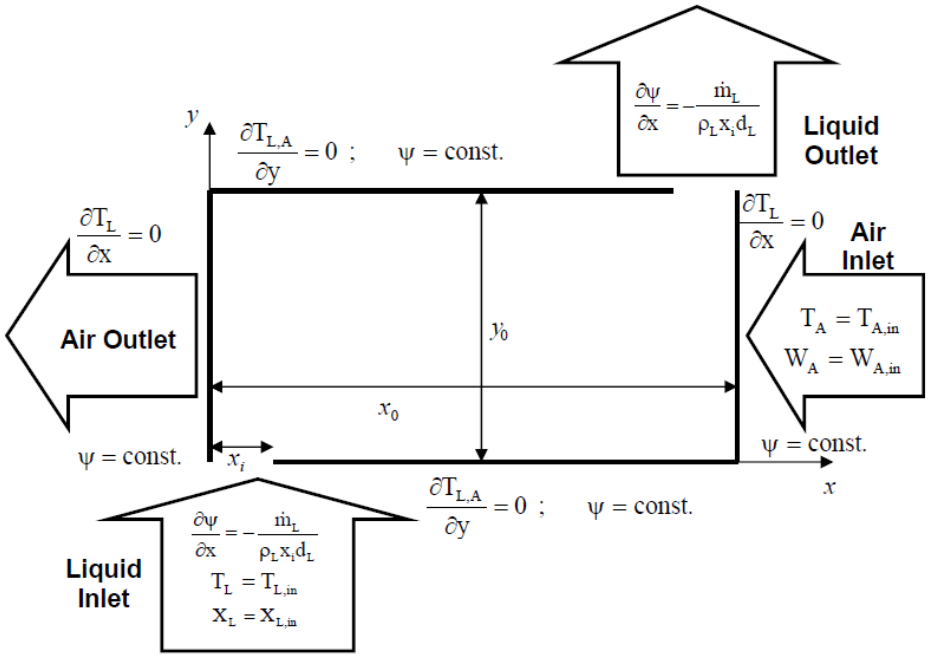

Figure 2.5 *Boundary conditions for determining the bulk liquid distribution and for solving the heat and mass transfer equations in the air and liquid streams*

2.4 Run-Around Membrane Energy Exchanger (RAMEE)

The mathematical model presented in the previous section can be used to solve the coupled heat and moisture transfer equations in each LAMEE. To model a RAMEE system, two LAMEEs are coupled in a closed loop. Additional equations are needed to determine the inlet boundary condition of each LAMEE and are presented in this section.

In this steady state model, according to assumption 9, the connecting pipes in the RAMEE system are perfectly insulated and impermeable, and heat and mass transfer occurs only between the air and the liquid in each LAMEE. Therefore, the bulk properties of liquid desiccant at the outlet of one LAMEE are the same as the inlet liquid desiccant properties for the other LAMEE in the RAMEE system. The inlet and outlet conditions of each LAMEE in a RAMEE system are given below and in Figure 2.6.

$$T_{Sol,in,S} = T_{Sol,out,E} \tag{2.29}$$

$$X_{Sol,in,S} = X_{Sol,out,E} \tag{2.30}$$

$$T_{Sol,in,E} = T_{Sol,out,S} \tag{2.31}$$

$$X_{Sol,in,E} = X_{Sol,out,S} \tag{2.32}$$

Where the subscripts S and E refer to supply and exhaust LAMEEs respectively.

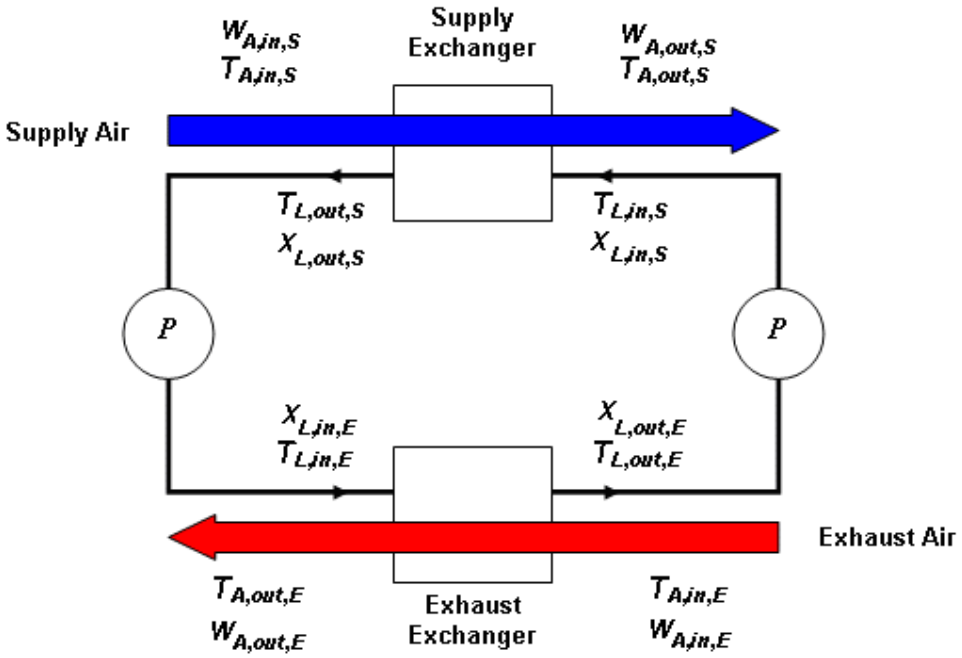

Figure 2.6 *Schematic diagram showing the inlet and outlet condition of each LAMEE in a RAMEE system*

The temperature and moisture content of the fluid streams at the outlet of each LAMEE are variable along the outlet headers. Therefore, the outlet bulk mean properties of the air and the liquid desiccant at each exchanger must be calculated to use the coupling equations (i.e. equations 2.29-2.32) and estimate the heat and moisture transfer rates in each LAMEE and the RAMEE system.

The following equations are applied to calculate the outlet bulk mean temperatures of the air and liquid salt solution in a counter/cross flow LAMEE:

$$T_{Air,out} = \frac{1}{\dot{m}_{Air} c_{pAir} y_0} \int_{y_0} \dot{m}_{Air} c_{pAir} T_{Air} dy \tag{2.33}$$

$$T_{Sol,out} = \frac{1}{\dot{m}_{Sol} c_{pSol} x_i} \int_{x_i} \dot{m}_{Sol} c_{pSol} T_{Sol} dx \tag{2.34}$$

Similarly, for a counter/cross flow LAMEE, the outlet bulk mean humidity ratio of the air and the outlet bulk mean water fraction of the liquid desiccant are estimated as follows:

$$W_{Air,out} = \frac{1}{y_0} \int_{y_0} W_{Air} dy \tag{2.35}$$

$$X_{Sol,out} = \frac{1}{x_i} \int_{x_i} X_{Sol} dx \tag{2.36}$$

As shown in Figure 2.6 the air inlet conditions are required to simulate the RAMEE system. In this thesis, AHRI summer and winter test conditions (AHRI 2005) are used mainly as the air inlet conditions of each LAMEE within a run-around system. When other operating conditions are used, they will be specified. The AHRI operating conditions are listed in Table 2.2.

Table 2.2 *AHRI Inlet Air Conditions Used in the RAMEE System Model*

Summer	$T_{Air,in,S}$	308.15 K (35°C)
	$W_{Air,in,S}$	17.5 g/kg
	$T_{Air,in,E}$	297.15 K (24°C)
	$W_{Air,in,E}$	9.3 g/kg
Winter	$T_{Air,in,S}$	274.85 K (1.7°C)
	$W_{Air,in,S}$	3.5 g/kg
	$T_{Air,in,E}$	294.15 K (21°C)
	$W_{Air,in,E}$	7.1 g/kg

2.5 Equilibrium Humidity Ratio of Aqueous Desiccant Solution

The equilibrium humidity ratio of the air in contact with salt solution at the air-solution interface is needed to solve the coupled heat and moisture transfer equations described in section 2.3.2. The humidity ratio of air can be obtained from the following equation (ASHRAE 2005):

$$W = 0.62198\frac{p_v}{P - p_v} \tag{2.37}$$

where p_v is the partial pressure of water vapor and P is the total pressure. Consequently, to determine the equilibrium humidity ratio of the salt solution, the partial water vapor pressure of the air in equilibrium with the salt solution must be known. The correlations developed by Cisternas and Lam (1991) are used to determine the vapor pressure of the salt solution.

$$\log p_v = KI[A - B/(T - E_s)] + [C - D/(T - E_s)] \tag{2.38}$$

where

$$A = A_s + 3.60591\times10^{-4}\cdot I + M_s/2303 \tag{2.39}$$

$$B = B_s + 1.382982 \cdot I - 0.031185 \cdot I^2 \quad (2.40)$$

$$C = C_s - 3.99334 \times 10^{-3} \cdot I - 1.11614 \times 10^{-4} \cdot I^2 + M_s \cdot I(1-\chi)/2303 \quad (2.41)$$

$$D = D_s - 0.138481.I + 0.027511 \cdot I^2 - 1.79277 \times 10^{-3} \cdot I^3 \quad (2.42)$$

$$\chi = 2 \cdot (\nu_+ + \nu_-)/(\nu_+ \cdot Z_+^2 + \nu_-.Z_-^2) \quad (2.43)$$

In equations (2.38)-(2.43), p_v is the vapor pressure (kPa), T is the temperature of salt solution (K), I is the ionic strength (mol/kg), M_s is the molar weight of solvent (g/mol), K is the electrolyte parameter, A_s, B_s, C_s, D_s, and E_s are solvent parameters that are constants, ν_+ is the number of moles of cation and ν_- is the number of moles of anion produced by dissociation of one mole of electrolyte, and Z_+ denotes the valency of the cation and Z_- the valency of the anion. The constants for $MgCl_2$ solution used in this study are listed in Table 2.3 (Cistrnas and Lam 1991)

Table 2.3 *The constants needed in equations (2.38)-(2.43) when the salt solution is $MgCl_2$ the solvent is water (Cistrnas and Lam 1991)*

A_s	B_s	C_s	D_s	E_s	K
-0.021302	-5.390915	7.192959	1730.2857	39.53	0.37678

Substituting the partial vapor pressure calculated from equation (2.38) into equation (2.37), the equilibrium humidity ratio of the salt solution can be determined. The equilibrium salt concentration lines for $MgCl_2$ solution on the psychometric chart are shown in Figure 2.7. As indicated in Figure 2.7, the equilibrium constant concentration lines are only shown for concentration less than or equal to 35.9% which is the saturation salt concentration of $MgCl_2$ solution. If the salt concentration is more than the saturation salt concentration, salt crystallization occurs which causes some problems in the exchanger. With deposition of the salt solution and formation of solid particles, the properties of the salt solution may not be determined correctly

from the correlations used for the liquid salt solution. Besides, the deposition of solid crystal particles on the membrane can lead to the obstruction of liquid channels and a reduction in the vapor transfer through the membrane. In this numerical model, the salt concentration of the $MgCl_2$ solution is limited to the saturation concentration and crystallization of the salt solution is not considered.

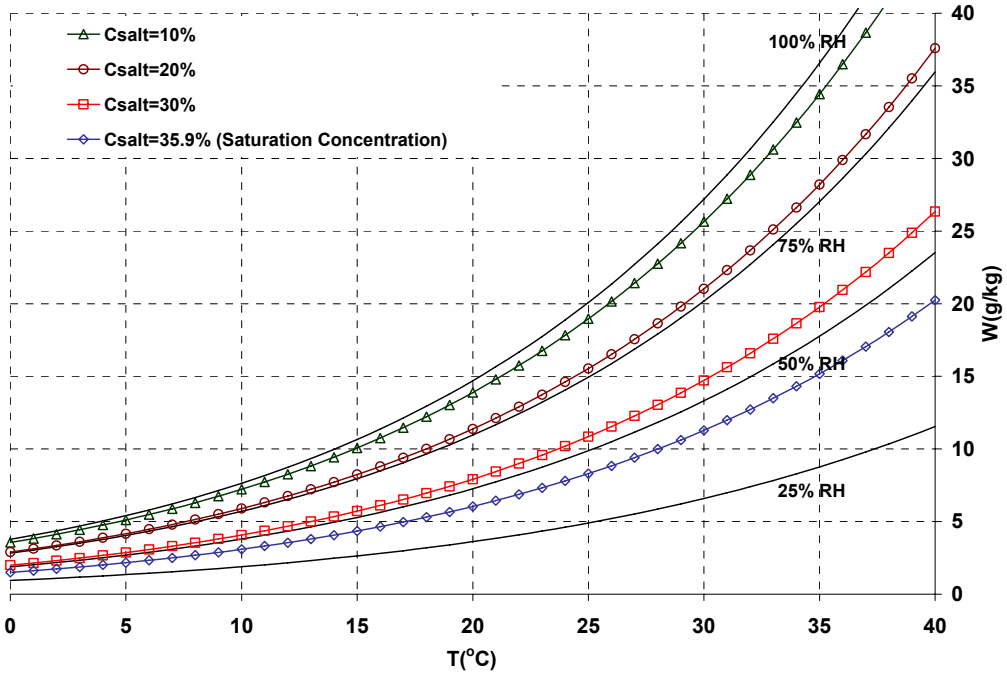

Figure 2.7 *Equilibrium salt concentration of $MgCl_2$ solution on the psychometric chart*

2.6 Numerical Solution Method

The governing equations and boundary conditions in each LAMEE are discretized using an implicit finite difference method. For both the air and the liquid streams, the backward (or upwind) differencing scheme is used and for liquid flow distribution a central differencing discretization scheme is used. A Gauss-Seidel iteration technique is used to solve the discretized equations. In this study 200×200 discrete nodes in x and y directions are used to solve the coupled heat and mass

transfer equations in each exchanger. Sensitivity studies show that the effect of increasing the number of nodes (e.g. to 300×300) on the predicted effectivenesses of the system is trivial. The sensitivity of the results to the number of spatial nodes is presented in Section 2.8.

Solving the coupled heat and mass transfer equations for each LAMEE gives the temperature and moisture content distributions in both the air and liquid salt solution. The additional equations, like those described in section 2.4, are used to couple two LAMEEs into a run-around loop.

The numerical model for the RAMEE system starts to iterate with arbitrary values for bulk properties of the liquid at the inlet of the supply exchanger ($T_{Sol,in,S}$ and $X_{Sol,in,S}$). The inlet conditions of the air streams to both supply and exhaust LAMEEs are known and constant (Table 2.1). From the numerical model for the LAMEE, the heat and moisture transfer equations are solved and the temperature and water content of the liquid are determined in the supply exchanger. The bulk mean outlet properties of the liquid at the outlet of the supply exchanger are used as the inlet conditions for the exhaust exchanger. Then, from the solution of the heat and moisture transfer equations in the exhaust exchanger, the new inlet conditions of the supply exchanger are determined. For subsequent iterations, the inlet conditions based on the previous iteration are adopted and the new outlet conditions are calculated. The numerical model keeps on iterating until it reaches steady state. Therefore, an appropriate quasi-steady state criterion is needed to determine when steady state occurs.

When the heat and moisture transfer between the RAMEE system and the surroundings are negligible (according to assumption 8), the heat and moisture transfers in both LAMEEs must be balanced. Thus at steady state, the amount of heat and moisture transferred between the air and liquid desiccant flows in the supply

exchanger must equal to the amount of heat and moisture transferred in the exhaust exchanger. Even though there is some external energy input such as the energy needed for pumping the liquid desiccant in the closed loop and the fan energy required to drive the air through the exchangers, it is very small in comparison with the energy transfer in the exchangers. Therefore, such external energy inputs are neglected in the model. As a result, the model of the RAMEE comes to the steady state conditions when

$$\begin{cases} q_S = q_E \\ m_S = m_E \end{cases} \tag{2.44}$$

where q_S, m_S , q_E, and m_E are the heat and moisture transfer rates between the liquid and the air in the supply and exhaust exchangers. Numerically, the following equations are used as steady state criteria.

$$\frac{|q_S - q_E|}{(q_S + q_E)/2} \le \lambda \tag{2.45}$$

$$\frac{|m_S - m_E|}{(m_S + m_E)/2} \le \lambda \tag{2.46}$$

where λ is the convergence criterion for the steady state condition in the model. A value of 1×10^{-3} is used for λ and the sensitivity of the results to changing convergence criterion is presented in section 2.8. The heat transfer in the supply and exhaust exchangers, respectively, is calculated from the following equations.

$$q_S = \dot{m}_{Air}(H_{A,in,S} - H_{A,out,S}) = C_{L,out,S}T_{L,out,S} - C_{L,in,S}T_{L,in,S} \tag{2.47}$$

$$q_E = \dot{m}_{Air}(H_{A,out,E} - H_{A,in,E}) = C_{L,in,E}T_{L,in,E} - C_{L,out,E}T_{L,out,E} \tag{2.48}$$

where H_A is the enthalpy of the moist air (J/kg) and is calculated using:

$$H = c_{pAir}(T - 273.15) + W(h_{fg} + c_{pW}(T - 273.15)) \tag{2.49}$$

ASHRAE 2005 simplifies equation (2.49) as follows.

$$H = 1006t + W\left(2.5\times10^{6} + 1805t\right) \tag{2.50}$$

where t is the air temperature in Celsius. Equation (2.50) is used in the model to determine the enthalpy of the moist air. The moisture transfer in the supply and exhaust LAMEEs can be determined from the following equations, respectively.

$$m_S = \dot{m}_{Salt}\left(X_{L,out,S} - X_{L,in,S}\right) = \dot{m}_{Air}\left(W_{A,in,S} - W_{A,out,S}\right) \tag{2.51}$$

$$m_E = \dot{m}_{Salt}\left(X_{L,in,E} - X_{L,out,E}\right) = \dot{m}_{Air}\left(W_{A,out,E} - W_{A,in,E}\right) \tag{2.52}$$

The detailed algorithm and the computer program in Visual Fortran for the RAMEE system are presented in Appendix C.

2.7 Dimensionless Parameters

The dimensional analysis used in this study is divided into two categories. The first group contains the dimensionless parameters used to investigate the effect of design characteristics, and the second category is applied for presenting the performance of the RAMEE system.

2.7.1 Design Dimensionless Groups

To analyze a RAMEE system with two counter/cross flow LAMEEs, the following dimensionless groups are used.

1. $NTU = \dfrac{2Ux_0y_0}{C_{min}}$ = the number of heat transfer units

2. $NTU_m = \dfrac{2U_m x_0 y_0}{\dot{m}_{min}}$ = the number of mass transfer units

3. $Cr^* = \dfrac{C_{Sol}}{C_{Air}}$ = the heat capacity ratio of the two fluids

4. $m^* = \dfrac{\dot{m}_{Salt}}{\dot{m}_{Air}}$ = mass flow rates ratio of the pure salt in the solution to the dry air

5. $\frac{y_0}{x_0}$ = the aspect ratio of the heat and moisture exchanger defined as the ratio of height to length of the exchanger (Figure 2.5)

6. $\frac{x_i}{x_0}$ = entrance length ratio which is the ratio of the length of the inlet and outlet headers to the length of the exchanger (Figure 2.5)

2.7.2 Effectiveness

Effectiveness is a dimensionless performance criterion which is widely applied as the best means to characterize, design and investigate the performance of most types of heat exchangers (Simonson and Besant 1999a). The classical definition of effectiveness is the ratio of actual heat transfer rate to the maximum possible heat transfer rate in an exchanger with infinite heat transfer surface area having the same inlet operating conditions as the actual one. This definition of the effectiveness can be extended to moisture (or latent energy) transfer and total energy (or enthalpy) transfer.

The inlet and outlet conditions of the RAMEE system under the steady state condition, as shown in Figure 2.8, are used to determine the overall effectiveness. The overall sensible effectiveness of the RAMEE system when the mass flow rates in both exchangers are equal ($\dot{m}_{Air,S} = \dot{m}_{Air,E}$) is calculated from the following equation

$$\varepsilon_{o,s} = \frac{T_{A,in,S} - T_{A,out,S}}{T_{A,in,S} - T_{A,in,E}} = \frac{T_{A,out,E} - T_{A,in,E}}{T_{A,in,S} - T_{A,in,E}} \tag{2.53}$$

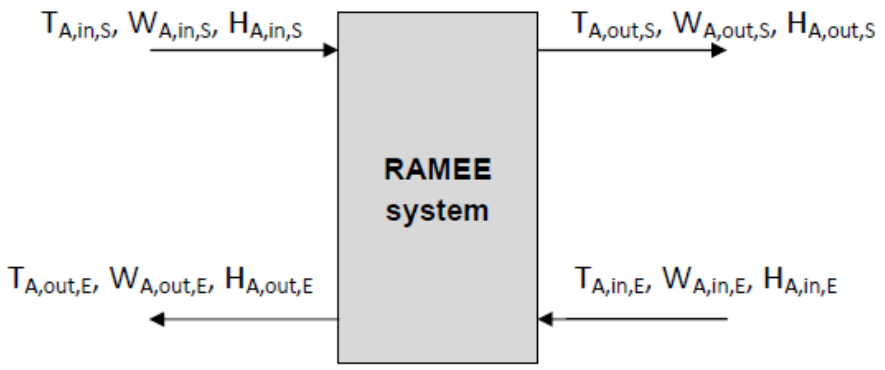

Figure 2.8 *Schematic diagram showing the inlet and outlet of the air streams in a RAMEE system*

The overall latent effectiveness as the dimensionless moisture transfer rate of the RAMEE system can be expressed as the ratio of the actual moisture transfer to the maximum possible moisture transfer under the same operating conditions with an infinite moisture transfer surface area.

$$\varepsilon_{o,l} = \frac{W_{A,in,S} - W_{A,out,S}}{W_{A,in,S} - W_{A,in,E}} = \frac{W_{A,out,E} - W_{A,in,E}}{W_{A,in,S} - W_{A,in,E}} \tag{2.54}$$

Eventually, the overall total effectiveness (dimensionless energy transfer rate) of the RAMEE system is calculated from following equation

$$\varepsilon_{o,t} = \frac{H_{A,in,S} - H_{A,out,S}}{H_{A,in,S} - H_{A,in,E}} = \frac{H_{A,out,E} - H_{A,in,E}}{H_{A,in,S} - H_{A,in,E}} \tag{2.55}$$

2.8 Numerical Accuracy

The accuracy of the effectivenesses calculated by the numerical model of the RAMEE system is related to the number of spatial nodes in the computation domain and the accuracy of the energy and mass balance in the supply and exhaust exchangers. In this section, the AHRI summer operating conditions listed in Table 2.2 are used and the system parameters are given in Table 2.1.

The sensitivity of the predicted overall effectiveness of the system to the number of spatial nodes is defined as:

$$\Delta\varepsilon_o = \left|\varepsilon_o - \varepsilon_{o,\text{Smallest number of nodes}}\right| \tag{2.56}$$

where ε_o is the overall effectiveness of the RAMEE system. The results are presented in Figure 2.9.

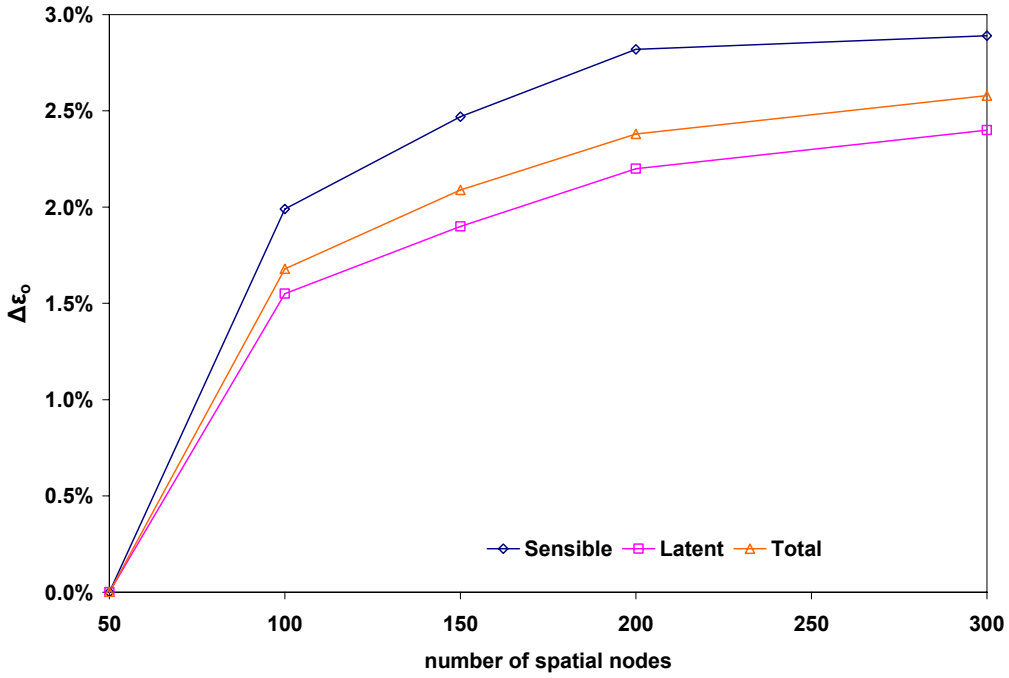

Figure 2.9 *Effect of the number of spatial nodes on the predicted effectiveness of a RAMEE system at AHRI summer test conditions.*

The results in Figure 2.9 are calculated with the energy and mass balance convergence criterion of $\lambda=10^{-3}$ (see equations (2.45) and (2.46)). Figure 2.9 shows that increasing the number of spatial nodes from 200 to 300 has little effect on the effectiveness (i.e. less than 0.2%). In selecting the appropriate number of spatial nodes, the computation time must be taken into account. Increasing the number of nodes from 200 to 300 increases the computation time by a factor of 4. Therefore, 200

spatial nodes are used to solve the coupled heat and moisture transfer equations in this thesis.

As mentioned in section 2.7, the numerical model comes to a quasi-steady state condition when both equations (2.45) and (2.46) are satisfied. The value of λ, the convergence criterion defined by equations (2.45) and (2.46), can affect the numerical results. Consequently, the accuracy of the numerical results is also attributed to λ. The sensitivity of the predicted effectivenesses to different λ values is defined as:

$$\Delta\varepsilon_o = \left|\varepsilon_o - \varepsilon_{o,\text{largest convergence criterion}}\right| \tag{2.57}$$

where ε_o is the overall effectiveness of the RAMEE system. The results are presented in Figure 2.10.

The results presented in Figure 2.10 are calculated with 200 spatial nodes. Reducing the energy and mass balance criterion (λ) from 10^{-3} to 10^{-4} does not change the result significantly, but it increases the solution time by the factor of 2.5. Therefore, $\lambda=10^{-3}$ is used as the convergence criterion in this thesis.

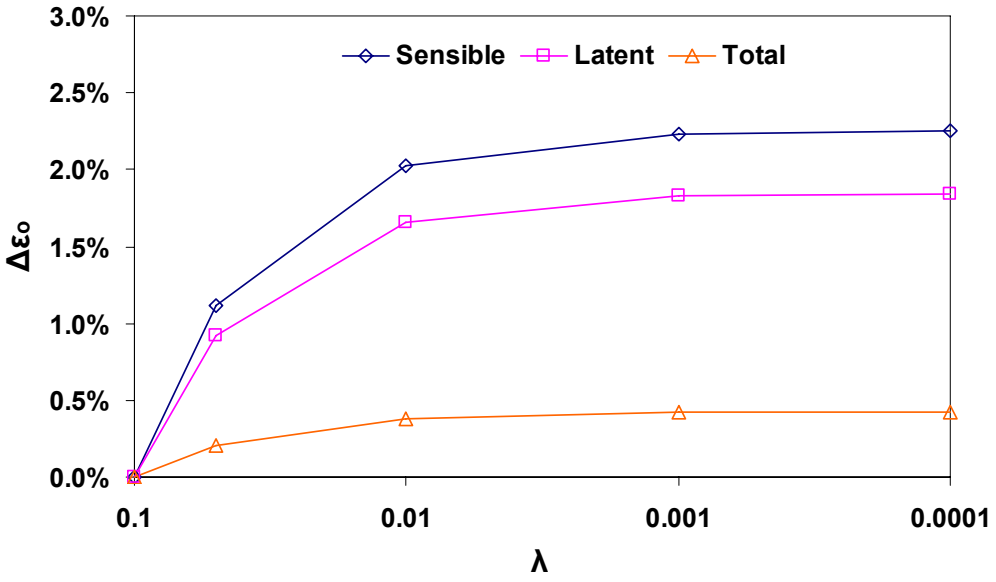

Figure 2.10 *Effect of the energy and mass balance convergence criteria, λ, on the predicted effectiveness of a RAMEE system at AHRI summer test conditions.*

2.9 Sensitivity Studies

In this section, the effects of some parameters and certain assumptions on the numerically predicted performance of a RAMEE system are investigated. By analyzing the sensitivity of the numerical results to the parameters and assumptions, the uncertainty in predicted effectivenesses can be estimated.

The parameters investigated in this chapter are the thermal conductivity of the membrane, membrane permeability, and thickness of the membrane. The LAMEE parameters listed in Table 2.1 and AHRI summer operating conditions given in Table 2.2 are used in this section. The sensitivity of the numerical results is presented as the changes in the effectiveness values with the change in various parameters.

2.9.1 Thermal Conductivity of the Semi-Permeable Membrane

Equation (2.13) shows that the overall heat transfer coefficient of the exchanger depends on the thermal conductivity of the semi-permeable membrane. Similarly, NTU is a function of overall heat transfer coefficient. An exchanger with greater overall heat transfer coefficient has greater value of NTU (i.e. greater heat transfer rate per unit of area) and as a result higher effectiveness, $\varepsilon = f(\mathrm{NTU}, \mathrm{Cr}^*)$. Thus, NTU and overall effectiveness of the RAMEE system depend on the thermal conductivity of the membrane. In this section the sensitivity of the predicted overall effectiveness of the RAMEE system to variations in the membrane thermal conductivity is studied. The fact that the value used in the model for thermal conductivity has a large uncertainty makes this study more critical to evaluate the predicted results.

According to equation (2.13), the overall heat transfer coefficient is also a function of convective heat transfer coefficient of the air and the liquid desiccant flows. The order of convective heat transfer resistance (1/h) of the two fluid flows in

equation (2.13) is much greater than the thermal resistance of the membrane (δ/k). Consequently, it is expected that the variation of the thermal conductivity of the membrane does not affect the numerical results significantly.

The effects of changing the thermal conductivity of the membrane on the overall sensible effectiveness of the RAMEE system are presented in Figure 2.11 in the form of effectiveness difference,

$$\Delta\varepsilon_{o,s} = \varepsilon_{o,s}(k \pm \varphi_k) - \varepsilon_{o,s}(k) \tag{2.56}$$

Variations of $\Delta\varepsilon_{o,s}$ are shown in Figure 2.11 with the change in Cr*. As shown, changing the thermal conductivity of the membrane by a factor of 2 changes the overall sensible effectiveness $\Delta\varepsilon_{o,s}$ only within ±0.12%.

Increasing the thermal conductivity of the membrane increases the heat flux through the membrane and increases the overall sensible effectiveness of the system. However, the maximum $\Delta\varepsilon_{o,s}$ is about 0.06%. On the contrary, the sensible heat transfer in the system will be reduced as the thermal conductivity of the membrane decreases. As shown, the effectiveness reduction is quite small. The effects of the variation of thermal conductivity on the overall latent effectiveness are very small and not presented.

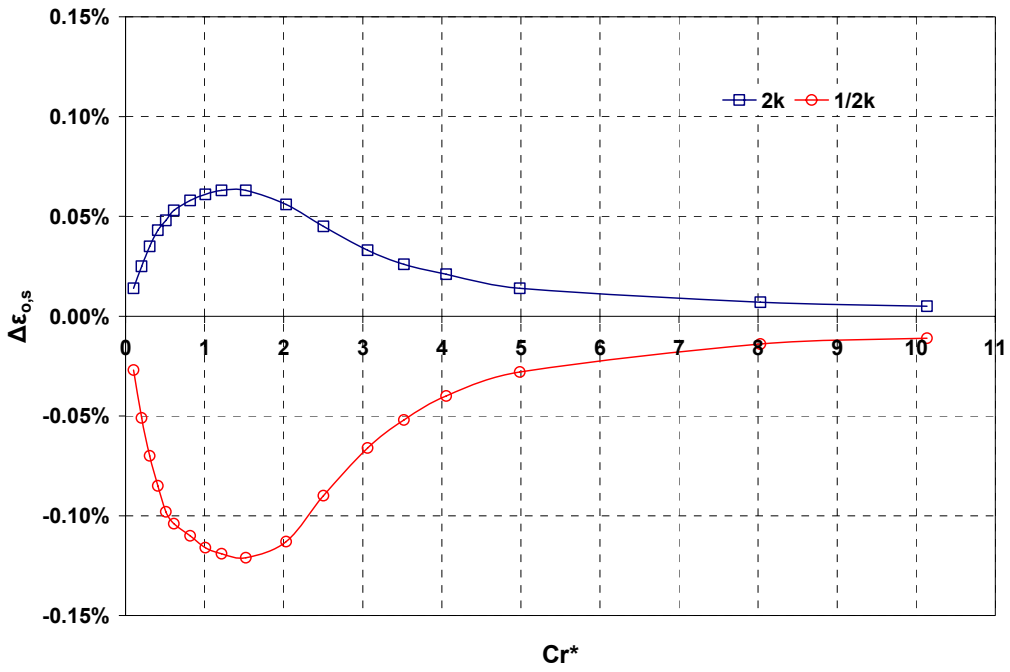

Figure 2.11 *Change in the predicted overall sensible effectiveness of the RAMEE system versus Cr* as a result of membrane thermal conductivity variation* $[\Delta\varepsilon_{o,s} = \varepsilon_{o,s}(k \pm \varphi_k) - \varepsilon_{o,s}(k)]$ *when NTU=10,* y_0/x_0*=0.5 and* x_i/x_0*=0.1 for AHRI summer condition*

2.9.2 Mass Conductivity of the Semi-Permeable Membrane (Permeability)

The overall mass transfer coefficient, U_m, defined with equation (2.10) is directly affected by the mass conductivity, also known as the membrane permeability, k_m. Because the effectiveness of the RAMEE system depends on NTU_m, which is the non-dimensional parameter for U_m, the predicted effectiveness of the system is affected by the permeability of the membrane. As mentioned previously, the value of $k_m=1.66\times10^{-6}$ kg/(m·s), which was measured and reported by Larson (2006) for Propore, is applied for permeability in the model. The uncertainty associated with this measurement was estimated as $\varphi_{km}= \pm\ 3.5\times10^{-7}$ kg/(m·s) which is approximately ±20% of the measured value and is reasonably large (Larson 2006). Thus, the effects of the change in permeability on the predicted results need to be addressed.

As the membrane permeability affects the overall mass transfer coefficients, it mostly influences the moisture transfer in the RAMEE system. The variations of the overall latent effectiveness of the RAMEE system with the heat capacity ratio (Cr*) and the uncertainty of the permeability are illustrated in Figure 2.12.

As revealed by Figure 2.12, the change in predicted effectiveness, in the form of

$$\Delta\varepsilon_{o,l} = \varepsilon_{o,l}\left(k_m \pm \varphi_{k_m}\right) - \varepsilon_{o,l}\left(k_m\right) \tag{2.57}$$

is greater than zero and can be as high as 2.2% when k_m increases by the maximum uncertainty $\varphi_{km}= 3.5\times10^{-7}$ value. Conversely, $\Delta\varepsilon_{o,l}$ are less than zero and can be as low as -3% when k_m decreases by the maximum uncertainty $\varphi_{km}= -3.5\times10^{-7}$ value. This can be explained as increasing or decreasing the permeability of the membrane results in higher or lower mass flux through the membrane and consequently higher or lower overall latent effectiveness of the system.

According to Figure 2.12, $\Delta\varepsilon_{o,l}$ values change almost linearly with Cr* for $Cr^*\leq3$ at a given permeability. The maximum change occurs when $Cr^*\approx3$, and when $3<Cr^*<10$, the uncertainty in effectiveness ($\Delta\varepsilon_{o,l}$) is almost at its maximum with $\Delta\varepsilon_{o,l}\approx2.2\%$ or -3%. That is, for higher Cr* ($Cr^*>3$) the predicted overall latent effectiveness of the RAMEE system is quite sensitive to changes of the permeability of the membrane. The overall sensible effectiveness ($\Delta\varepsilon_{o,s}$) of the RAMEE system is also affected by the variation of the membrane permeability. As the permeability changes by $\pm3.5\times10^{-7}$ kg/(m.s), the overall sensible effectiveness changes up to ±1.5% (not presented graphically).

Unlike thermal conductivity, the permeability of the membrane impacts the overall effectiveness of the RAMEE system fairly significantly, which should be considered during data analysis and interpretation.

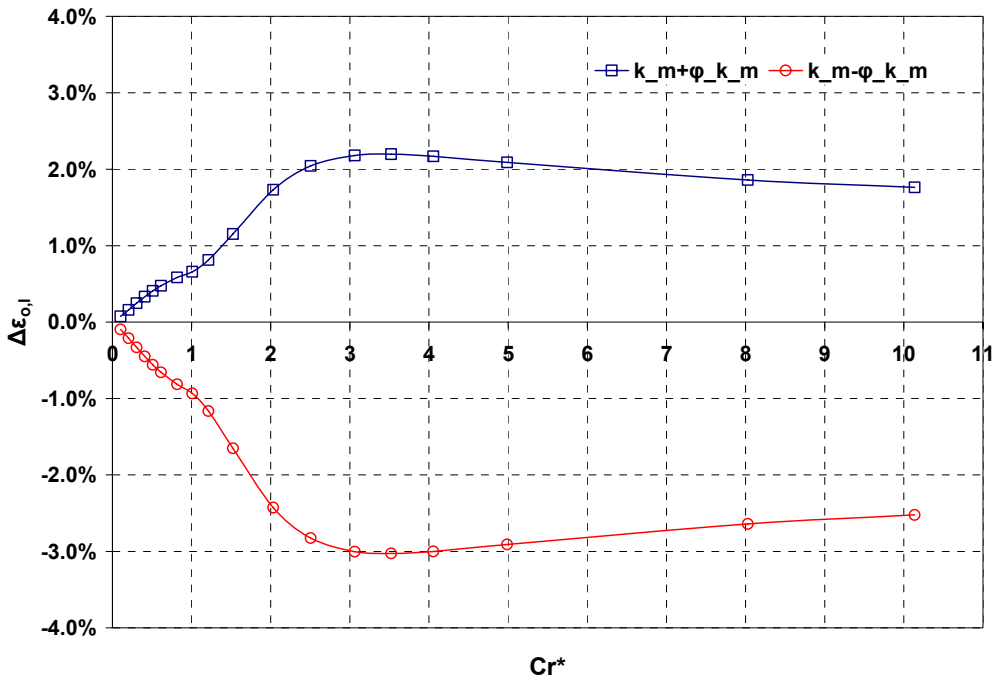

Figure 2.12 *Change of predicted overall latent effectiveness of the RAMEE system versus Cr* as a result of membrane permeability variation* $[\Delta\varepsilon_{o,l} = \varepsilon_{o,l}(k_m \pm \varphi_{k_m}) - \varepsilon_{o,l}(k_m)]$ *when NTU=10,* y_0/x_0*=0.5 and* x_i/x_0*=0.1 for AHRI summer condition*

2.9.2 Thickness of the Semi-Permeable Membrane

Another parameter that has impact on the overall mass transfer coefficient and the number of mass transfer units is the thickness, δ, of the membrane. As the membrane thickness increases, the mass transfer resistance of the semi-permeable membrane increases. This reduces the overall mass transfer coefficient and the number of mass transfer units in the exchanger. Consequently, the overall latent effectiveness of the RAMEE system decreases as the membrane thickness increases. Conversely, a membrane with lower thickness results in higher overall latent effectiveness. The membrane thickness used in this study (i.e. δ=0.2 mm) is based on measurement with an associated uncertainty. The thickness of the membrane when it is compressed is 0.2 mm, but it can be measured up to 0.5 mm. The corresponding

change ($\Delta\varepsilon_o$) of the predicted overall sensible, latent and total effectiveness of the RAMEE system as the membrane thickness (δ) changes from 0.2 mm to 0.5 mm is depicted in Figure 2.13 as a function of Cr*.

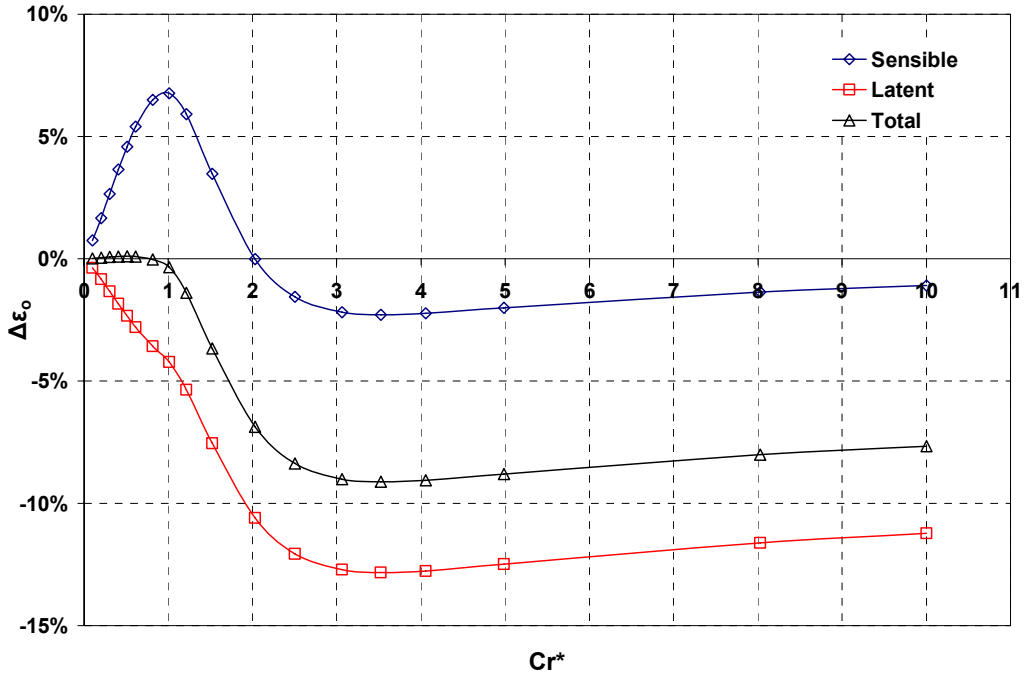

Figure 2.13 *Change of predicted overall effectiveness of the RAMEE system versus Cr* as a result of membrane thickness variation from δ=0.2 mm to δ=0.5 mm* $[\Delta\varepsilon_o = \varepsilon_o(\delta = 0.5\text{mm}) - \varepsilon_o(\delta = 0.2\text{mm})]$ *when NTU=10, y_0/x_0=0.5 and x_i/x_0=0.1 for AHRI summer condition*

As indicated in Figure 2.13, the $\Delta\varepsilon_o$ values increase or decrease depending on the Cr* values applied in the model. The overall latent effectiveness of the RAMEE system decreases when a thicker (0.5 mm) semi-permeable membrane is used as $\Delta\varepsilon_{o,l}<0$. The maximum reduction of the overall latent effectiveness of the RAMEE system (at Cr*≈3) is approximately 13% which is significant. The overall sensible and total effectiveness of the RAMEE system are also reduced by 2% and 9%, respectively, when Cr*≈3 as the membrane thickness increases to 0.5 mm, which are not shown graphically.

2.10 Summary

In this chapter, a numerical model that is used to simulate the heat and moisture transfer in a RAMEE system with two counter/cross flow exchangers has been developed. The assumptions, governing equations, boundary conditions and numerical solution method are explained in detail. The model is two-dimensional and steady state. A finite difference method is used to solve the governing equations.

The model solves the fluid flow distribution to determine the bulk mean velocity of the liquid desiccant in the exchangers. As the liquid flow is pressure driven, the continuity and momentum equations are solved independently of the temperature and concentration distribution. The coupled heat and mass transfer governing equations are solved to determine the temperature and moisture content distributions of each fluid flow in a LAMEE. In this model, the convective heat and moisture transfer in fluid flows and water vapor phase change are taken into account. The energy released from the phase change is assumed to be entirely delivered to the liquid flow. The fluid properties at the outlet of each LAMEE are calculated by averaging the local properties and are used to couple the two LAMEEs in a closed loop to simulate a RAMEE system. The outlet air properties under steady-state conditions are used to predict the overall sensible, latent and total energy effectivenesses of the RAMEE system.

Several dimensionless parameters are defined to predict the performance of the RAMEE system under different operating conditions and to investigate the effect of different design characteristics on the performance of the system. The dimensionless parameters enable the numerical results to be used for similar designs which have the same dimensionless variables.

The numerical accuracy of the predicted effectiveness based on grid size and convergence criteria is less than 0.2%. The uncertainty of the numerical results is estimated by investigating the effects of some input data uncertainties that were measured. It is shown that changing the thermal conductivity of the membrane does not impact the performance of the RAMEE system substantially because the overall sensible effectiveness changes by only ±0.12% at the maximum. The predicted effectivenesses of the system are more sensitive to variations in the permeability and thickness of the membrane. The change of the permeability in the range of its measurement uncertainty results in up to ±3% change for overall latent effectiveness and up to ±1.5% change for overall sensible effectiveness of the RAMEE system. The change of the membrane thickness from 0.2 mm to 0.5 mm (which represents the thickness of the membrane when no pressure is applied with the caliper) reduces the overall sensible, latent, and total effectiveness of the RAMEE system by up to 2%, 13% and 9%, respectively. The impacts of the uncertainties for the permeability and thickness of the membrane on the numerical results are quite important, and must be taken in to account in the data analysis.

Chapter 3

Validation and Effectiveness Correlations for Heat Recovery Systems

3.1 Introduction

Numerical data can be correlated into functional relationships for convenience and accurate engineering design when the numerical model has been developed based on accurate mathematical equations. In addition, the assumptions and constraints applied should have a small impact on the predicted results. Finally, the numerical results have to be validated with valid experimental, analytical or other numerical data. Numerical data has been used previously in order to generate useful correlations for design purposes. Simonson and Besant (1999b) used results from a numerical model which was validated with experimental data and developed correlations for the sensible, latent and total effectivenesses of energy wheels. The same method is used in this study to generate performance correlations for counter/cross flow heat exchanger and heat recovery systems (exchanges only sensible energy) made of two counter/cross flow heat exchangers.

The purpose of this chapter is to validate the numerical model presented in Chapter 2 for the case of only heat transfer using the well known effectiveness correlations presented in Incropera and Dewitt (2002). This comparison is performed for a single purely cross-flow heat exchanger and a purely counter-flow heat exchanger. The numerically predicted overall sensible effectiveness of the run-around heat exchanger (RAHE) is also validated with the analytical equations based on Zeng (1990). Effectiveness correlations are also developed for the RAHE with two counter/cross flow heat exchangers.

3.2 Verification of the Model

In this section, the accuracy of the model is verified for the case of no moisture transfer and only heat or sensible energy transfer in a single exchanger and a run-around system.

3.2.1 Heat Exchanger

Because the energy equation (equation (2.16)) on the liquid side contains the advection terms in both the x and the y directions, the model is able to study heat transfer in heat exchangers with cross-flow, counter-flow or counter/cross flow arrangements. Incropera and Dewitt (2002) provide correlations and analytical solutions for determining the effectiveness of heat exchangers in the following form.

$$\varepsilon = f\left(\mathrm{NTU}, \mathrm{Cr}, \text{Flow Arrangement}\right) \tag{3.1}$$

Where $\mathrm{NTU}=\mathrm{UA}/\mathrm{C_{min}}$ is the number of heat transfer units and $\mathrm{Cr}=\mathrm{C_{min}}/\mathrm{C_{max}}$ is the heat capacity rate ratio of two fluids.

The effectiveness of cross-flow heat exchangers with both fluids unmixed can be calculated from the following correlation (Incropera and Dewitt 2002):

$$\varepsilon_{\mathrm{cross}} = 1 - \exp\left[\left(\frac{1}{\mathrm{Cr}}\right)\left(\mathrm{NTU}\right)^{0.22}\left\{\exp\left[-\mathrm{Cr}\left(\mathrm{NTU}\right)^{0.78}\right]-1\right\}\right] \tag{3.2}$$

For a counter-flow heat exchanger, the effectiveness can be determined from the following analytical solution (Incropera and Dewitt 2002):

$$\varepsilon_{\mathrm{counter}} = \frac{1-\exp\left(-\mathrm{NTU}\left(1-\mathrm{Cr}\right)\right)}{1-\mathrm{Cr}\exp\left(-\mathrm{NTU}\left(1-\mathrm{Cr}\right)\right)} \tag{3.3}$$

In Figure 3.1, the sensible effectivenesses of a cross-flow heat exchanger and a counter-flow heat exchanger calculated by the present numerical model for over 160 simulated cases are compared with the effectiveness values from equations (3.2) and (3.3). In Figure 3.1, when the simulation and the effectiveness equations predict

exactly the same values for the effectiveness the simulated data point must be on the solid line which referred as exact. The dash lines show the region where the discrepancy between the simulation and the effectiveness equations is within ±2%. That is, the simulated data points for the effectiveness in this region differ from predicted values from equations (3.2) and (3.3) with up to ±2%. The difference between the computed values and correlations lies within ±0.02 for $0<Cr\leq 1$ and $0<NTU\leq 15$.

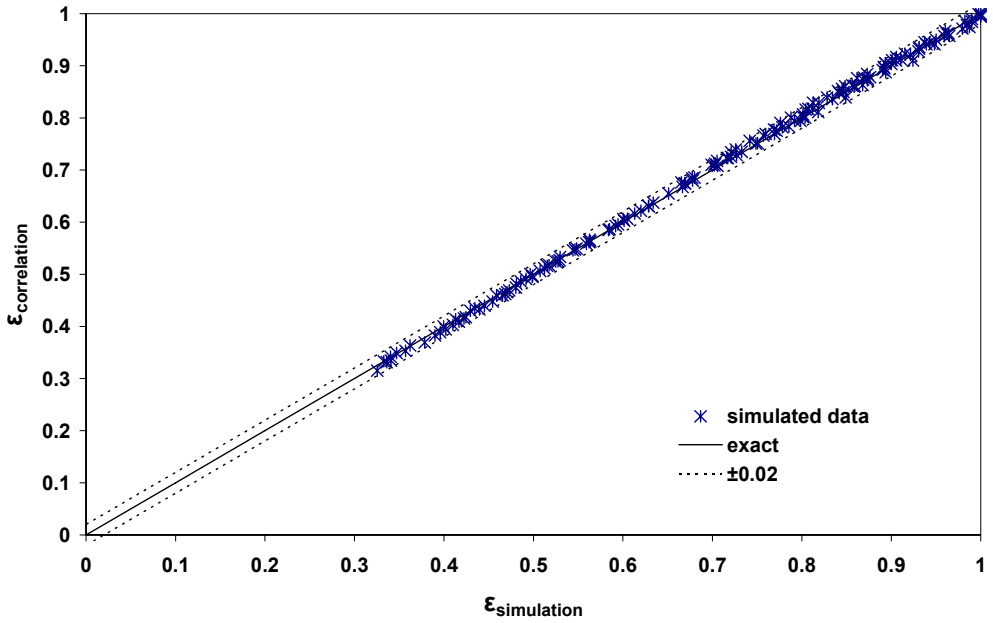

Figure 3.1 *Effectiveness of flat-plate cross-flow and counter-flow heat exchangers determined from correlations in the literature (equations (3.2) and (3.3)) compared to the simulated effectiveness for range of $0<Cr\leq 1$ and $0<NTU\leq 15$*

3.2.2 Run-Around Heat Exchanger (RAHE)

In this section, equations developed by Zeng (1990) for a run-around heat exchanger (RAHE) will be used to verify the present numerical model for a RAHE with two cross-flow or two counter-flow heat exchangers. Zeng (1990) showed that the overall effectiveness of the RAHE was a function of the effectiveness of the

individual exchangers (ε_S and ε_E) and the thermal capacity of the air and liquid streams in each exchanger.

The functional relationship can be written as follows.

$$\frac{1}{\varepsilon_o} = \frac{C_{min,A}}{\varepsilon_E . C_{min,E}} + \frac{C_{min,A}}{\varepsilon_S . C_{min,S}} - \frac{C_{min,A}}{C_L} \tag{3.4}$$

For a RAHE made of two identical heat exchangers, which is the focus of this section, equation (3.4) can be simplified as follows.

For $C_A \leq C_L$,

$$\frac{1}{\varepsilon_o} = \frac{1}{\varepsilon_E} + \frac{1}{\varepsilon_S} - Cr \tag{3.5}$$

And for $C_A > C_L$,

$$\frac{1}{\varepsilon_o} = \frac{1}{Cr}\left(\frac{1}{\varepsilon_E} + \frac{1}{\varepsilon_S} - 1\right) \tag{3.6}$$

where ε_o is the overall sensible effectiveness of the system, ε_E and ε_S are the effectiveness of exhaust and supply heat exchangers respectively and Cr ($Cr = C_{min}/C_{max}$) is the thermal capacity rate ratio.

A comparison of the sensible effectiveness data obtained from equations (3.5) and (3.6) with the results from the numerical model is shown in Figure 3.2. The effectivenesses of the RAHE with two identical cross-flow or counter-flow heat exchangers calculated from the correlation (equations (3.5) and (3.6)) agrees with the simulated effectiveness within ±0.025 for $0 < Cr \leq 1$ and $0 < NTU \leq 15$ for over 350 simulated data points.

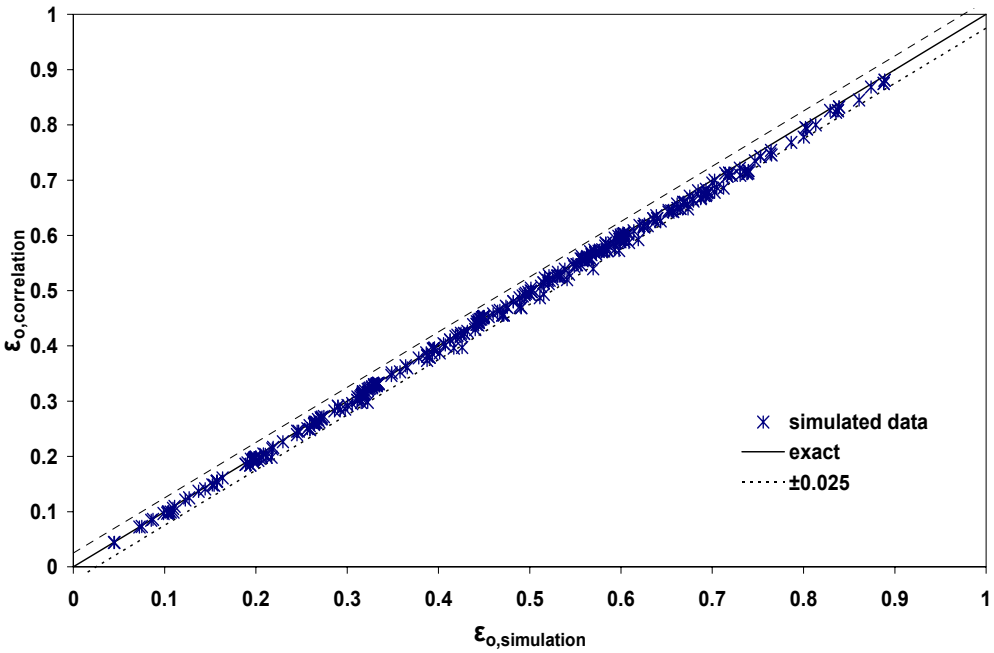

Figure 3.2 *Overall sensible effectiveness of the RAHE with two identical flat-plate cross-flow or counter-flow heat exchangers correlated by equations (3.5) and (3.6) compared to the simulated effectiveness for range of $0<Cr\leq1$ and $0<NTU\leq15$*

3.3 Effectiveness Correlations

In this section, the numerical model, which was developed in Chapter 2 and validated for the case of heat transfer in the previous sections, is used to generate effectiveness data and develop effectiveness correlations for counter/cross-heat exchangers and RAHE made with two identical counter/cross flow heat exchangers.

3.3.1 Counter/Cross Flow Heat Exchanger

The effectiveness of a counter/cross flow flat-plate heat exchanger is a function of NTU (number of heat transfer units), Cr (heat capacity ratio of two unmixed fluids), and some characteristic dimensionless length ratios of the heat exchanger. These include the aspect ratio (y_0/x_0) of the exchanger and the ratio of the

length of the inlet and outlet headers to the length of the heat exchanger (entrance ratio, x_i/x_0). The functional relationship is:

$$\varepsilon_{counter/cross} = f\left(NTU, Cr, \frac{x_i}{x_0}, \frac{y_0}{x_0} \right) \tag{3.7}$$

where $Cr=C_{min}/C_{max}$ is the heat capacity ratio of the two fluids

From sensitivity studies it is found that the effect of the entrance ratio (x_i/x_0) on the effectiveness of the counter/cross flow heat exchanger is minor for a range of $0<x_i/x_0\leq 0.25$. For example with NTU=3, Cr=1 and $y_0/x_0=0.25$ the computed effectiveness of the heat exchanger changes by less than 2% as x_i/x_0 increases from 0 to 0.25. It is expected that the performance of a counter/cross flow heat exchanger will decrease with increasing the entrance ratio. Thus, the dependence of $\varepsilon_{counter/cross}$ on x_i/x_0 can be neglected and the calculation of $\varepsilon_{counter/cross}$ will not include x_i/x_0.

It is expected, for the same total heat transfer surface area, the effectiveness of counter/cross flow heat exchangers ($\varepsilon_{counter/cross}$) will fall between the effectiveness of pure counter-flow exchangers ($\varepsilon_{counter}$) and pure cross-flow exchangers (ε_{cross}). Furthermore, for small aspect ratios (y_0/x_0), $\varepsilon_{counter/cross}$ will approach $\varepsilon_{counter}$ while as y_0/x_0 approaches 1, $\varepsilon_{counter/cross}$ will approach ε_{cross}. Considering this and the effectiveness data from numerous simulations, the effectiveness correlation of a counter/cross flow exchanger ($\varepsilon_{counter/cross}$) is proposed as follows.

$$\varepsilon_{counter/cross} = \left[\left(\frac{y_0}{x_0} \right) \left(1 + \frac{NTU}{200} \right) \varepsilon_{cross} + \left(1 - \frac{y_0}{x_0} \right) \varepsilon_{counter} \right] \tag{3.8}$$

In this correlation, $\varepsilon_{counter/cross}$ is calculated directly by knowing the aspect ratio of the exchanger and the effectiveness of a cross-flow heat exchanger and a counter-flow heat exchanger with the same NTU and Cr values. ε_{cross} and $\varepsilon_{counter}$ are obtained

from equations (3.2) and (3.3), respectively. This correlation can be used for a range of parameters $0<y_0/x_0\leq 1$ and $0<x_i/x_0\leq 0.25$.

In Figure 3.3, the effectivenesses of the counter/cross- flow heat exchanger calculated using equation (3.8) are compared to the effectivenesses determined from more than 200 simulation cases. Figure 3.3 shows that the values from equation (3.8) agrees with over 200 simulated data points within ±0.02 for $0<Cr\leq 1$, $0.5\leq NTU\leq 15$, $0<x_i/x_0\leq 0.25$ and $0<y_0/x_0\leq 1$.

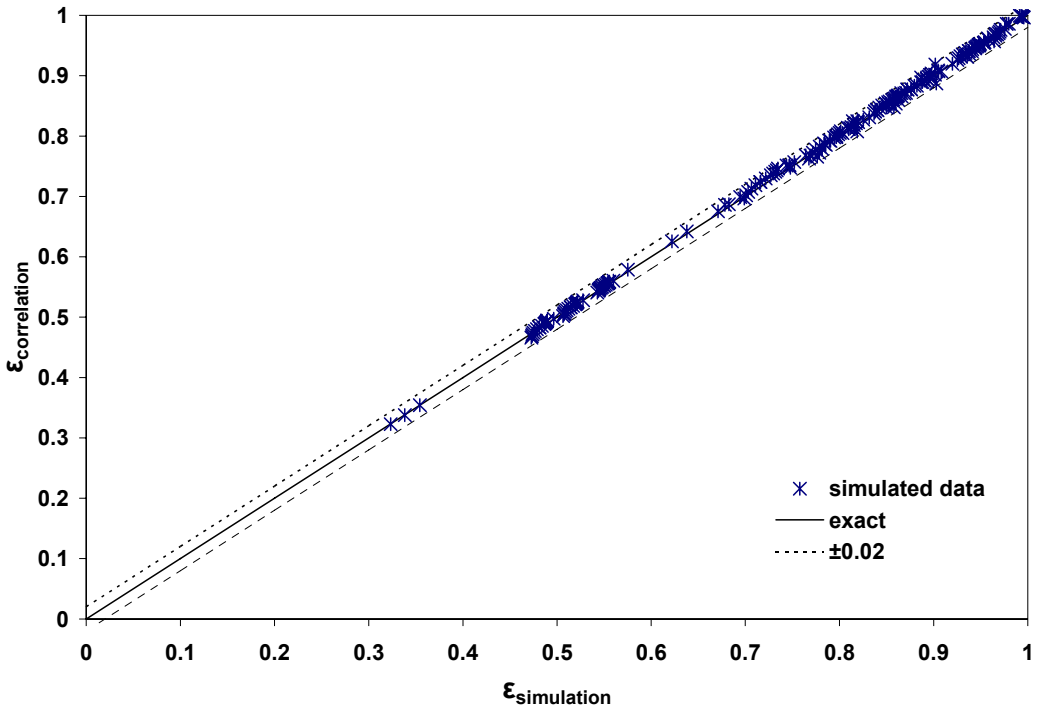

Figure 3.3 *Effectiveness of the counter/cross flow heat exchanger calculated using correlations (equation (3.8)) compared to the simulated effectiveness for range of* $0<Cr\leq 1$, $0<NTU\leq 15$, $0<x_i/x_0\leq 0.25$ *and* $0<y_0/x_0\leq 1$

3.3.2 Run-Around Heat Exchangers (RAHE)

As indicated in Figure 3.2, the equations of Zeng (1990) show good agreement with the simulation data for RAHEs using two identical cross-flow heat exchangers or two identical counter-flow heat exchangers. A comparison between the simulation

and the data from equations (3.5) and (3.6) where the effectiveness of the individual counter/cross flow heat exchangers are calculated using the new correlation, equation (3.8), is presented in Figure 3.4. As it can be seen, the correlated data for the effectiveness of the RAHE with two counter/cross flow heat exchangers agree with over 400 simulated data point within ±0.02 for $0<C_L/C_A\leq 10$, $0<Cr\leq 1$, $0<NTU\leq 15$, $0<x_i/x_0\leq 0.25$ and $0<y_0/x_0\leq 1$.

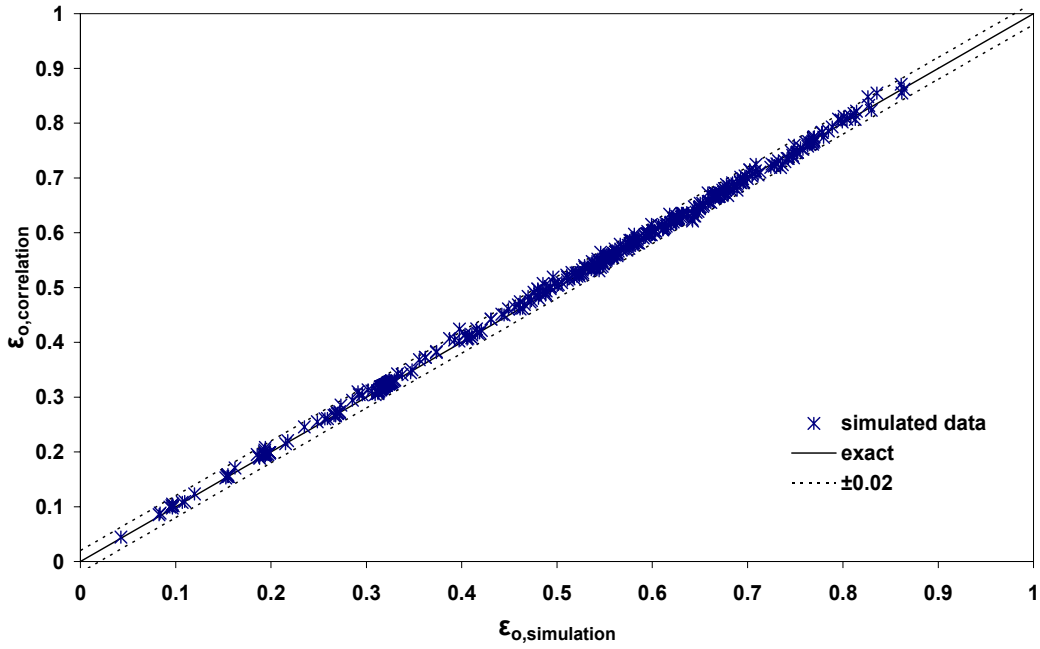

Figure 3.4 *Overall sensible effectiveness of the run-around heat recovery system with two identical counter/cross flow heat exchangers calculated from correlations (equations (3.8) and (3.5) or (3.6)) compared to the simulated effectiveness for range of $0<C_L/C_A\leq 10$, $0<Cr\leq 1$, $0<NTU\leq 15$, $0<x_i/x_0\leq 0.5$ and $0<y_0/x_0\leq 1$*

3.4 Applications and Limitations of the Correlations

As shown in the previous section, the correlations for counter/cross flow exchangers individually and coupled in a RAHE system agree well with the present numerical model and can be used for design purposes. In this section, the newly-

developed correlations are applied to justify the effects of different design characteristics and show the limitations of the new correlations.

3.4.1 Correlation for a Counter/Cross Flow Heat Exchanger

The performance of the counter/cross flow heat exchanger is investigated for the selected operating condition of $T_{A,in}$=308.15 K (35^{o}C) and $T_{L,in}$=297.15 K (24^{o}C). Even though the performance of the LAMEE with both the heat and moisture transfer depends on the operating inlet temperature and moisture content of the air and liquid streams, the effectiveness of a heat exchanger is not affected by the operating condition. The effects of different parameters on the effectiveness of the heat exchanger are shown in the next few figures. In all figures, the simulation is compared with the correlation developed for the counter/cross flow heat exchanger. The physical properties of the heat exchanger that is modeled in this section are given in Table 2.1.

3.4.1.1 Effect of Entrance Ratio (x_i/x_0)

The effectiveness of a heat exchanger decreases with increasing entrance ratio as it is shown in Figure 3.5. On the other hand, the correlation does not account for change in entrance ratio and predicts a constant effectiveness value and therefore is limited to $0<x_i/x_0\leq0.25$ with the maximum uncertainty of ±0.02 in this range. Since it is unlikely that one would design a heat exchanger with the entrance ratio greater than 0.25 and the effect of x_i/x_0 is trivial in the range of $0<x_i/x_0\leq0.25$ this parameter was neglected in developing the correlation. It limits the correlation to the range of $0<x_i/x_0\leq0.25$ and extrapolation beyond an entrance ratio of 0.25 will lead to errors greater than 2% (Figure 3.5).

Figure 3.5 also shows that the effectiveness of a counter/cross flow exchanger is always between the effectiveness of a pure counter-flow and a pure cross-flow exchanger with the same NTU and Cr (where in Figure 3.5 the effectiveness of a counter-flow exchanger is on the left vertical line and the effectiveness of a cross-flow exchanger is on the right vertical line). It should be noted even though the effectiveness values for cross-flow and counter-flow exchangers have been presented as entrance ratio is 1.1 and zero in Figure 3.5, it does not mean that the entrance ratios are those values and it is only the way that the results are presented.

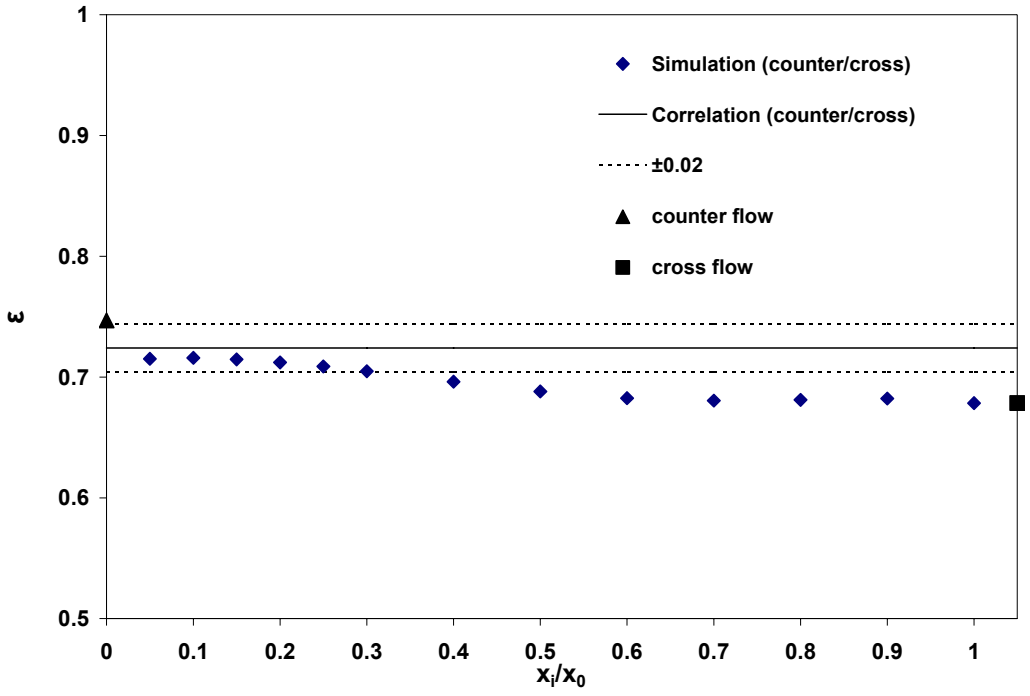

Figure 3.5 *Variation of the effectiveness of a counter/cross flow heat exchanger due to change in the size of the inlet header (entrance ratio, x_i/x_0) for NTU=3, Cr=1 and y_0/x_0=0.25. The simulated effectivenesses of pure cross-flow and pure counter-flow exchangers are included for comparison.*

Figure 3.6 shows the influence of the entrance ratio on the liquid flow distribution. As shown in Figure 3.6, as the entrance ratio increases from x_i/x_0=0.1 to 1, the flow patterns change from predominately counter-flow (horizontal streamlines

for the liquid flow means counter-flow because the airflow is horizontal from right to left) throughout the exchanger to cross-flow (vertical streamlines) throughout the exchanger. When $x_i/x_0=1$ the length of the inlet and outlet headers are equal to the exchanger length, which makes it a cross-flow heat exchanger (Figure 3.6 (d)).

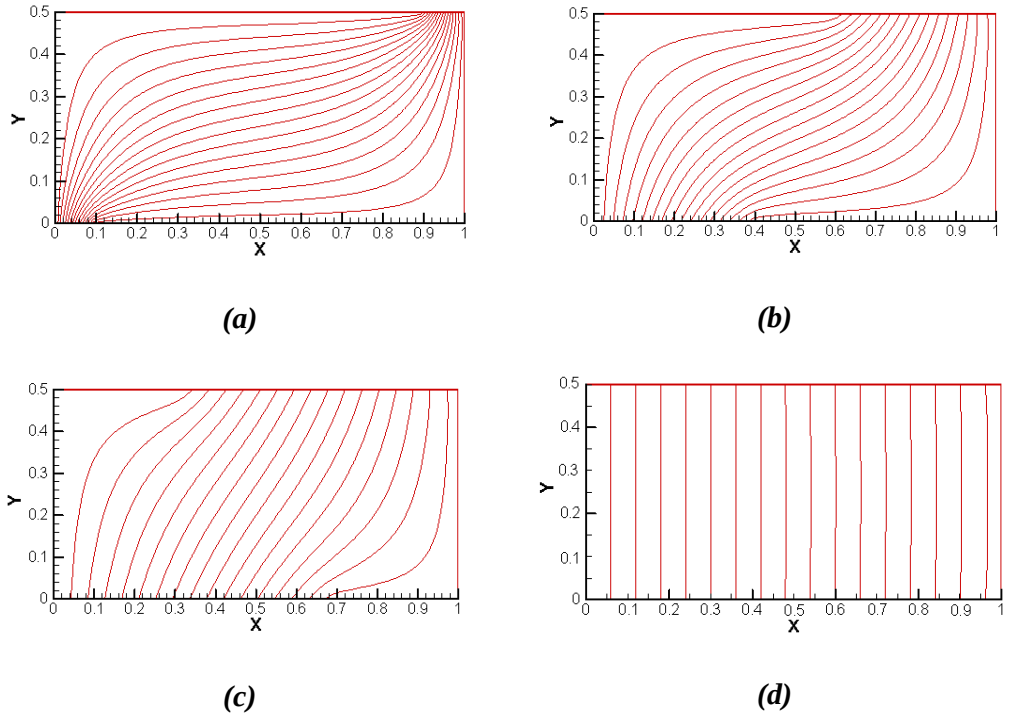

Figure 3.6 *Liquid stream lines in a heat exchanger with a combination of cross and counter-flow with the entrance ratio (x_i/x_0) of (a) 0.1, (b) 0.4, (c) 0.7 and (d) 1 when aspect ratio (y_0/x_0) is 0.5*

3.4.1.2 Effect of Aspect Ratio (y_0/x_0)

The effects of the aspect ratio (i.e. the ratio of height to length, y_0/x_0) on the effectiveness of the counter/cross flow heat exchanger ($\varepsilon_{counter/cross}$) are shown in Figure 3.7 for the case of $x_i/x_0=0.1$. For comparison, the effectivenesses of a pure cross-flow heat exchanger and a pure counter-flow heat exchanger with the same NTU and Cr are also shown in the figure. It can be seen that $\varepsilon_{counter/cross}$ decreases from a value near $\varepsilon_{counter}$ to a value near ε_{cross} as the aspect ratio (y_0/x_0) increases from 0.1 to

1. Figure 3.7 also shows that $\varepsilon_{counter/cross}$ is more sensitive to aspect ratio for high NTU values or that the difference between $\varepsilon_{counter}$ and ε_{cross} increases as NTU increases. The correlation also shows the same trend and agrees well with the simulation.

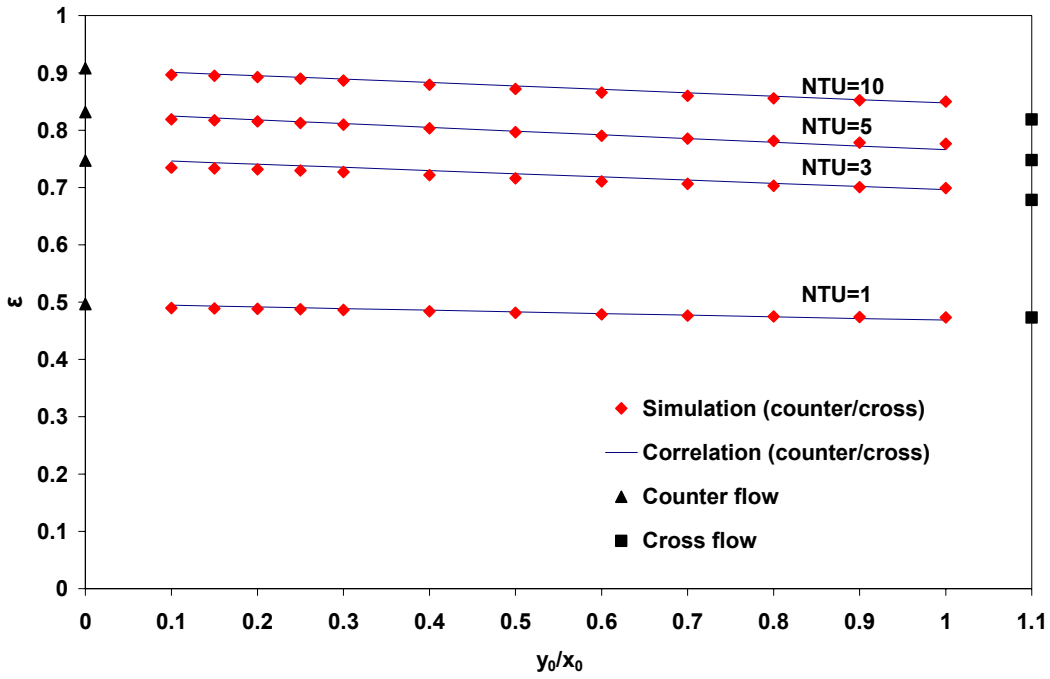

Figure 3.7 *Effectiveness of the counter/cross flow heat exchanger as a function of the aspect ratio (height to length) for Cr=1 and NTU as parameter. The simulated effectivenesses of pure cross and pure counter-flow exchangers are included for comparison,* x_i/x_0=0.1

The fluid flow distribution will change when the aspect ratio changes, which affects the effectiveness. Simulated liquid flow distributions for two designs with different aspect ratios are illustrated in Figure 3.8. As the aspect ratio decreases, the exchanger length increases compared to the height resulting in liquid streamlines that are more horizontal. This means that more of the liquid is flowing in the counter-flow arrangement with the air (the airflow is horizontal from right to left) and consequently the effectiveness increases as y_0/x_0 decreases. By increasing the aspect ratio, the

liquid-air flow configuration becomes more like a cross-flow arrangement and the effectiveness decreases.

For a very small aspect ratio ($y_0/x_0 \approx 0$) the effectiveness is close to the effectiveness of a similar counter-flow exchanger and for a large aspect ratio (e.g. $y_0/x_0 \approx 1$) although the streamlines are like a cross-flow exchanger and $\varepsilon_{counter/cross}$ is close to ε_{cross}.

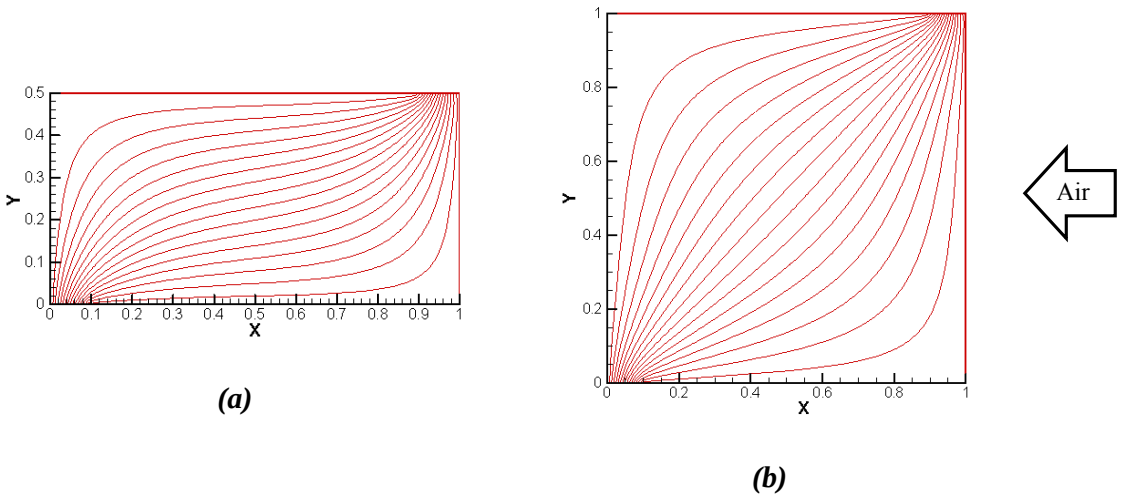

Figure 3.8 *Liquid streamlines in a counter/cross flow heat exchanger with the aspect ratio (y_0/x_0) of (a) 0.5 and (b) 1 when the entrance ratio (x_i/x_0) is 0.1*

3.4.1.3 Effect of NTU and Heat Capacity Rate Ratio

In Figure 3.9, $\varepsilon_{counter/cross}$ is presented as a function of NTU and Cr when $y_0/x_0=0.5$ and $x_i/x_0=0.1$. It should be noted that Cr is different from Cr* presented in section 2.7.1 as Cr is C_{min}/C_{max} but Cr* is C_L/C_A in each exchanger. Both the simulation and correlation data show that the effectiveness increases as NTU increases at a constant Cr. At a constant NTU, the effectiveness increases as Cr

decreases as expected from the literature. Similar trends and close agreement between the simulation and correlation verify the correlation for a wide range of NTU and Cr.

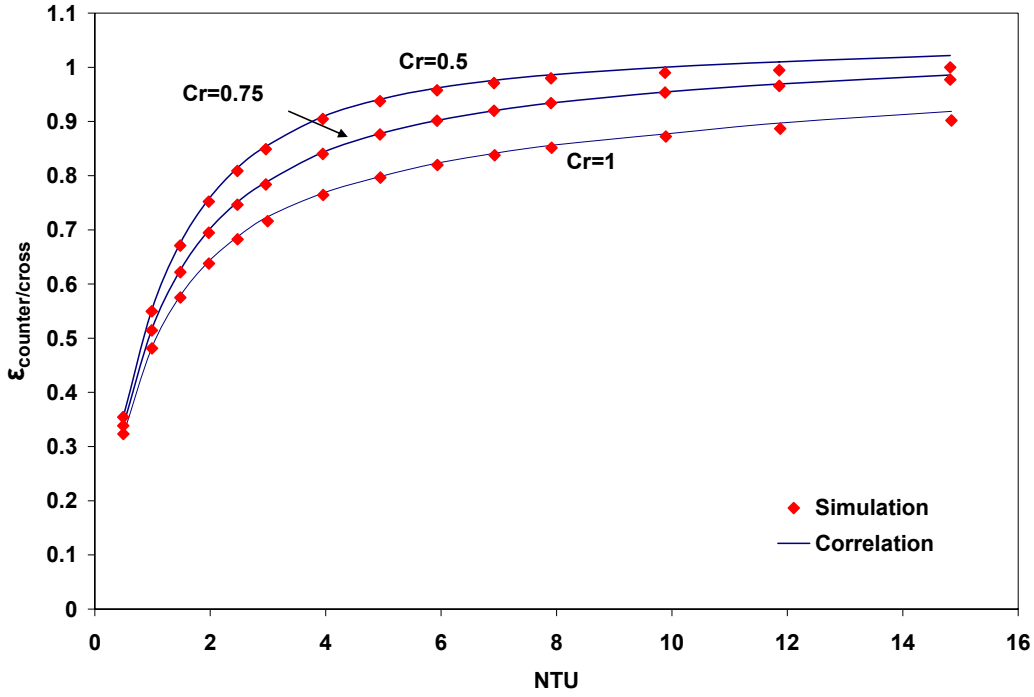

Figure 3.9 *Variation of the effectiveness of a counter/cross flow heat exchanger with NTU and Cr. The aspect ratio (y_0/x_0) is 0.5 and the entrance ratio (x_i/x_0) is 0.1*

3.4.1.4 Effect of Flow Arrangement

A direct comparison of the three different heat exchangers, cross-flow, counter-flow and counter/cross flow, is shown in Figure 3.10. The effectiveness of counter-flow exchanger is the highest as expected. The effectiveness of the counter/cross flow heat exchanger ($\varepsilon_{counter/cross}$) lies between the effectiveness of the counter-flow exchanger and the cross-flow exchanger. In this specific case where NTU=15 Cr=1, y_0/x_0=0.25, and x_i/x_0=0.1 $\varepsilon_{counter/cross}$ values are close to $\varepsilon_{counter}$ and are up to 8% higher compared to ε_{cross} values.

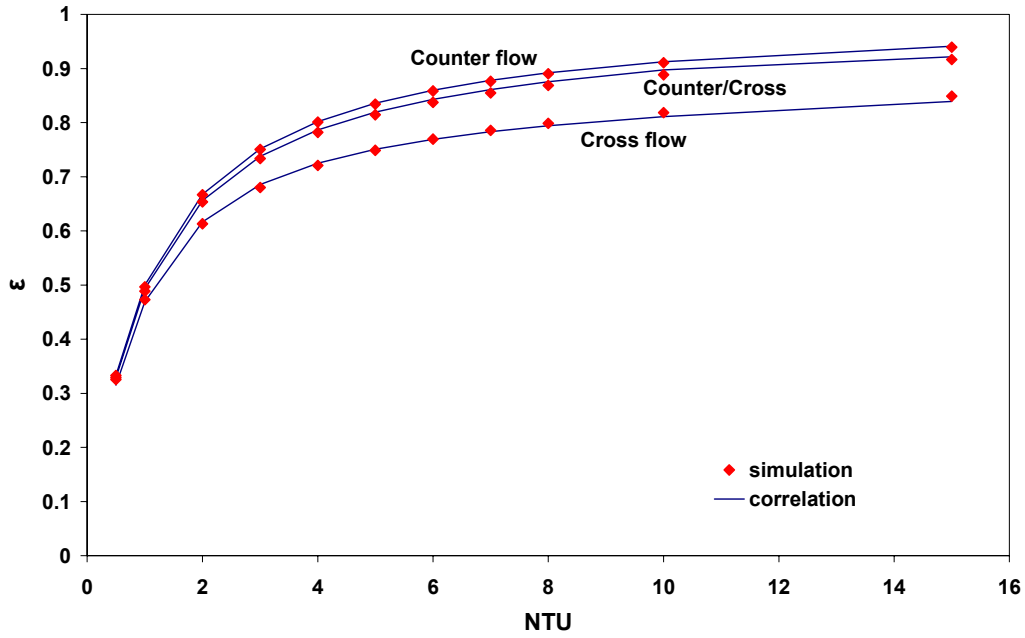

Figure 3.10 *Effectiveness of a single heat exchanger with pure cross-flow, pure counter-flow and a combination of cross and counter (counter/cross) flow arrangements as a function of NTU when Cr=1. The counter/cross flow exchanger has an entrance ratio (x_i/x_0) of 0.1 and an aspect ratio (y_0/x_0) of 0.25*

3.4.2 Correlation for Run-Around Heat Exchanger (RAHE)

The overall sensible effectiveness results for the RAHE with two identical counter/cross flow heat exchangers are presented and compared with the correlation developed for this system in this section. The supply and exhaust air mass flow rates are equal here. The operating conditions for the run-around system are AHRI summer test conditions given in Table 2.2.

The effects of the aspect ratio (y_0/x_0) and NTU of the exchangers on the overall sensible effectiveness of the RAHE ($\varepsilon_{o,counter/cross}$) are presented in Figure 3.11. The same trends as a single counter/cross flow exchanger are observed for the run-around system. As the aspect ratio decreases, $\varepsilon_{o,counter/cross}$ increases. However, in case of aspect ratio of one ($y_0/x_0=1$), the effectiveness of the RAHE system is slightly higher than the effectiveness of the run-around system with cross-flow exchangers for

the same NTU and Cr (Therefore, the effectiveness of the cross-flow exchanger is plotted at an aspect ratio of 1.1 in Figure 3.11). In Figure 3.9 also, $\varepsilon_{o,counter/cross}$ is close to $\varepsilon_{o,counter}$ when the aspect ratio is small ($y_0/x_0 \approx 0$).

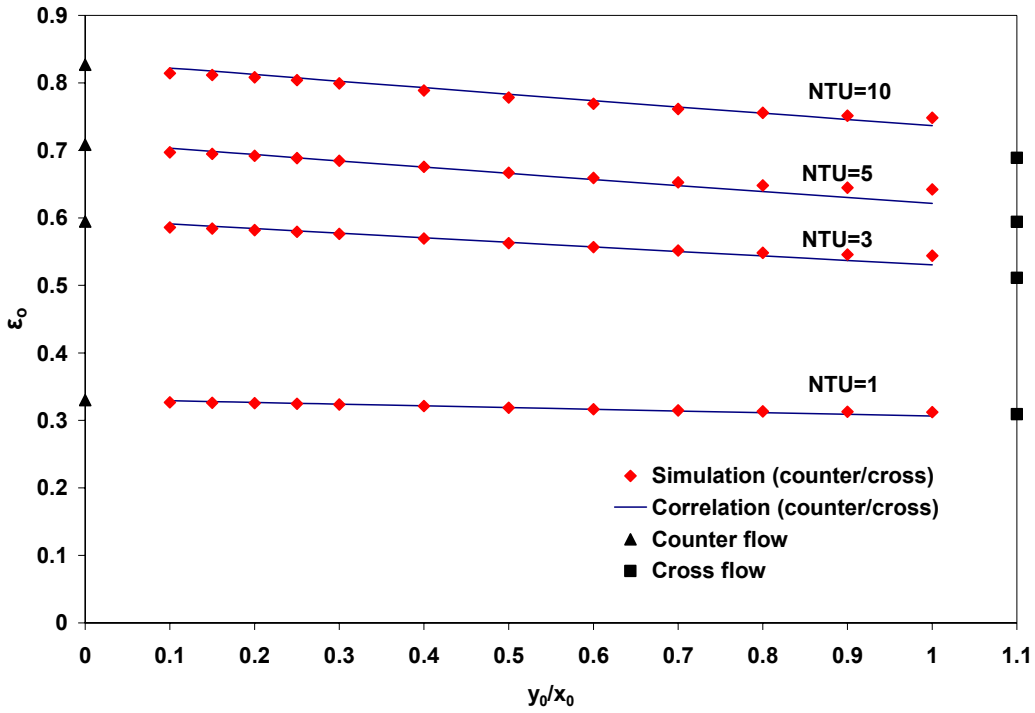

Figure 3.11 *Variations of the overall effectiveness of the run-around heat recovery system made of two identical counter/cross flow heat exchangers with changing aspect ratio (height to length of heat exchangers) and NTU as parameter when Cr=1 and x_i/x_0=0.1 The simulated effectivenesses of pure cross-flow and pure counter-flow exchangers are included for comparison.*

It is also revealed in Figure 3.11 that the overall effectiveness is more sensitive to the aspect ratio for high NTU values (e.g. NTU=10). For example, changing y_0/x_0 from 0 to 0.4 causes the overall effectiveness to decrease by 0.03 and 0.01 when NTU=10 and NTU=1 respectively.

The overall effectiveness of the RAHE is presented for a range of NTU and Cr for the case of $C_A > C_L$ and $C_A < C_L$ in Figure 3.12 (a) and (b) respectively. The results show that ε_o increases as NTU and Cr increase.

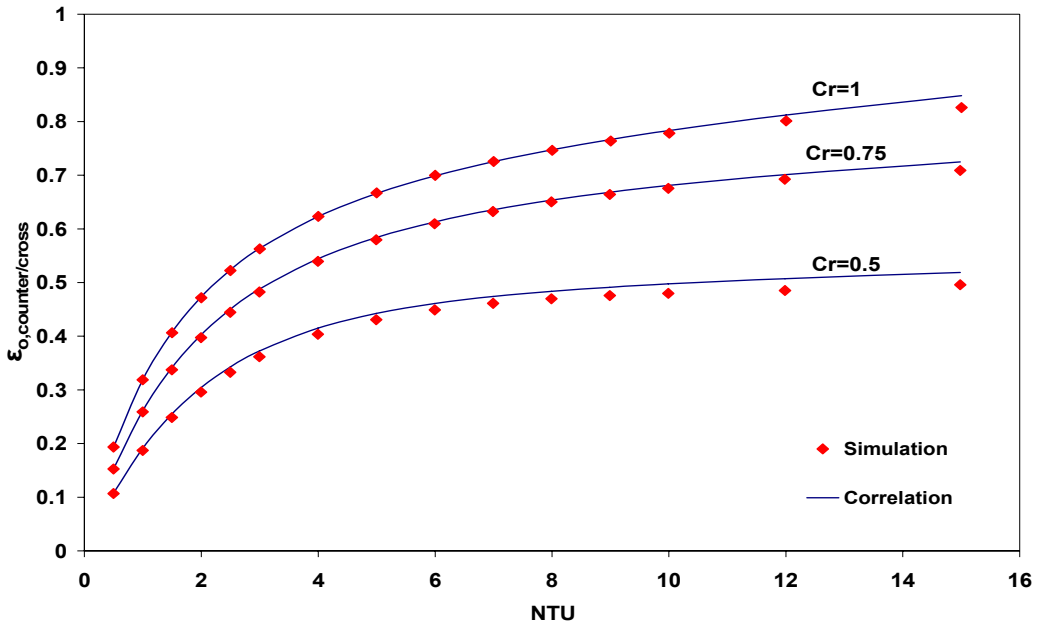

(a)

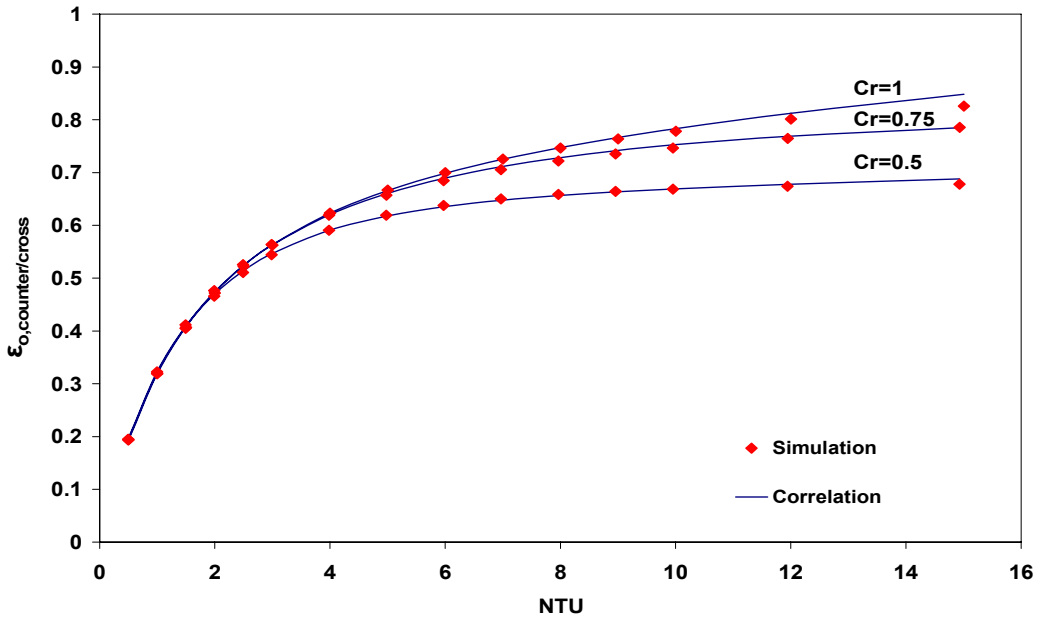

(b)

Figure 3.12 *Variation of overall effectiveness of run-around heat recovery system with two identical counter/cross flow heat exchangers with NTU for (a) $C_A>C_L$ and (b) $C_A<C_L$, $x_l/x_0=0.1$and $y_0/x_0=0.5$*

The effectiveness depends strongly on Cr for NTU>3. For NTU<3, the effectiveness of the RAHEs changes substantially with NTU. However, ε_0 is almost constant with NTU for each Cr when NTU≥6. Although the effectiveness of a single heat exchanger is minimum when Cr=1 (Figure 3.9), the maximum effectiveness of the RAHE occurs when Cr=1. It signifies that a single heat exchanger and a RAHE system employing that exchanger must be treated differently. From a comparison between Figures 3.12(a) and 3.12(b), it can be found that for case of $C_A>C_L$ the overall effectiveness is more sensitive to Cr, but for the same value of Cr the overall effectiveness is higher when $C_A<C_L$.

When NTU=5, $y_0/x_0=0.5$ and $x_i/x_0=0.1$, the overall effectiveness of the RAHE system with two counter/cross flow heat exchangers is shown in Figure 3.13 as a function of C_L/C_A and is compared to the overall effectiveness of the RAHE systems with two counter-flow and two cross-flow heat exchangers. As can be seen, the maximum overall effectiveness occurs when $C_L=C_A$ and counter/cross flow design improves the maximum overall effectiveness of the RAHE system by 7% compared to the similar RAHE system with two cross-flow heat exchangers. The good agreement between the simulation and the correlation for the RAHE system with counter/cross flow exchangers verifies the accuracy of the correlation for a wide range of NTU and Cr.

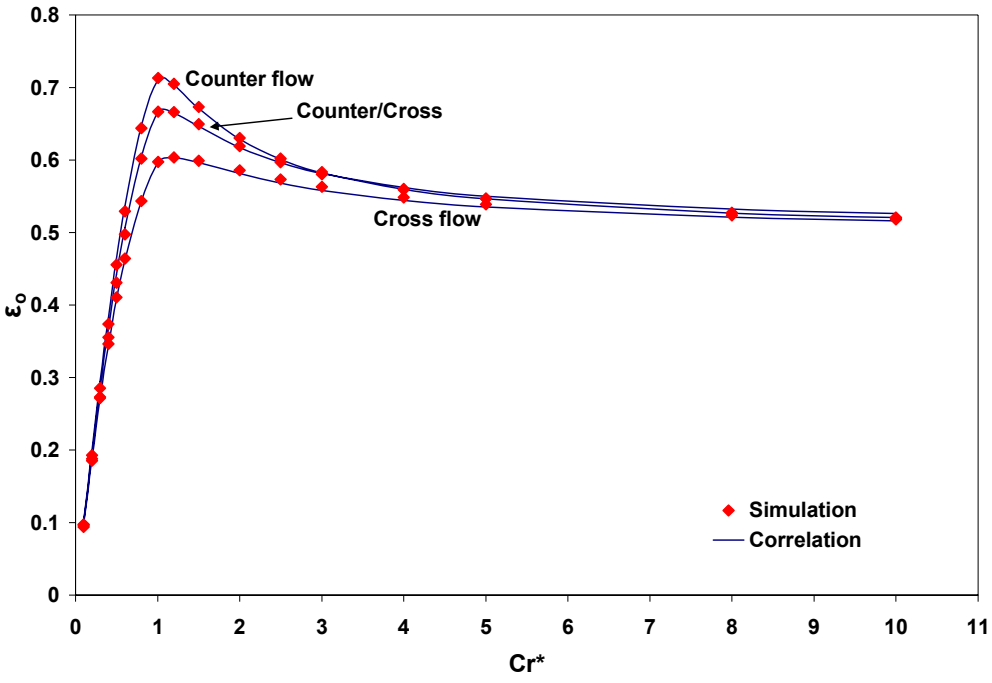

Figure 3.13 *Overall effectiveness of run-around heat recovery system with two identical counter/cross flow heat exchangers compared to the overall effectiveness of the RAHE with two counter-flow and two cross-flow heat exchangers, NTU=5, $x_i/x_0=0.1$ and $y_0/x_0=0.5$*

Although it is not presented visually in a figure, it should be noted that $\varepsilon_{o,counter/cross}$ changes by about 0.02 over the range of $0<x_i/x_0\leq 0.25$ for NTU=15. For lower NTU values, $\varepsilon_{o,counter/cross}$ is less sensitive to the entrance ratio. This is similar to the findings of a single heat exchanger presented in Figure 3.5.

The findings of this study about the effectiveness of single heat exchanger and RAHE agree with Fan et al. (2005) for cross-flow heat exchangers and the RAMEE systems using cross-flow heat exchangers.

3.5 Summary

The numerical/mathematical model developed in Chapter 2 for a LAMEE and the RAMEE system was validated in this chapter for the case of heat transfer (i.e.

sensible energy) only. The accuracy of the model was verified by correlations from the literature for both single heat exchangers and two exchangers coupled in run-around loop for exchangers with pure cross-flow or pure counter-flow arrangement. Comparisons showed that the difference between the predicted effectiveness from simulation and the effectiveness from correlations was less than ±2% and ±2.5% for single and run-around heat exchangers, respectively.

The validated numerical model was used to develop new performance correlations for flat-plate counter/cross flow heat exchangers and run-around heat exchangers (RAHE) made of two counter/cross flow heat exchangers. The new correlations agree with the model within ±2% for both single heat exchangers and RAHEs. These performance correlations can be used in engineering design to select and predict the performance of RAHEs under different operating conditions and different design characteristics.

The overall sensible effectiveness of a RAHE made of two identical counter/cross flow heat exchangers is a function of number of heat transfer units (NTU), the heat capacity rate ratio of the fluids (Cr), the aspect ratio (i.e. the ratio of height to length) of the exchanger (y_0/x_0) and the ratio of the length of the inlet/outlet headers to the length of the heat exchanger (entrance ratio, x_i/x_0). The effect of x_i/x_0 is ignored in the correlations based on the practical considerations. The correlations developed are for the range of $0<Cr\leq1$, $0.5\leq NTU\leq15$, $0<x_i/x_0\leq0.25$ and $0<y_0/x_0\leq1$.

The effectiveness of counter/cross flow heat exchangers is generally less than counter-flow exchangers. However, if this heat exchanger is designed such that the entrance ratio and aspect ratio are small, it can have almost the same effectiveness as that of a counter-flow heat exchanger. A counter/cross flow exchanger with small entrance ratio (e.g. $x_i/x_0=0.1$) and small aspect ratio (e.g. $y_0/x_0=0.25$) has

approximately 10% higher effectiveness compared to a similar cross-flow heat exchanger and a 1.5% lower effectiveness compared to a similar counter-flow exchanger (when NTU=15 and Cr=1). A RAHE with two counter/cross flow exchangers (with x_i/x_0=0.1 and y_0/x_0=0.25) has about 7% greater and 5% lower overall sensible effectiveness compared to that of an equivalent RAHE system with two cross and counter-flow heat exchangers, respectively (NTU= 5 and $C_L/C_A \approx 1$).

To achieve a high overall effectiveness for the RAHE, the following can be recommended: (i) high NTU value, (ii) $0.8<C_L/C_A<1.2$, (iii) the aspect ratio of the heat exchanger in the range of 0 to 0.3 and (iv) the entrance ratio in range of 0 to 0.25.

Chapter 4

Validation of the Model for RAMEE system

4.1 Introduction

The purpose of this chapter is to present the results from the numerical model (presented in Chapter 2) for the case of coupled heat and water vapour transfer. The results are presented in the form of the effectiveness of the RAMEE system with two identical LAMEEs. The overall effectivenesses are compared with numerical (Seyed Ahmadi 2008) and experimental (Mahmud 2009) data to validate the model.

4.2 Numerical Validation

Seyed Ahmadi (2008) developed a mathematical/numerical model to study the transient behavior of a RAMEE system made from two identical cross-flow LAMEEs. A comparison between the effectiveness of the present model with cross-flow exchangers and the effectiveness determined by Seyed Ahmadi (2008) model when the system reaches steady state is presented in Figures 4.1. The AHRI summer and winter operating conditions (AHRI 2005) are applied in both models. The effectivenesses of the RAMEE system with two counter/cross flow exchangers are also included in Figure 4.1. The LAMEE parameters are presented in Table 2.1.

As shown in Figure 4.1, both numerical models give almost the same results for the overall sensible and latent effectivenesses of the RAMEE system with two cross-flow exchangers under steady state conditions (differences are within ±1%).

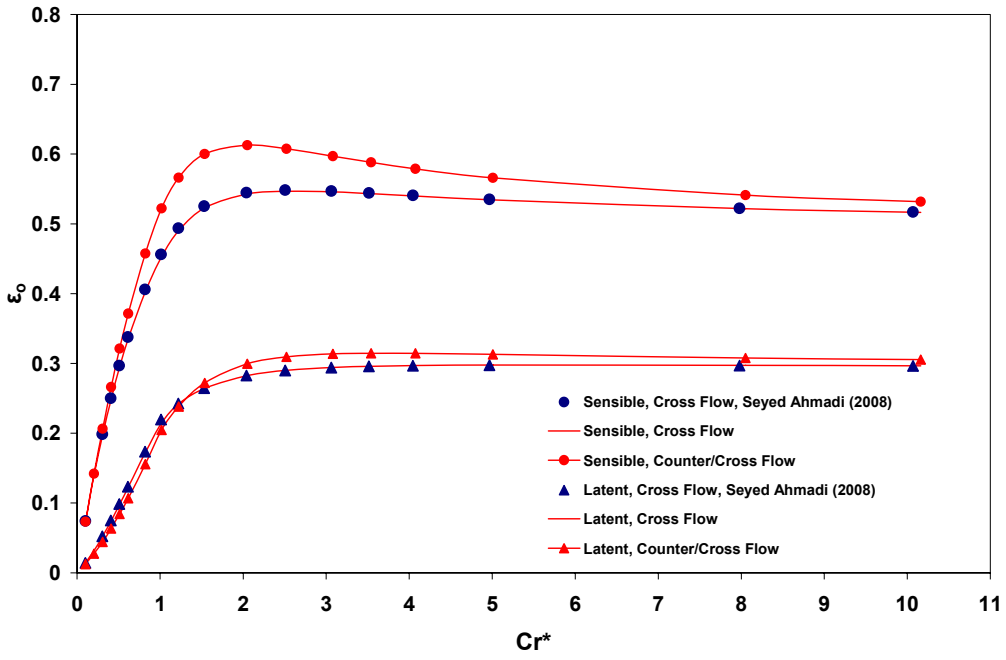

(a)

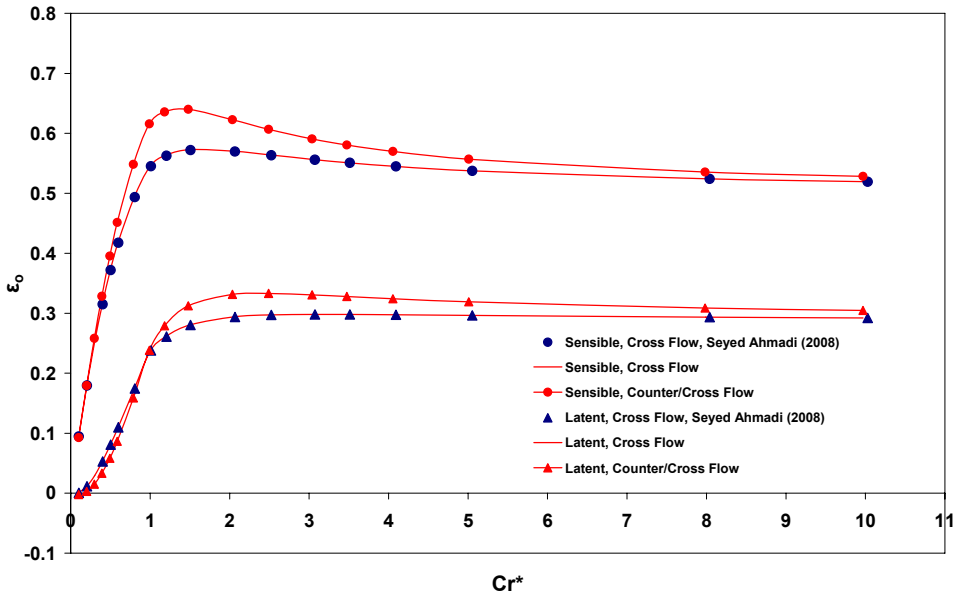

(b)

Figure 4.1 *Comparisons of steady state overall sensible and latent effectiveness of the RAMEE system with two cross-flow exchangers calculated from the present numerical model and the numerical model of Seyed Ahmadi (2008). The results are for NTU=5 and AHRI (a) summer and (b) winter conditions. The predicted effectiveness of the system with two counter/cross flow exchangers is for* $x_i/x_0=0.1$ *and* $y_0/x_0=0.5$

4.3 Experimental Validation

The purpose of this section is to validate the present numerical model with experimental data. The validation is done with data obtained from a laboratory testing prototype which was built and tested by another graduate student (Mahmud 2009) at the University of Saskatchewan. The comparison uses data measured on a RAMEE system composed of two counter/cross flow LAMEEs.

4.3.1 RAMEE Prototype

The laboratory testing prototype (prototype 3) made of two counter/cross flow LAMEEs was tested by Mahmud (2009) under the operating conditions similar to AHRI summer and winter operating conditions. The counter/cross flow LAMEE designed by Mahmud (2009) is depicted in Figure 4.2 and the design parameters are given in Table 4.1.

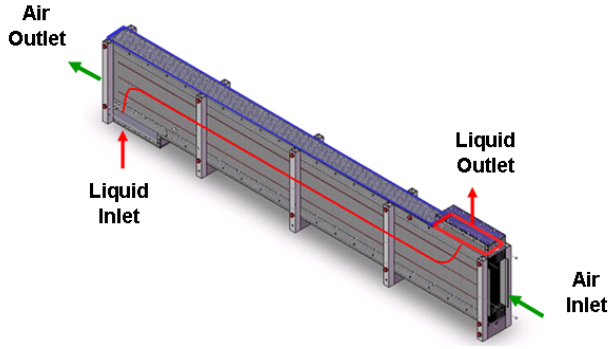

Figure 4.2 *Counter/cross flow LAMEE in prototype 3 of Mahmud (2009).*

In prototype 3, the length of liquid headers was decreased and the liquid channels were widened to provide more uniform liquid flow compared to RAMEE prototype 2 (Erb 2007). The liquid desiccant was pumped from the bottom to the top header following the suggestions of Erb (2007). In prototype 3, Propore was used as

the semi-permeable membrane (Larson et al. 2007) and $MgCl_2$ was adopted as the coupling fluid.

Table 4.1 *Design parameters of counter/cross flow LAMEE used in prototype 3*

Name	Symbol	Value
Size of exchanger	$x_0 \times y_0 \times z_0$	1.8×0.2×0.075 m
Header length	x_i	0.075 m
Channel thickness, air side	d_A	4.4 mm
Channel Thickness, liquid side	d_L	2.7 mm
Number of air channels	n_A	11
Number of liquid channels	n_L	10
Membrane thickness	δ	0.2 mm
Thermal conductivity of the membrane	k	0.3 W/(m.K)
Moisture conductivity of the membrane	k_m	1.66×10^{-6} kg/(m.s)

As shown in Table 4.1, each LAMEE in prototype 3 has a length of 1.8 m and a height of 0.2 m, which makes it a counter/cross flow LAMEE with an aspect ratio (the ratio of the height to the length of exchanger) of 1/9. The length of the liquid headers is 0.075 m, so the entrance ratio (the ratio of the header length to the length of exchanger) of each LAMEE is approximately 0.042. Due to the small aspect ratio and entrance ratio of the exchangers used in the RAMEE prototype 3, the liquid-air flow configuration within the exchanger is almost counter-flow and the overall effectiveness of the prototype 3 is expected to be very close to a RAMEE system with two counter-flow exchangers with the same design characteristics. The sensitivity of the performance of the RAMEE system to aspect ratio and entrance ratio are presented in Chapter 5.

4.3.2 RAMEE Test Apparatus (RAMEETA)

The Run-Around Membrane Energy Exchanger Testing Apparatus (RAMEETA) used to test prototype 3 is shown schematically in Figure 4.3 (Erb

2007). The facility is composed of two air streams each driven by two fans (one downstream and one upstream), an environmental chamber, and two LAMEEs (one on the supply side and another on the exhaust side). The LAMEEs are coupled in a closed loop with connecting pipes and two pumps recirculating the $MgCl_2$ solution. The fans are used to control the air flow rate.

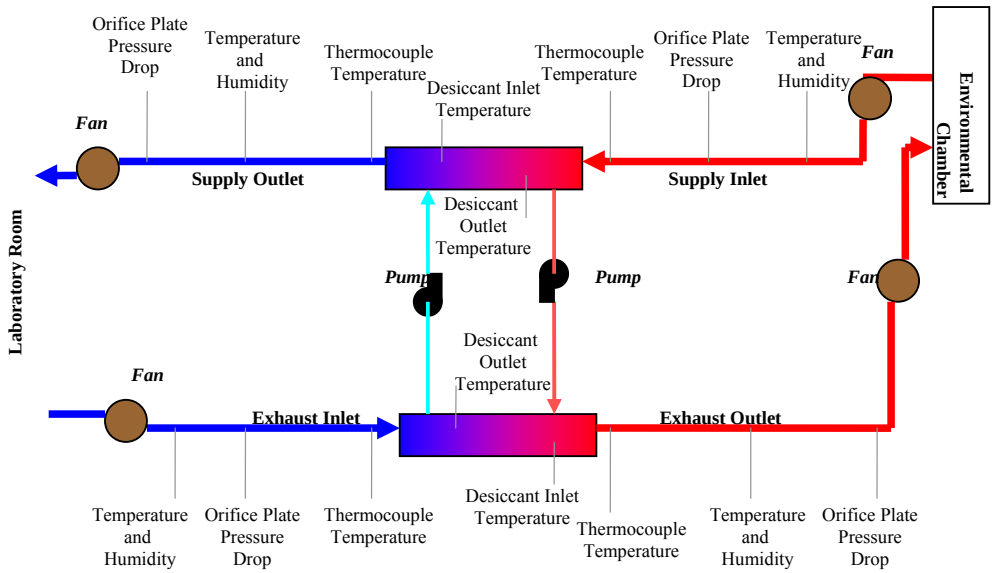

Figure 4.3 *Schematic of Run-Around Membrane Energy Exchanger Testing Apparatus (RAMEETA). (Erb 2007)*

The environmental chamber provides the outdoor operating conditions or supply air stream. The supply air stream enters the supply LAMEE, and after transferring heat and moisture with coupling liquid in the exchanger the air is released into the laboratory room. The indoor conditions in the laboratory are almost constant and can be used as the source for the exhaust air stream. Heat and moisture transfer between the exhaust air stream and liquid desiccant occurs in the exhaust LAMEE.

The temperature, relative humidity and mass flow rate of the air are measured on both sides of each LAMEE to determine the sensible, latent and total effectivenesses (equations (2.51)-(2.53)). In the experiments, the mass flow rates of

both supply and exhaust air streams are equal and mass flow rates are measured with pressure transducers and orifice plates. The air temperature is measured using T-type thermocouples and resistance temperature detectors (RTD's). The relative humidity of the air on both side of each LAMEE is measured using capacitive humidity sensors.

The liquid desiccant ($MgCl_2$ solution) flows in a closed loop between two exchangers and transfers heat and moisture from one air stream to the other. The salt solution is pumped in a closed loop and its mass flow rate is measured by a rotameter. To reduce the heat transfer to the surrounding, the air and liquid pipes and the pumps are insulated.

4.3.3 Comparison between Numerical and Experimental Results

In this section, the results from the numerical model are compared to the experimental results. It should be noted that due to the limitations in controlling the inlet air conditions during the tests, slightly different inlet air temperatures and humidity ratios than the AHRI summer conditions were used in the tests. However, for the simulations, AHRI test conditions were used. A computational sensitivity study showed that the overall sensible and latent effectivenesses of the RAMEE system with counter/cross flow exchangers changed only by ±1% if the inlet air humidity ratio changes in range of ± 2 g/kg which is the maximum difference between the experimental conditions and AHRI conditions. The impact of changing the inlet air temperature on the overall effectiveness of the system is also trivial. A computational sensitivity study revealed that the overall sensible effectiveness of the RAMEE system changes less than 1% with a $2^{o}C$ temperature variation around AHRI summer test conditions. This temperature difference is larger than the difference between the experimental conditions and AHRI testing conditions.

The comparison between the numerical and experimental data for RAMEE prototype 3 is presented in Figure 4.4. The trends of the experimental and numerical effectivenesses as a function of Cr* compare well (both the experimental and numerical data peak at certain values of Cr*), but the effectiveness values differ. These differences can be in the ranges of 1% to 30%, 0.5% to 14%, and 1% to 17% for overall sensible, latent and total effectivenesses of the RAMEE system, respectively. As shown in Figure 4.4 (a), even though the numerical model can predict the change of overall sensible effectiveness of the RAMEE system with Cr*, the simulated effectiveness is up to 30% different (at large NTUs) from the experimental data. It also can be seen that the experimental sensible effectiveness of the RAMEE is not as sensitive as the numerical results to the change of NTU.

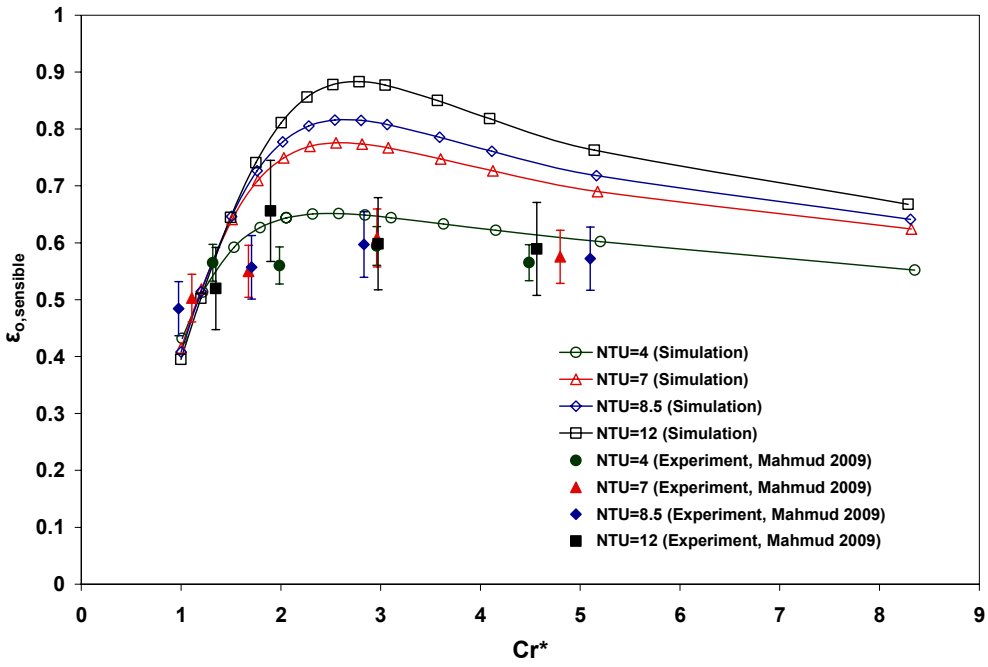

(a)

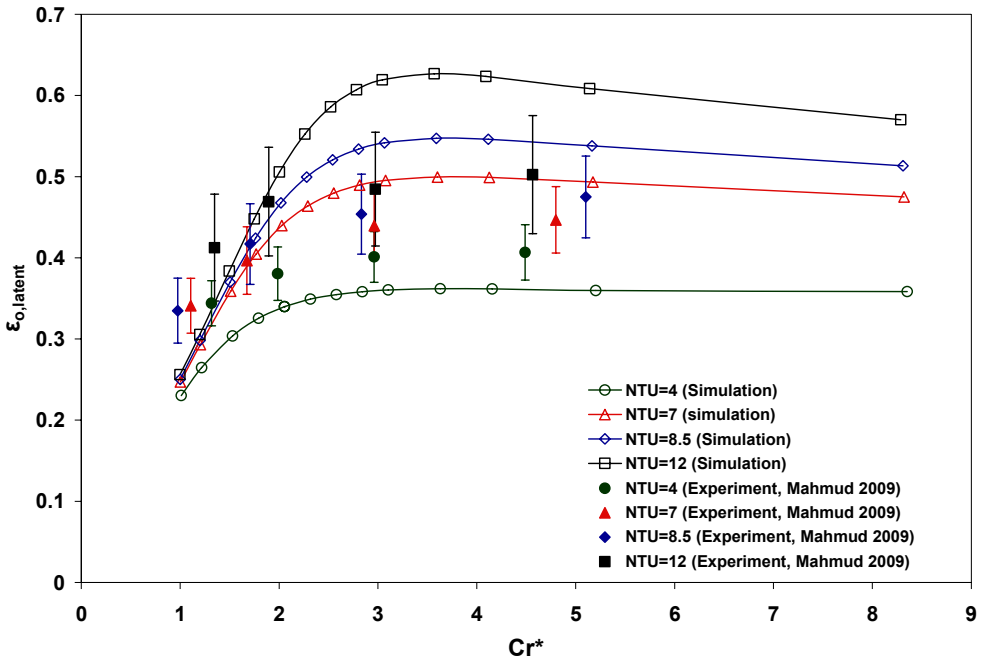

(b)

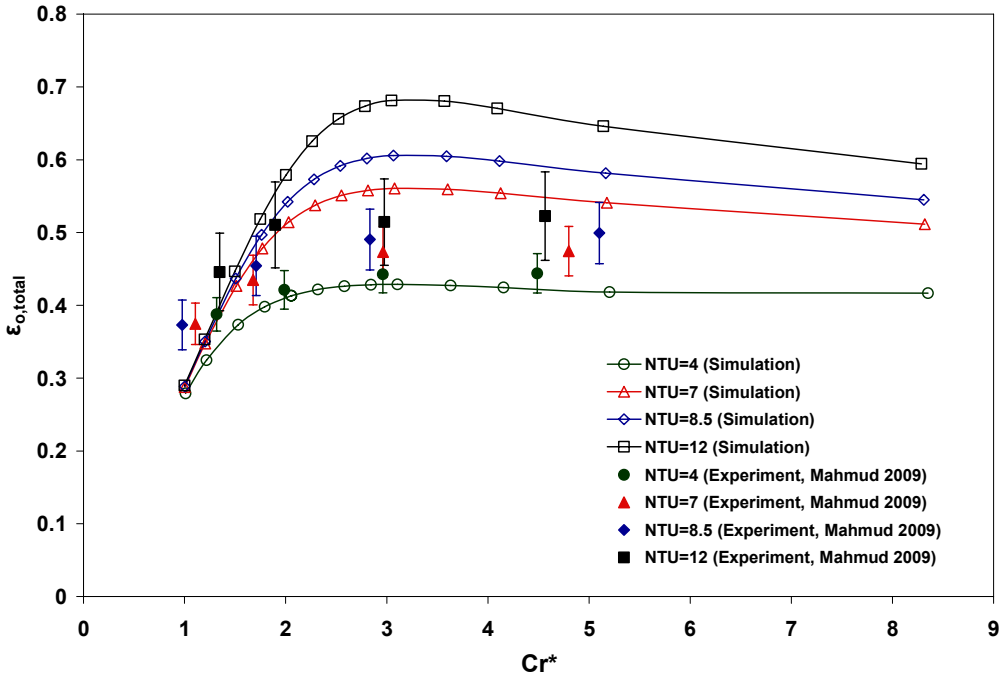

(c)

Figure 4.4 *Experimental and numerical overall (a) sensible, (b) latent and (c) total effectivenesses of the RAMEE system with two counter/cross flow exchangers between numerical model and experimental data (prototype 3) for summer operating conditions*

The same data for the overall total effectiveness as in Figure 4.4 (c) are also presented in Figure 4.5 (a) to Figure 4.5 (d) for further illustration. Each graph in Figure 4.5 compares the numerical and experimental data at a constant NTU value, and includes the uncertainty in Cr* (mass flow rate) the mass flow rate uncertainty in the experimental data.

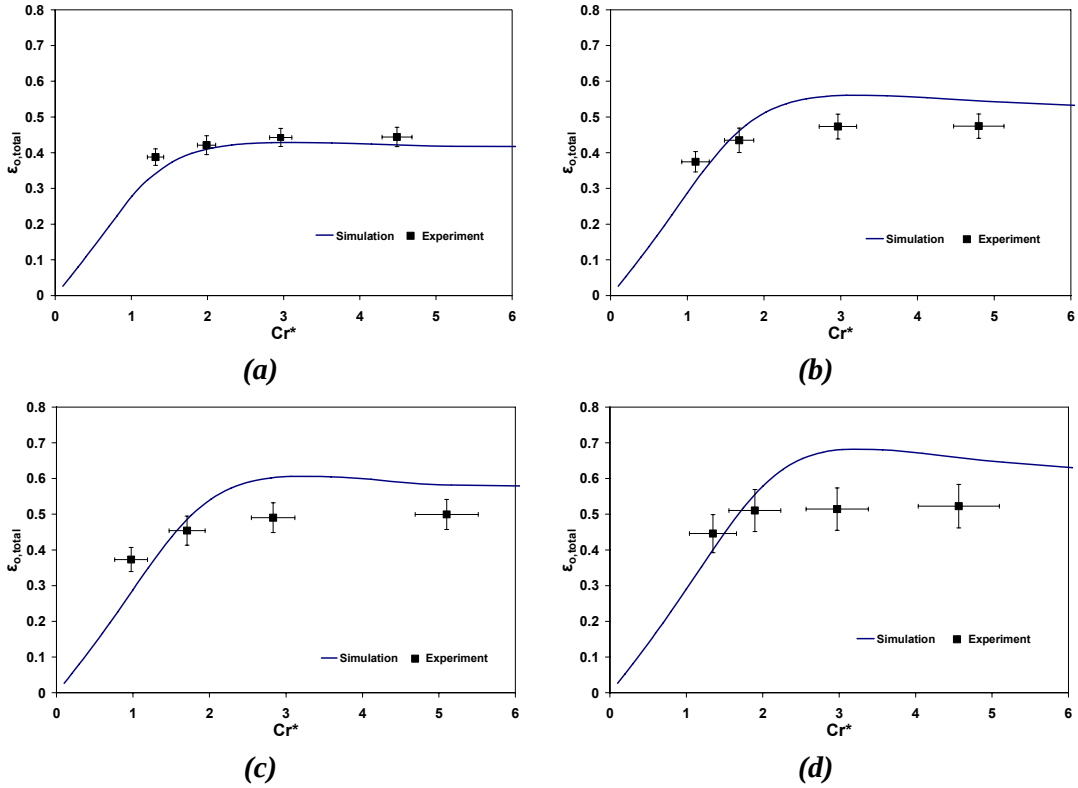

Figure 4.5 *Experimental and numerical overall total effectiveness of the RAMEE system with two counter/cross flow exchangers (prototype 3) for summer operating conditions when (a) NTU=4, (b) NTU=7, (c) NTU=8.5 and (d) NTU=12*

As indicated in Figure 4.5, the numerical and experimental results agree mainly within the experimental uncertainty at lower NTUs. For example as shown in Figure 4.5 (a) the discrepancy between simulations and experiments is 1-4% which is mostly within experimental uncertainty. However, as NTU increases, the differences between the numerical and experimental total effectiveness increase. As shown in Figures 4.4 and 4.5, even though the uncertainties of the experimental data increase

with NTU, the simulations exceed the experimental uncertainty at large NTUs (e.g. up to 17% difference in total effectiveness at NTU=12).

Further investigation should be conducted to better explain the reasons for such discrepancies. However, it is speculated that the liquid flow may not have been distributed uniformly unlike the prediction by simulation. In the model, it is assumed that all the liquid channels are filled with equal amount of the liquid desiccant. However, practically, liquid desiccant might not flow thought the channels uniformly and there are some channels with more flow and some other with less flow. In addition, at lower flow rates, there might be some liquid channels without flow or very low flow. At a constant Cr*, the NTU of the RAMEE prototype 3 is increased by reducing the fluids flow rates. In this case, the heat and mass transfer surface area might be less than that used by the numerical model. As a result, the measured effectivenesses are lower than the simulated effectivenesses at higher NTUs.

The experimental results differ less from the simulated effectiveness at lower NTUs (e.g. NTU=4). The higher liquid desiccant mass flow at low NTU (for a constant Cr*) may results in more uniformly distributed flow within the exchangers in agreement with the numerical prediction.

The salt solution might leak into the air channels during these tests. At lower NTUs, the liquid desiccant mass flow rate is higher which may result in more liquid leakage within the exchangers. Liquid leakage in the air channels can result in higher moisture transfer rate because of direct contact between the leaked liquid and air stream. At NTU=4, perhaps because of leakage in the tests the moisture transfer rate is higher than that predicted in the numerical model with no leakage. Consequently, the overall latent and total effectivenesses of the RAMEE prototype 3 calculated from measured data are higher than the simulated effectivenesses.

The discrepancy between the experimental and numerical results can be also attributed to the fact that the system might not have reached the steady state conditions when the data were collected. Seyed Ahmadi (2008) investigated the transient behaviour of the RAMEE system with two cross-flow exchangers. He found that sometimes it took a long period of time for the system to reach the quasi-steady state conditions. This time period is a function of NTU, Cr*, initial salt concentration, volume of the salt solution in the system, and the operating conditions (Seyed Ahmadi 2008). However, the experimental measurements were recorded after 3 to 5 hours of running time of the system regardless of this fact.

The discrepancy between the experimental and numerical results, in Figures 4.4 and 4.5, may be due to the incorrect membrane thickness and permeability values applied in the numerical model. Because of the uncertainties in the measurements of the membrane thickness and permeability, the measured values employed in the numerical model might not exactly represent the physical membrane employed in the tests. The sensitivities of the numerical results to the variations of the permeability and the thickness of the membrane are analyzed in Chapter 2. As it is presented, the effectiveness results significantly vary with changes in the membrane permeability and thickness.

4.4 Summary

In this Chapter, the present numerical model developed for coupled heat and water vapor transfer in the RAMEE system is compared with previously reported numerical and experimental data. A RAMEE system with two cross-flow exchangers is compared with Seyed Ahmadi (2008) for quasi-steady state operating conditions. The comparison shows the effectiveness results computed by both the numerical models are almost equal (less than 1% difference).

The numerical model for the RAMEE system with two counter/cross flow exchangers is compared to the experimental results for the RAMEE prototype 3 (Mahmud 2009). The comparison shows that both the experimental and numerical results show the same general trends of changing effectiveness as Cr* changes. The numerical and experimental results for overall total effectiveness are in good agreement for lower NTU values (e.g. NTU=4). The discrepancy between the measured and computed overall total effectiveness is within experimental uncertainty for NTU=4 (1-4% difference). However, at higher NTUs the differences between the numerical and experimental results become more noticeable (up to 17% difference). The discrepancies between the simulated and measured results may be attributed to the non-uniform liquid flow in tests, the liquid desiccant leakage into the air channels in the tests, the incorrect permeability and thickness of the membrane employed in the simulation, and the test data acquisition before the RAMEE system reaches the full steady-state condition.

Chapter 5

Sensitivity study for dimensionless groups

5.1 Introduction

It is the purpose of this section to investigate the impacts of different dimensionless parameters on the performance of the RAMEE system composed of two counter/cross flow LAMEEs. The dimensionless parameters studied in this chapter include the entrance ratio (x_i/x_0), aspect ratio (y_0/x_0), the number of heat transfer units ($NTU=UA/C_{min}$), heat capacity rate ratio ($Cr^*= C_{Sol}/C_{Air}$), the number of mass transfer units ($NTU_m= U_m A / \dot{m}_{min}$), and the mass flow rate ratio of pure salt to dry air ($m^*=\dot{m}_{Salt}/\dot{m}_{Air}$). In addition, the influence of the liquid and air flow configuration on the predicted overall effectiveness of the RAMEE system are examined.

There are other parameters which also affect the performance of the RAMEE system. These parameters are the temperature and humidity ratio of the inlet air stream and the type of salt solution used as the coupling liquid. In this chapter, the results are presented for two different inlet operating conditions, AHRI summer and winter (AHRI 2005). The computational results in this study are for $MgCl_2$ solution as the coupling fluid. The investigation of the performance of the system with different types of salt solution is not performed. The impact of this parameter will be addressed as a part of the RAMEE project in the future. A similar dimensional study is performed for a counter/cross flow LAMEE and the results are presented and interpreted in Appendix D.

The LAMEE parameters and design characteristics which are used for the RAMEE system investigated are described in Table 2.1. The performance of the run-around system is presented under the AHRI summer and winter operating conditions

(AHRI 2005) provided in Table 2.2. In all simulations, equal air mass flow rates are used for the supply and exhaust exchangers (i.e. $\dot{m}_{Air,S} = \dot{m}_{Air,E}$).

5.2 Effect of Entrance Ratio

The effects of the entrance ratio, or the ratio of the length of the inlet and outlet headers to the length of the exchanger, on the overall effectiveness of a RAMEE system are shown in Figure 5.1. The effectiveness of RAMEE system, with two counter-flow and with two cross-flow LAMEEs are also presented for comparison. As illustrated in Figure 5.1, increasing the exchanger entrance ratio, by increasing the header length for a given length of the exchanger, results in the reduction of the overall sensible, latent, and total effectivenesses of the RAMEE system.

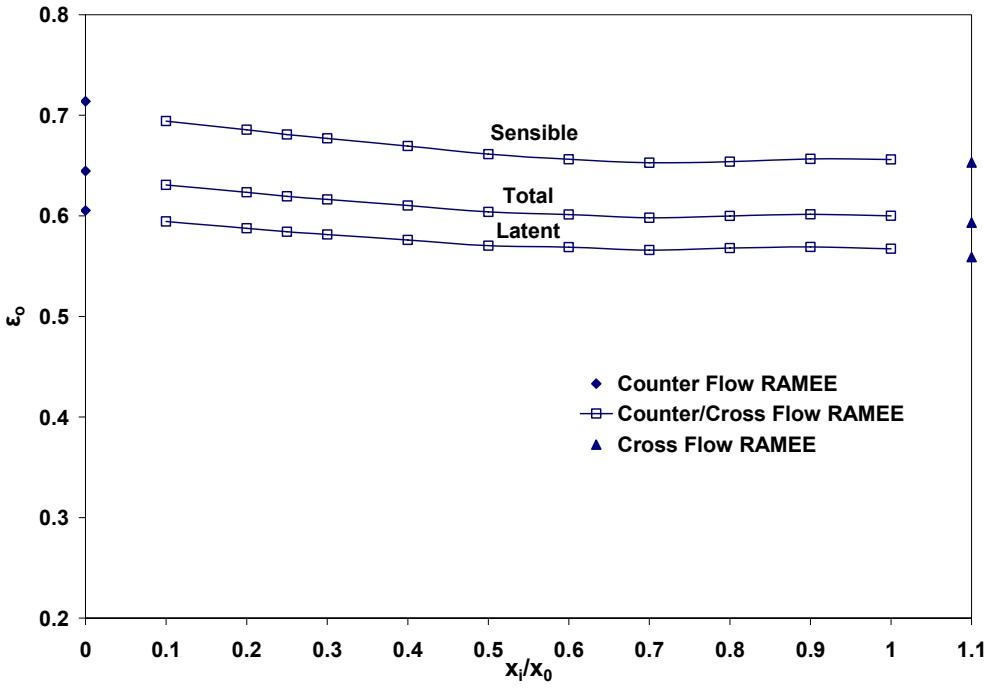

Figure 5.1 *Variation of the overall sensible, latent and total effectivenesses of a RAMEE system with two counter/cross flow exchangers due to change entrance ratio, x_i/x_0 for NTU=10, Cr*=3, y_0/x_0=0.5, and AHRI summer conditions. The effectivenesses of the RAMEE with two pure cross-flow and two pure counter-flow exchangers are included for comparison.*

The inlet and outlet headers of the counter/cross flow exchanger are in the cross-flow direction. The flow streamlines, Figure 3.6, change to the counter-flow direction (horizontal streamlines mean the liquid flows in the counter-flow arrangement relative to the air stream. The air stream is horizontal from right to left) as liquid passes through the exchanger. The velocity of the liquid flow near the corners of the exchanger boundaries is lower. The local heat and moisture transfer near the corners reduce significantly. If the header length is small compared to the exchanger length, the effects of the corners become smaller and the flow configuration is mostly counter-flow (refer to Figure 3.6). The counter/cross flow RAMEE with small entrance ratio is more favorable for the heat and moisture transfer between the air and liquid desiccant streams. As implied by Figure 5.1, the RAMEE system with two counter/cross flow exchangers should have an entrance ratio less than 0.2 to have a high performance.

It is also indicated in Figure 5.1, that the overall effectiveness values of the counter/cross flow RAMEE system reach almost the overall effectiveness of the cross-flow RAMEE when $0.6<x_i/x_0<1$. This happens as the liquid velocity is oriented more in cross-flow (vertical) direction with the higher entrance ratio (refer to Figure 3.6)

5.3 Effect of Aspect Ratio

The aspect ratio, the ratio of the height to the length of the exchanger (y_0/x_0), affects the overall effectiveness of the RAMEE system with two counter/cross flow heat and moisture exchangers as presented in Figure 5.2. As the aspect ratio increases, the sensible, latent and total effectivenesses of the RAMEE system decrease.

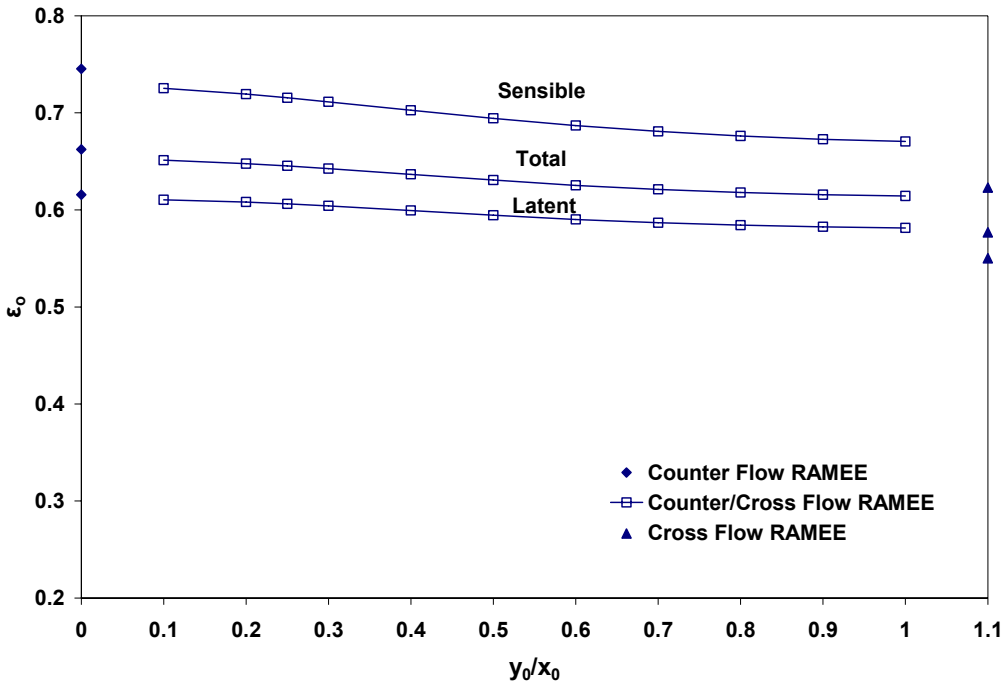

Figure 5.2 *Overall sensible, latent and total effectiveness of a RAMEE system with two counter/cross flow LAMEEs as a function of the aspect ratio (height to length) for NTU=10, Cr*=3, x_i/x_0=0.1 and AHRI summer conditions. The effectivenesses of the system with two pure cross and two pure counter-flow exchangers are included for comparison.*

Figure 5.2 shows that the overall effectiveness of the RAMEE system with two counter/cross flow exchangers is between the effectiveness of a RAMEE with two counter-flow exchangers and a RAMME with two cross-flow exchangers. For the case of a small entrance ratio (x_i/x_0=0.1), the effectiveness of the system is close to the effectiveness of an equivalent RAMEE system with two counter-flow exchangers.

It should be noted that the overall effectivenesses of the pure counter-flow and pure cross-flow RAMEEs are independent of aspect ratio at a constant NTU and Cr*. However, for a given NTU and Cr*, the values of the overall effectiveness of the RAMEE system with two counter/cross flow exchanger change as y_0/x_0 varies. This occurs since the liquid and air flow configuration relative to each other is different for different values of y_0/x_0 (refer to Figure 3.8)

5.4 Effect of NTU and Cr*

For the RAMEE system consisting of two identical counter/cross flow exchangers each with parameters used from Table 2.1, the variations of the overall effectivenesses with Cr* and NTU are presented in this Figures 5.3 and 5.4. The results in Figure 5.3 are shown for the AHRI summer condition and in Figure 5.4 are for the AHRI winter operating condition. The entrance ratio and aspect ratio of the exchangers employed are 0.1 and 0.5, respectively. As indicated in both figures, the overall sensible, latent and total effectivenesses of the RAMEE system increase as NTU increases. As Cr* increases the effectiveness values increase to a maximum value as Cr* reaches a critical value, Cr^*_{crit} Where, for the summer operating condition in Figure 5.3, Cr^*_{crit} is located between Cr*=2 and Cr*=3. Fan et al. (2006) found that the peak overall total effectiveness occured at approximately Cr*=3 which is in good agreement with the results presented for the AHRI summer condition. For the winter operating condition in Figure 5.4, Cr^*_{crit} is located between Cr*=1 and Cr*=2. As Cr* increases for $Cr^* > Cr^*_{crit}$ the $\varepsilon_{o,counter/cross}$ values remain nearly constant for both the summer and winter test conditions when NTU≤5. However, the $\varepsilon_{o,counter/cross}$ values for NTU=10 in both Figures 5.3 and 5.4 decrease moderately as Cr* increases beyond Cr^*_{crit}.

Under most conditions, it is desired to keep the RAMEE system operating at the condition when Cr* is close to Cr^*_{crit}. For constant NTU the mass flow rate of the salt solution can be adjusted with the pump speed or valve opening at the pump exit so that $Cr^* \approx Cr^*_{crit}$ to achieve the maximum effectiveness. Under part-load conditions, it is desirable to reduce the heat and moisture transfer of the RAMEE system by reducing Cr* (i.e., reducing the flow rate of the liquid). The slope of the effectiveness

curves in Figure 5.3 and 5.4 for $Cr^* < Cr^*_{crit}$ are higher for higher NTU values. This means that $\varepsilon_{o,counter/cross}$ is more sensitive to changes in Cr* (or liquid flow control) as the NTU of the system increases.

Comparing Figures 5.3 (c) and 5.4 (c), shows that the effectiveness depends on the operating conditions. The maximum overall total effectiveness at the AHRI winter conditions is greater than the overall total effectiveness at AHRI summer conditions for a certain value of NTU. For example, at NTU=10, the maximum total effectiveness of the RAMEE during the AHRI winter conditions is about 6% greater than the maximum total effectiveness of the system under AHRI summer test conditions. Also, the maximum overall total effectiveness occurs at different values of Cr* during the AHRI summer and winter conditions.

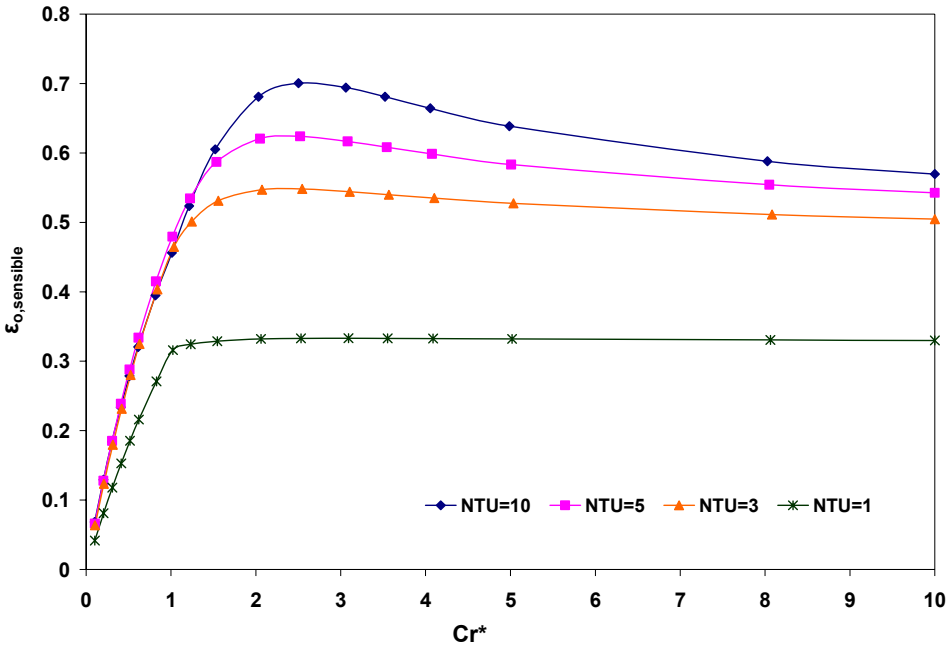

(a)

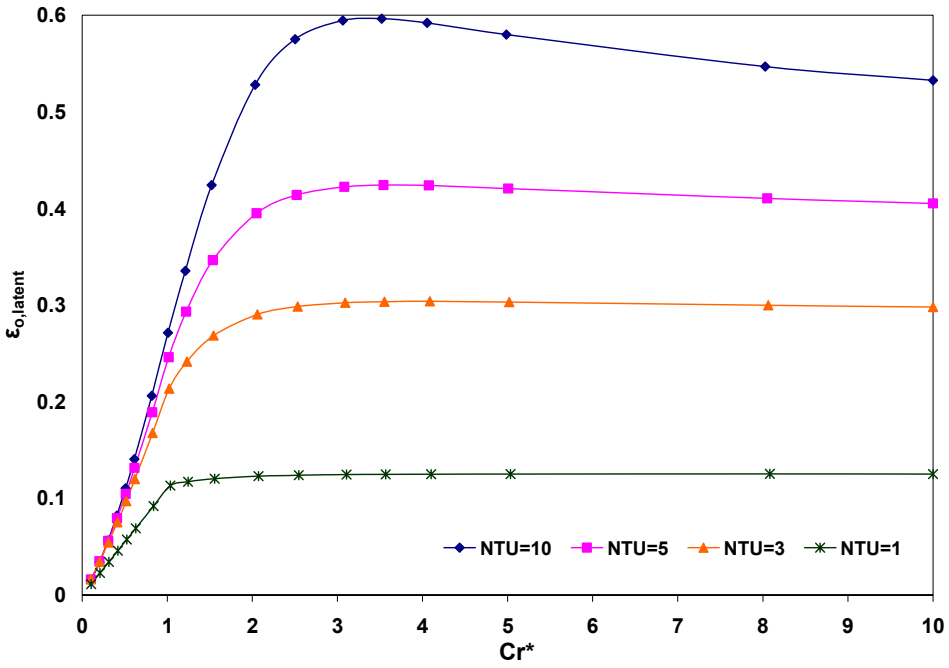

(b)

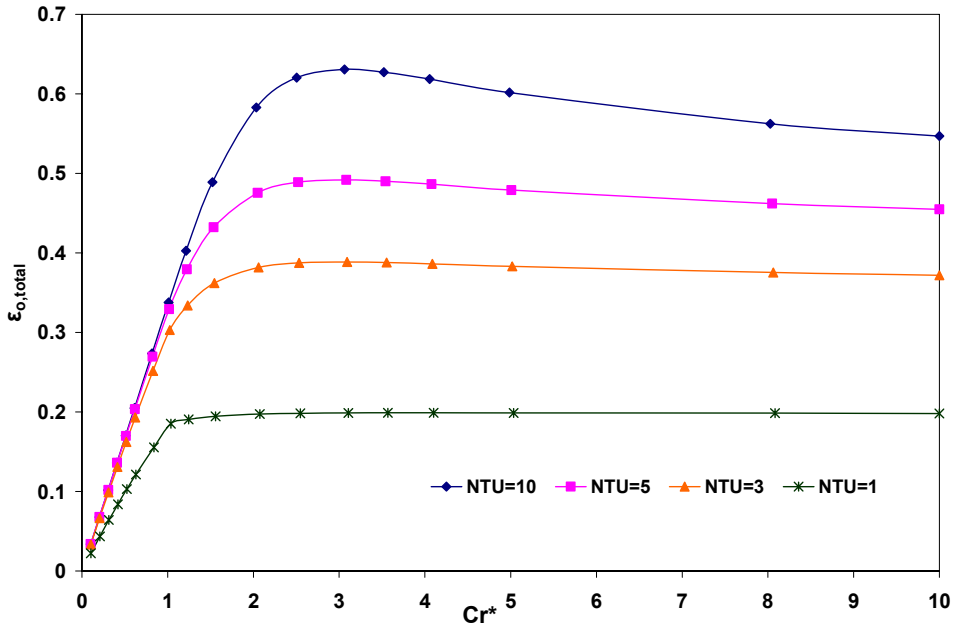

(c)

Figure 5.3 *Overall (a) sensible, (b) latent and (c) total effectiveness of a RAMEE system with two counter/cross flow exchangers as a function of Cr* and for different NTU values under AHRI summer operation condition,* $y_0/x_0=0.5$ *and* $x_i/x_0=0.1$

As shown in Figure 5.4 (b), for Cr*<0.5 the overall latent effectiveness of the RAMEE system can be negative. Negative latent effectiveness has been measured and

was simulated by Simonson et al. (2000) for air-to-air energy wheels when the rotational speed of the wheel was low (e.g. less than 5 rpm). A similar effect is seen here with the RAMEE system for low flow rates of coupling fluid. As can be seen in Appendix D Figure D.5, the large temperature difference caused the moisture transfer in reverse direction. For the RAMEE system, at low salt solution mass flow rates (i.e. Cr*<0.5 at constant air mass flow rate) and high NTUs (i.e. NTU>5), the heat flux is great and the temperature difference between the salt solution and air flow is large. Like the energy wheel, this causes the moisture to transfer in the opposite direction to its normal direction. Further explanation of negative latent effectiveness is presented in Appendix D.

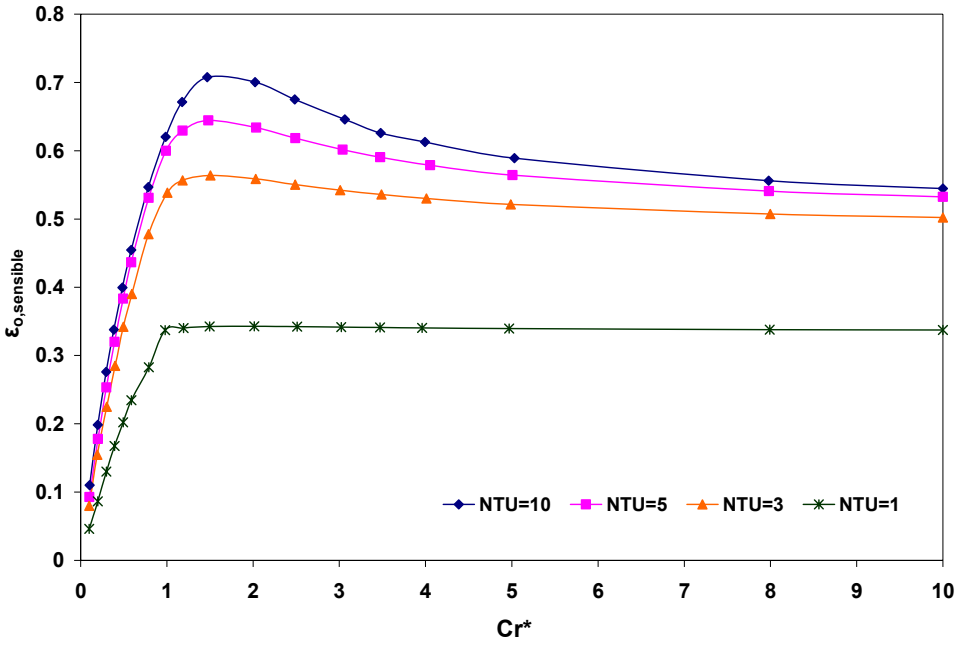

(a)

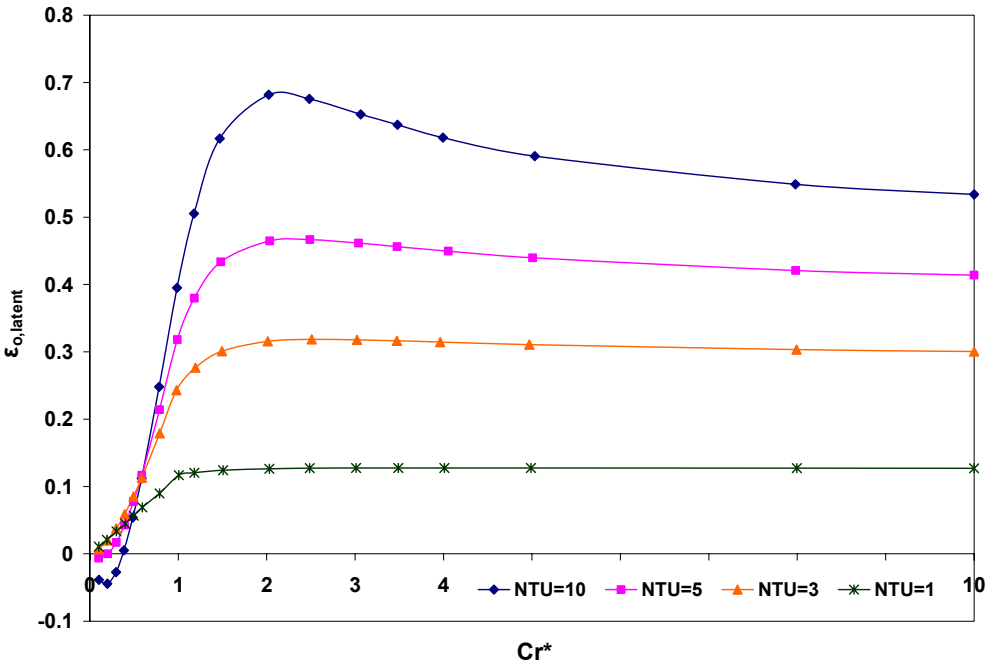

(b)

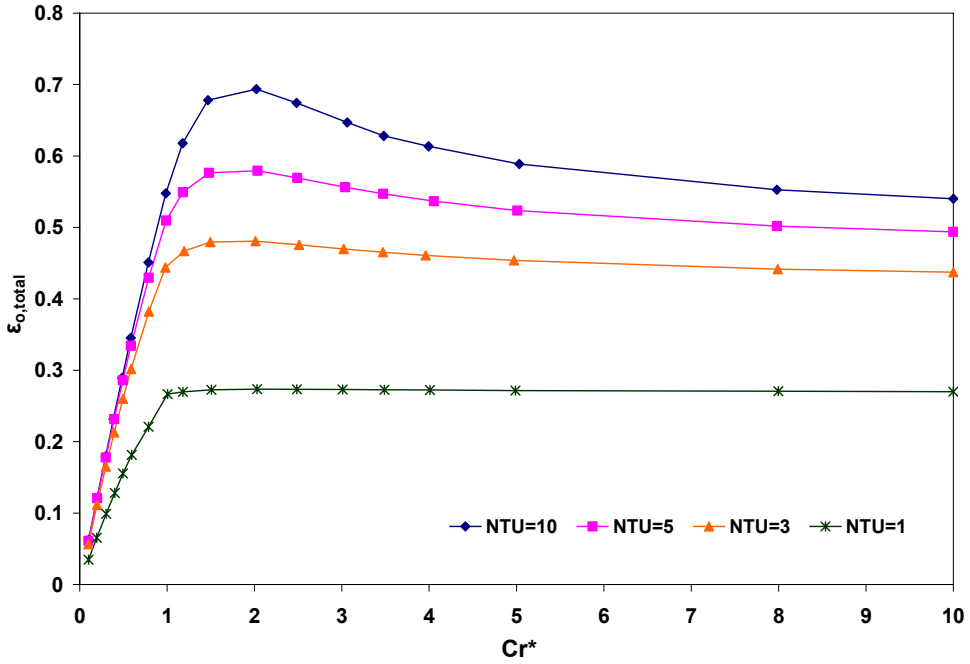

(c)

Figure 5.4 *Overall (a) sensible, (b) latent and (c) total effectiveness of a RAMEE system with two counter/cross flow exchangers as a function of Cr* and for different NTU values under AHRI winter operation condition, y_0/x_0=0.5 and x_i/x_0=0.1*

Figures 5.3 and 5.4 show that the RAMEE effectiveness peaks at Cr*≈3 (summer) and Cr*=1.5 (winter), while Chapter 3 showed a peak for run-around heat

exchanger (RAHE) effectiveness at Cr*=1 (i.e. at a lower solution flow rate). This difference in Cr^*_{crit} between the RAHE and RAMEE can be attributed to the latent heat of water vapour released or absorbed by the desiccant solution in the RAMEE. In summer, the supply air is hot and humid, so the salt solution obtains heat and moisture from the air stream in the supply exchanger. The water vapour condenses at the liquid-air interface and it releases latent heat to the liquid desiccant. Therefore, the heat capacity rate of the solution must be higher to absorb both the sensible and latent heat from the supply air stream.

Simonson and Besant (1999a) presented an operating condition factor, H*, which represents the ratio of latent to sensible energy change of inlet air streams and is defined as.

$$H^* = \frac{h_{fg}\Delta W}{c_p \Delta T} \approx 2500 \frac{W_{Air,in,S} - W_{Air,in,E}}{T_{Air,in,S} - T_{Air,in,E}} \tag{5.1}$$

This parameter may be used to explain why the maximum ε_o in the RAMEE occurs at different Cr* under the two different operating conditions (AHRI summer and winter). When H* is positive, the heat of phase change decreases the effective sensible heat transfer decreasing the sensible effectiveness. A RAMEE system operating under conditions with a positive H* releases the latent energy to the liquid stream in the supply exchanger, which decreases the ability of the coupling liquid to gain sensible heat from the supply air, resulting in a lower sensible effectiveness. On the other hand, if H* is negative, it enhances the ability of the coupling liquid to gain more heat from the air stream and the sensible effectiveness increases.

All in all, a system operating under positive H* needs a higher heat capacity rate of solution to air (i.e. greater Cr*) for optimum overall effectiveness. In other words, when H* is high and positive it means that the heat of phase change is greater

compared to the sensible heat transfer. In order to change the temperature of the air, the mass flow rate of the salt solution must be increased at a given NTU. The values of H* for AHRI summer and winter operating conditions are 1.86 and 0.47, respectively. Therefore, under the AHRI summer condition the maximum effectiveness occurs at greater Cr* compared to the case under the AHRI winter condition.

5.5 Effect of NTU_m and m*

The performance of the RAMEE system also depends on two other dimensionless groups which are associated with the mass transfer in the system. These are the number of mass transfer units (NTU_m) and mass flow rate ratio of pure salt in liquid desiccant to dry air ($m^* = \dot{m}_{Salt} / \dot{m}_{Air}$). The variations of the overall sensible, latent and total effectivenesses of the RAMEE system with the ratio of m* for different values of NTU_m are shown in Figures 5.5 and 5.6 for the AHRI summer and winter operating condition, respectively. As indicated in the figures, the overall effectivenesses increase initially with m* and then decrease moderately to a constant level as m* increases further (i.e. m*>3). The overall sensible, latent and total effectiveness distributions of the RAMEE system also increase with increasing NTU_m in general for both operating conditions. The ε_o is more sensitive to changes in NTU_m for lower values of NTU_m similar to what was seen in Figures 5.3 and 5.4 for ε_o versus NTU.

Similar to Figures 5.3 and 5.4, the maximum overall effectivenesses occur at a certain value of $m^* = m^*_{crit}$ which depends on the value of NTU_m and the operating conditions. For example, under the AHRI summer operating condition and for NTU_m=3 the maximum overall total effectiveness in Figure 5.5 (c) is approximately at m*≈1. However, for NTU_m=10 the maximum $\varepsilon_{o,}$ is at m*≈0.6. It can be concluded

from Figures 5.5 and 5.6 that the value of m^*_{crit} is reduced as NTU_m increases. It implies that for greater NTU_m lower salt solution mass flow rate is needed at the optimum performance for a given NTU_m. The slopes of the ε_o distributions in Figures 5.5 and 5.6 are higher at $m^*<m^*_{crit}$. This reveals that the effectiveness is more sensitive to m* at lower salt solution flow rates irrespective of the NTU_m values of the system.

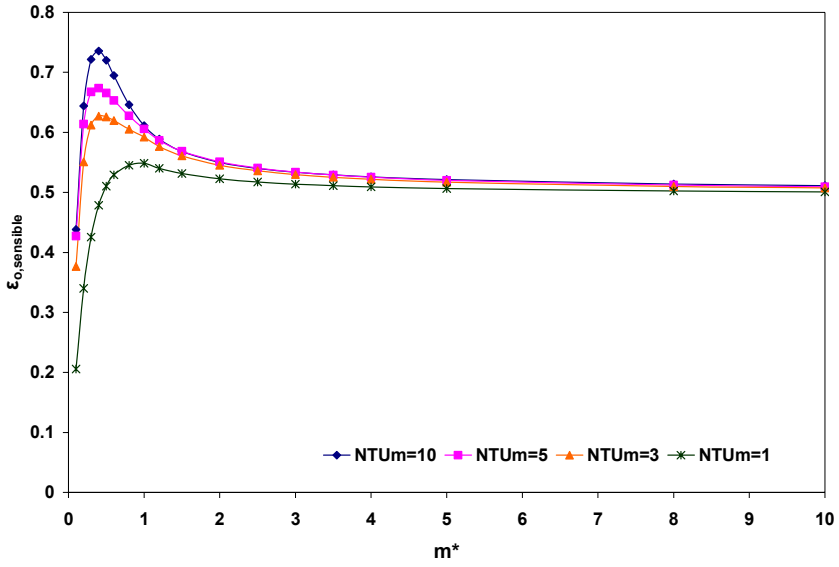

(a)

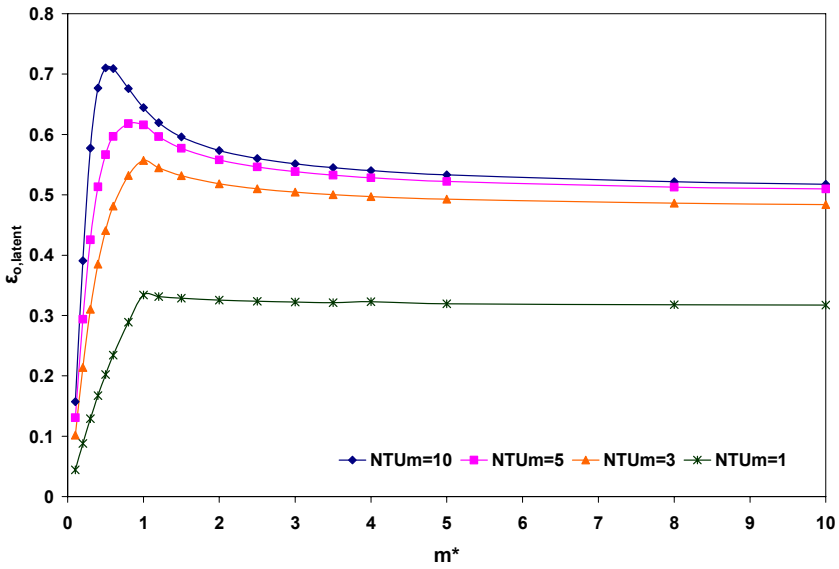

(b)

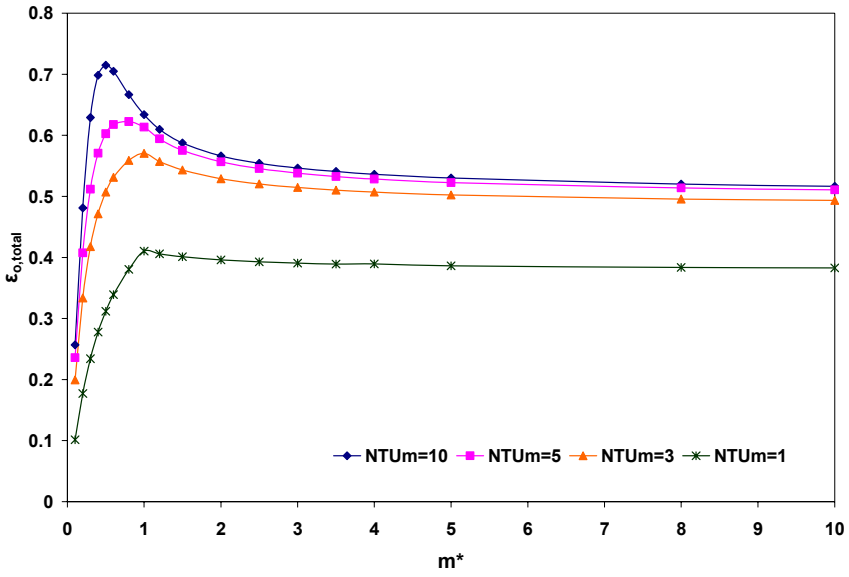

(c)

Figure 5.5 *Overall (a) sensible, (b) latent and (c) total effectiveness of a RAMEE system with two counter/cross flow exchangers as a function of m* and for different NTU_m values under AHRI summer operation conditions, $y_0/x_0=0.5$ and $x_i/x_0=0.1$*

The maximum overall effectiveness of the system for the winter operating conditions occurs at a lower m* than for the summer conditions. As discussed previously, a greater salt solution mass flow rate is required during summer conditions to achieve the maximum performance.

Under both AHRI summer and winter operating conditions, the values of overall effectiveness are almost independent from m* when m*>5. Fan et al. (2006) studied the RAMEE system with two identical cross-flow exchangers and the same trend was reported for the overall effectiveness as a function of NTU_m and m*.

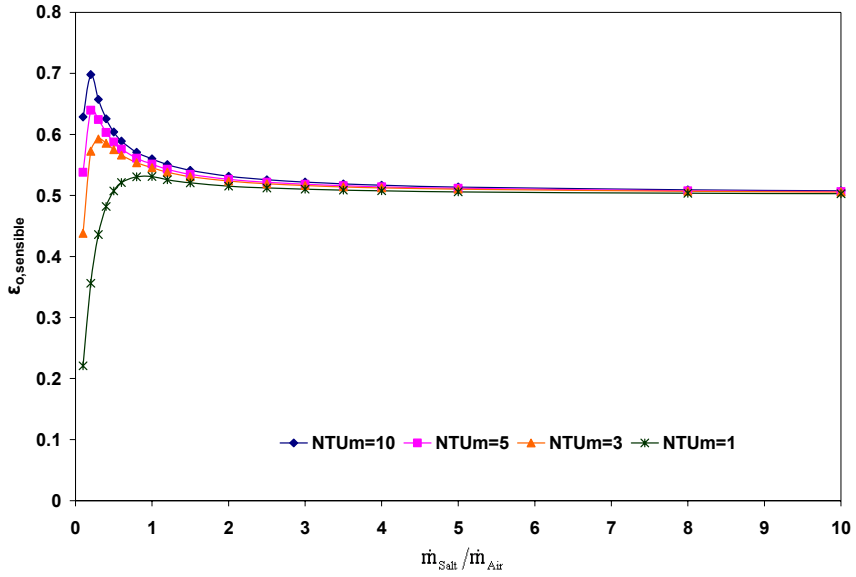
0.8
0.7
0.6
0.5
0.4
0.3
0.2
0.1
0
$\varepsilon_{o,sensible}$
NTUm=10
NTUm=5
NTUm=3
NTUm=1
0
1
2
3
4
5
6
7
8
9
10
$\dot{m}_{Salt}/\dot{m}_{Air}$

(a)

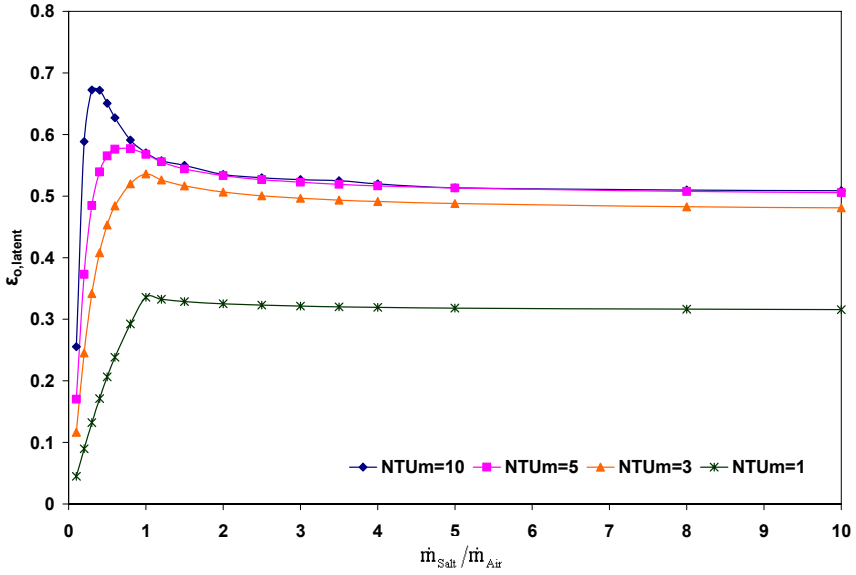
0.8
0.7
0.6
0.5
0.4
0.3
0.2
0.1
0
$\varepsilon_{o,latent}$
NTUm=10
NTUm=5
NTUm=3
NTUm=1
0
1
2
3
4
5
6
7
8
9
10
$\dot{m}_{Salt}/\dot{m}_{Air}$

(b)

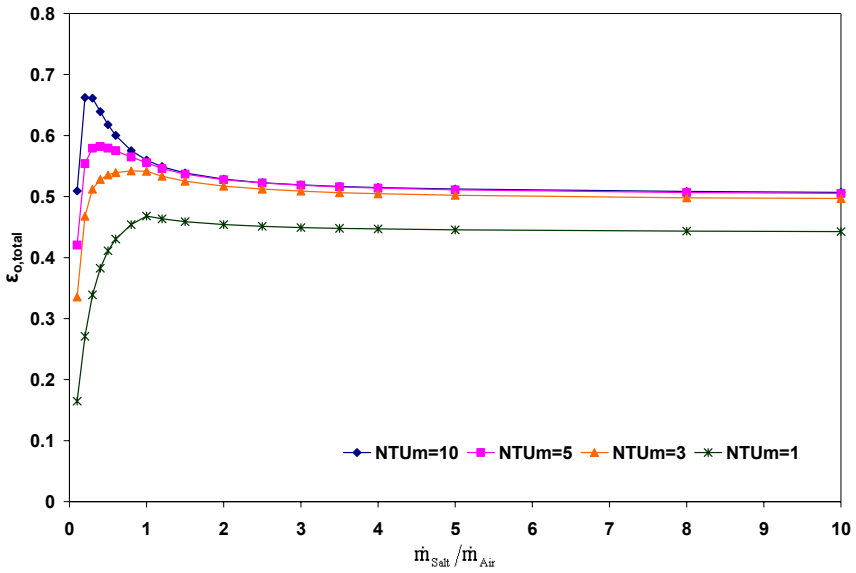

(c)

Figure 5.6 *Overall (a) sensible, (b) latent and (c) total effectiveness of a RAMEE system with two counter/cross flow exchangers as a function of* $\dot{m}_{Salt}/\dot{m}_{Air}$ *and for different* NTU_m *values under AHRI winter operation conditions,* $y_0/x_0=0.5$ *and* $x_i/x_0=0.1$

5.6 Effect of Flow Arrangement

One of the main purposes of this study is to develop a model for a RAMEE system consisting of two identical counter/cross flow exchangers to improve its performance compared to the RAMEE system with cross-flow exchangers (Fan et al. 2006, Erb 2007, Seyed Ahmadi 2008 and Erb et al. 2009). In this section, a comparison among three RAMEE systems is presented. These RAMEEs include purely counter-flow exchangers, counter/cross flow exchangers, and purely cross-flow exchangers. The comparison of the overall total effectiveness is shown in Figure 5.7. The LAMEE parameters employed for the simulations are listed in Table 2.1 with NTU=10, $x_i/x_0=0.1$ and $y_0/x_0=0.5$.

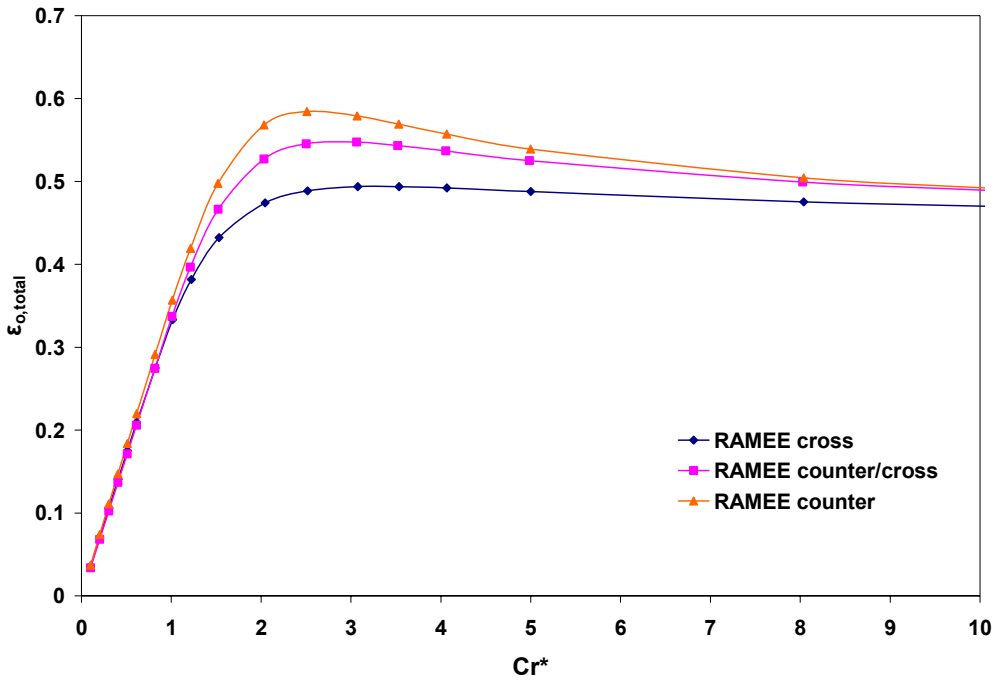

Figure 5.7 *Overall total effectiveness of the RAMEE system with two pure cross-flow, pure counter-flow and counter/cross flow heat and moisture exchangers with NTU=10. The counter/cross flow exchanger has an entrance ratio (x_i/x_0) of 0.1 and an aspect ratio (y_0/x_0) of 0.5*

As expected, Figure 5.7 shows that a RAMEE system with two counter-flow exchangers has the highest effectiveness at any given Cr* among the three RAMEE designs. However, as was mentioned previously, installing counter-flow exchangers in HVAC ducting has practical difficulties. Cross-flow exchangers are simplest to install in HVAC systems, but as expected, Figure 5.7 shows that they have the lowest effectiveness. The trends of $\varepsilon_{o,total}$ as a function of Cr* are similar for three RAMEEs.

Counter/cross flow exchangers are proposed for future RAMEE system in order to take advantage of the good performance of the counter-flow arrangement and to avoid the design problem associated with the counter-flow exchangers. As illustrated in Figure 5.7, the overall total effectiveness of the RAMEE system with two counter/cross flow LAMEEs falls between the overall total effectiveness of the

other two RAMEEs. The maximum $\varepsilon_{o,total}$ of the RAMEE system with two counter-flow exchangers is only 4% higher than the RAMEE system with two counter/cross flow exchangers when $x_i/x_0=0.1$, $y_0/x_0=0.5$ and NTU=10. The difference in $\varepsilon_{o,total}$ distributions are even smaller at other Cr* values. The RAMEE system with two counter/cross flow exchangers has a maximum of $\varepsilon_{o,total}$ which is 6% greater than the equivalent RAMEE system with two cross-flow exchangers.

Even though the performance of the RAMEE system with counter-flow exchangers is the best, a well-designed counter/cross flow RAMEE can have a high overall effectiveness that is quite close to the effectiveness of the system with counter-flow exchangers. In order to improve the performance of the RAMEE system with two counter/cross flow LAMEEs, the liquid-air flow arrangement must be as close as possible to the counter-flow configuration. It was illustrated in Figures 5.1 and 5.2 that a small aspect ratio and a small liquid entrance ratio of the exchanger in the counter/cross flow RAMEE would modify the liquid flow arrangement close to counter-flow configuration relative to the air stream. In the case where the exchangers aspect ratio is 0.5, entrance ratio is 0.1, Cr*>8, and NTU=10 the overall total effectiveness of the counter/cross flow RAMEE nearly equals the overall total effectiveness of the counter-flow RAMEE.

5.7 Summary

In this chapter, the effects of various dimensionless parameters on the performance of a RAMEE system with two counter/cross flow exchangers were presented. The impacts of the entrance ratio, aspect ratio, number of heat transfer units, heat capacity rate ratio, number of mass transfer units, mass flow rate ratio and the liquid-air flow configuration have been investigated. In general, the computed

overall effectiveness of the RAMEE model increases with Cr*, NTU, NTU_m and m*, but decreases as the x_i/x_0 and y_0/x_0 are increased.

It has been shown that the performance of the RAMEE system depends on the operating inlet air temperature and humidity. The numerical results have revealed that the overall effectiveness of a counter/cross flow RAMEE system falls between the overall effectivenesses of a counter-flow and a cross-flow RAMEE system with similar design and operating parameters. A well-designed counter/cross flow exchanger should have a small aspect ratio ($y_0/x_0<0.2$) and entrance ratio ($x_i/x_0<0.1$) to provide a RAMEE overall effectiveness that is almost as high as a counter-flow RAMEE system.

Chapter 6

Summary, Conclusions and Future Work

6.1 Summary and Conclusions

The main purpose of this study is to develop, validate and apply a numerical model to investigate the steady-state performance of a run-around membrane energy exchanger (RAMEE) system consisting of two counter/cross flow liquid-to-air membrane energy exchangers (LAMEEs). The counter/cross flow exchangers are employed in the RAMEE system to improve its performance. The overall objectives of this study can be summarized by two questions: (1) How effective is a RAMEE system using counter/cross flow exchangers compared to a similar RAMEE system with two cross-flow exchangers? (2) What are the parameters affecting the performance of a counter/cross flow RAMEE system and how can they be adjusted to optimize the performance of the system? To answer these questions, the RAMEE effectiveness has been presented for various geometric and flow design parameters. The following steps have been taken in this research

1. The numerical model to simulate the heat and moisture transfer in a RAMEE system with two counter/cross flow exchangers has been developed based on the physical principles in Chapter 2. The model is two-dimensional and steady state. A finite-difference method is used to solve the governing equations. The continuity and momentum equations are solved to determine the bulk mean velocity of the liquid desiccant flow at each point in the exchangers. With the bulk mean fluid velocity, the coupled heat and mass transfer governing equations are solved to determine the temperature and moisture contents of each fluid at each point in a LAMEE. The outlet properties calculated by the model are used to predict the overall sensible, latent and total energy effectiveness of the RAMEE system. The numerical model can predict

the performance of a RAMEE system using two cross-flow, counter-flow, or counter/cross flow LAMEEs. Some sensitivity studies are also performed to show the influence of the uncertainty of several design characteristics on the accuracy of the simulated results. It is revealed that the overall effectiveness of the RAMEE is noticeably sensitive to changing the membrane thickness and permeability. The overall latent effectiveness of the RAMEE decreases up to 13% as the membrane thickness is changed from 0.2 mm to 0.5 mm. changing the permeability with ±20% of the value used in the numerical model for Propore (1.66×10^{-6} kg/m^2.s) changes the latent effectiveness of the RAMEE in the range of ±3%.

2. The numerical model developed in Chapter 2 is validated, for the case of heat (i.e. sensible energy) transfer only, using correlations from the literatures in Chapter 3. Based on the comparisons presented between the numerical model and the correlations for the case of heat transfer only (i.e. no moisture transfer), it can be concluded that the numerical model provides reliable results. The discrepancies between simulated results and correlations are ±2% and ±2.5% for single heat exchangers and run-around heat exchangers (RAHE), respectively. The validated numerical model is then used to develop a new performance correlation for the flat-plate counter/cross flow heat exchangers. The new correlation is:

$$\varepsilon_{counter/cross} = \left[\left(\frac{y_0}{x_0}\right)\left(1+\frac{NTU}{200}\right)\varepsilon_{cross} + \left(1-\frac{y_0}{x_0}\right)\varepsilon_{counter}\right] \tag{6.1}$$

The values for the effectiveness of supply and exhaust LAMEEs can be determined from equation (6.1) and be used in Zeng's (1990) correlations for the RAHE to predict the overall sensible effectiveness of the counter/cross flow RAHE. The results from the new correlations agree with simulated results within ±2% for the single counter/cross flow heat exchangers and ±2% for the counter/cross flow RAHEs

(for over 200 and 400 simulated data points, respectively). These performance correlations can then be used for engineering design applications to select and predict the performance of the run-around systems. It should be noted that the effects of x_i/x_0 (i.e. entrance ratio) are ignored in the correlations based on the practical considerations. The new correlation is restricted to $0<x_i/x_0\leq0.25$ and extrapolation beyond $x_i/x_0=0.25$ will result in errors greater than 2%.

Both the model and the correlations have revealed that using counter/cross flow heat exchangers in a RAHE system improves its performance compared to the case of cross-flow exchangers. The improvement depends on design characteristics such as NTU, Cr and x_i/x_0 and y_0/x_0. For example, a counter/cross flow exchanger with a small entrance ratio (e.g. $x_i/x_0=0.1$) and small aspect ratio (e.g. $y_0/x_0=0.25$) has approximately 10% higher effectiveness compared to a similar cross-flow heat exchanger and a 1.5% lower effectiveness compared to a similar counter-flow exchanger (when NTU=15 and Cr=1). A RAHE with two counter/cross flow exchangers (with $x_i/x_0=0.1$ and $y_0/x_0=0.25$) has about 7% greater and 5% lower overall sensible effectiveness compared to the cross-flow and counter-flow RAHEs respectively (NTU= 5 and $C_L/C_A\approx1$).

To achieve a high overall effectiveness for the counter/cross flow RAHE, the followings can be recommended: (i) high NTU value, (ii) $0.8<C_L/C_A<1.2$, (iii) $0<y_0/x_0\leq0.3$, and (iv) $0<x_i/x_0\leq0.25$.

3. In Chapter 4, the numerical model for both the heat and moisture transfer was validated with numerical and experimental data. When the model is compared with another numerical model (Seyed Ahmadi 2008), the results differ by less than 1% of the overall effectiveness. The numerical model is also compared with the results from experiments on the RAMEE system. The experimental data were

measured by another graduate student at the University of Saskatchewan on a counter/cross flow RAMEE. The comparison shows that the experimental and numerical effectivenesses have similar sensitivities to *Cr**. The numerical and experimental results for the overall total effectiveness of the system also reveal good agreement for lower NTUs (e.g. NTU=4) where the differences are less than 4%. However, discrepancies between the numerical and experimental data increase as NTU increases (e.g. up to 17% difference in total effectiveness at NTU=12). The discrepancies exceed the experimental uncertainty bound at large NTUs (e.g. NTU>4)

4. The effects of various dimensionless parameters on the numerical performance of a RAMEE system using two counter/cross flow exchangers are presented in Chapter 5. The performance of the system is shown to be influenced by the change of the exchanger entrance ratio (the ratio of the length of the inlet and outlet headers to the total length of the exchanger) and exchanger aspect ratio (the ratio of the height over the length of the exchanger), number of heat transfer units, heat capacity rate ratio, number of mass transfer units, mass flow rate ratio of pure salt in desiccant solution to dry air, liquid-air flow configuration, and operating inlet temperature and humidity ratio. It is revealed that counter/cross flow exchangers in a RAMEE system can improve the performance when they are designed with the small aspect ratio (e.g. $y_0/x_0<0.2$) and entrance ratio (e.g. $x_i/x_0<0.1$) compared to a cross-flow RAMEE. Using the counter/cross flow exchangers can increase the overall maximum total effectiveness of the RAMEE system by 6% (at NTU=10, $Cr^*\approx3$, $y_0/x_0=0.5$ and $x_i/x_0=0.1$) compared to a similar system with two cross-flow exchangers. This counter/cross flow RAMEE has about 4% lower maximum total effectiveness compared to the similar counter-flow RAMEE. This difference can be

reduced as the aspect ratio, y_0/x_0, and entrance ratio, x_i/x_0, of the counter/cross flow LAMEEs are decreased.

6.2 Future Work

This study is part of a research project developing a run-around membrane energy exchanger (RAMEE) system and is focused on modeling the performance of a RAMEE consisting of two counter/cross flow exchangers.

In the study presented in this thesis, the numerical model has been compared with experimental data. It is speculated that several modifications are needed in the model to decrease the discrepancy between the experiment and the simulation. One of the modifications is the inclusion of non-uniformity in the fluid flow through the exchanger channels. In the current model it is assumed that the flow channels are uniform and the air and liquid desiccant flow rates are distributed uniformly (i.e. every channel has the same size and flow rate). In reality, this is not the case. As a result of pressure variation through the exchangers, the fluid channels are deformed and it causes a variation in the channel sizes and different flow rates through different channels. The study of the non-uniform flow distributions, which could include flow visualization, may explain the difference between the numerical and experimental data.

From this study it is revealed that the properties of the membrane (e.g. permeability) are very important factors which affect the performance of the RAMEE system. A study is recommended to search for a new membrane material with uniform properties across its volume.

The value used in this study for the thickness of the membrane was measured with large uncertainty. As shown in this study, the thickness of the membrane affects the results substantially. Therefore, the thickness of the membrane should be

measured using the measurement conditions according to available standards (e.g., textile standards).

The impacts of frosting on the air side and crystallization of the salt solution on the performance of the system are other important topics for investigation. These effects can be very critical under certain operating conditions. Frosting on the air side and crystallization of the desiccant can change the permeability of the membrane which affects the heat and mass transfer in the system significantly. Besides, in this study only $MgCl_2$ salt solution as the coupling liquid has been examined. It is believed that the type of the salt solution also affects the system performance. Therefore, the behavior of a RAMEE system using different salt solutions should be studied to search and determine the best desiccant for the RAMEE system. The best salt solution should be determined considering the performance, cost, operating conditions, and environment.

A study is also recommended to investigate the part load control of the RAMEE system. The transient behavior of the system has been examined (Seyed Ahmadi 2008) and it has been shown that the required time for the system to reach equilibrium under certain operating conditions is very long. This may limit the application of the system in cases when the system is run periodically. Therefore, methods are needed to control the system and reduce transient times.

This study has developed effectiveness correlations for the system when it only transfers heat between two participating air streams (RAHE system). Another study should be done to develop correlations for the overall sensible, latent, and total effectiveness of the RAMEE system.

REFRENCES

Ali, A., Vafai, K. and Khaled, A.-R.A., 2003. Comparative study between parallel and counter-flow configurations between air and falling film desiccant in the presence of nanoparticle suspensions, *Int. J. Energy Res.*, **27** (8), 725–745

Ali, A., Vafai, K. and Khaled, A.-R.A., 2004. Analysis of heat and mass transfer between air and falling film in a cross flow configuration, *International Journal of Heat and Mass Transfer* **47**, 743-755.

Abdou, O.A., Lorsch, H.G., 1994. Impact of the building indoor environment on occupant productivity - part 3: effects of indoor air quality. *ASHRAE Transactions* **100**(2), 902-913

ANSI/AHRI Standard 1060-2005, *Standard for Rating Air-to-Air Exchangers for Energy Recovery Ventilation Equipment*, Air-Conditioning & Refrigeration Institute, Arlington

ANSI/ASHRAE Standard 55-2004, *Thermal environmental conditions for human occupancy*, ASHRAE, Atlanta

ANSI/ASHRAE Standard 62.1-2004, *Ventilation for acceptable indoor air quality*, ASHRAE, Atlanta

ANSI/ASHRAE Standard 84-2008, *Method of Test for Air to Air Heat/Energy Exchangers*, ASHRAE, Atlanta

ANSI/ASME Standard PTC 19.1-1998, Measurement uncertainty, ASME, New York

ASHRAE, 2004. *ASHRAE Handbook-HVAC System and Equipment*, ASHRAE, Atlanta

ASHRAE, 2005. *ASHRAE Handbook-Fundamentals*, ASHRAE, Atlanta

Bennett, I.J.D., Besant, R.W. and Schoenau, G.J., 1994. Validation of a run-around heat recovery system model, *ASHRAE Transactions* **100**(1), 230-237.

Bennett, I.J.D., Besant, R.W., Schoenau, G.J. and Johnson, A.B., 1994. Procedure for optimizing coils in a runaround heat exchanger system, *ASHRAE Transactions* **100**(1), 442-451.

Besant, R.W. and Simonson, C.J., 2000. Air-to-air energy recovery, *ASHRAE Journal*, **42**(5), 31-42.

Besant, R.W. and Simonson, C.J., 2003. Air-to-air exchangers, *ASHRAE Journal,* **45**(4), 42-52.

Cisternas, L.A. and Lam, E.J., 1991. Analytic correlation for the vapor pressure of aqueous and non-aqueous solutions of single and mixed electrolytes: Part II - Application and extension, *Fluid phase equilibria,* **62**(1), 11-27.

Dhital, P., Besant, R.W. and Schoenau, G.J., 1995. Integrating run-around heat exchanger systems into the design of large office buildings, *ASHRAE Transactions* **101**(2), 979-991.

Dieckmann, J., Roth, K.W. and Brodrick, J., 2003. Air-to-air energy recovery heat exchangers, *ASHRAE Journal*, 57–58.

Erb, B., 2006. *Designing and Testing a Run-Around Heat and Moisture Recovery System*, Summer Work Report, Department of Mechanical Engineering, University of Saskatchewan, Saskatoon, Saskatchewan

Erb, B., 2007. Run-*around membrane energy exchanger prototype 2 testing*, Summer Work Report, Department of Mechanical Engineering, University of Saskatchewan, Saskatoon, Saskatchewan

Erb, B., Seyed-Ahmadi, M., Simonson, C.J. and Besant, R.W., 2009. Experimental measurements of a run-around membrane energy exchanger (RAMEE) with comparison to numerical modeling, *ASHRAE Transactions*, **115**(2) (in press)

Fan, H., Simonson, C.J., Besant, R.W. and Shang, W., 2005. Run-around heat recovery system using cross-flow flat-plate heat exchangers with aqueous ethylene glycol as the coupling fluid. *ASHRAE Transactions* **111**(1), 901-910.

Fan, H., Simonson, C.J., Besant, R.W. and Shang, W., 2006. Performance of a run-around system for HVAC heat and moisture transfer applications using cross-flow plate exchangers coupled with aqueous lithium bromide. *HVAC&R Research* **12**(2), 313-336

Fan, H., 2005. *Modeling a Run-Around Heat and Moisture Recovery System,* M.Sc thesis, Department of Mechanical Engineering, University of Saskatchewan, Saskatoon, Saskatchewan

Fang, L., Clausen, G. and Fenger, P.O., 2000. Temperature and humidity: important factors for perception of air quality and for ventilation requirements. *ASHRAE Transactions* **106**(1), 503-510

Fehrm, M., Reiners, W. and Ungemach, M., 2002. Exhaust air heat recovery in buildings, *International Journal of Refrigeration* **25**, 439–449

Fauchoux, M., Simonson, C.J. and Torvi, D.A., 2007. The effect of energy recovery on perceived air quality, energy consumption and economics of an office building, *ASHRAE Transactions,* **113**(2), 437-449.

Forsyth, B.I. and Besant, R.W., 1988a. The design of a run-around heat recovery system, *ASHRAE Transactions,* **94**(2), 511-531.

Forsyth, B.I. and Besant, R.W., 1988b. The performance of a run-around heat recovery system using aqueous glycol as a coupling liquid, *ASHRAE Transactions,* **94**(2), 532-545.

Hemingson, H. 2005. Preliminary testing for run around heat and moisture exchanger, Summer Work Report, Department of Mechanical Engineering, University of Saskatchewan, Saskatoon, Saskatchewan, 15 pages

Incropera, F.P. and Dewitt, D.P., 2002. *Fundamentals of Heat and Mass Transfer*, 5th ed. John Wiley & Sons, New York

Johnson, A.B., Besant, R.W. and Schoenau, G.J., 1995. Design of multi-coil run-around heat exchanger systems for ventilation air heating and cooling, *ASHRAE Transactions* **101**(2), 967-978.

Johnson, A.B. and Besant, R.W., 1995. Reducing energy costs using run-around systems, *ASHRAE Journal* **37** (2, Feb.), 41-46.

Kays, W.M. and London, A.L., 1984. *Compact Heat Exchangers.* McGraw-Hill, Toronto

Kuppan, T., 2000. *Heat exchanger design handbook*, Marcel Dekker, New York

Lagoudi, A., Loizidou, M., Santamouris, M. and Asimakopoulos, D., 1996. Symptoms experienced, environmental factors and energy consumption in office buildings. *Energy and Buildings,* **24**, 237-243

Larson, M.D., 2006. *The performance of membrane in a newly proposed run-around heat and moisture exchanger*, M.Sc. Thesis, Department of Mechanical Engineering, University of Saskatchewan, Saskatoon, Saskatchewan

Larson, M.D., Besant, R.W. and Simonson, C.J., 2008. The effect of membrane deflections on flow rate in cross-flow air-to-air exchangers, *HVAC&R Research*, **14**(2), 275-288

Larson, M.D., Simonson, C.J., Besant, R.W. and Gibson, P.W., 2007. The elastic and moisture transfer properties of polyethylene and polypropylene membranes for use in liquid-to-air energy exchangers, *Journal of Membrane Science*, 302, 136-149

London, A.L. and Kays, W.M., 1951. Liquid-coupled indirect-transfer regenerator for gas-turbine plants, *Transactions of the American Society of Mechanical Engineers,* **73**(5), 529-542.

Liu, X.H., Jiang, Y. and Qu, K.Y., 2007. Heat and mass transfer model of cross-flow liquid desiccant air dehumidifier/regenerator. *Energy conversion and management,* **48**(2), 546-554.

Luo, X. and Roetzel, W., 1998. Theoretical investigation on cross-flow heat exchangers with axial dispersion in one fluid, *Revue générale de thermique,* **37**(3), 223-233.

Mahmud, K., 2009. *Design and Testing of a Laboratory RAMEE System with Counter-Flow Exchangers to Transfer Heat and Moisture Vapour between Supply and Exhaust Air Flows*, M.Sc Thesis in progress , Department of Mechanical Engineering, University of Saskatchewan, Saskatoon, Saskatchewan

Mesquita, L.C.S., Harrison, S.J. and Thomey, D., 2006. Modeling of heat and mass transfer in parallel plate liquid –desiccant dehumidifiers, *Solar Energy*, **80**,1475-1482.

Moore, A.D., 1949. Fields from fluid flow mappers, *Journal of Applied Physics*, **20**, 790-804

Niu, J.L. and Zhang, L.Z., 2001. Membrane-based Enthalpy Exchanger: Material considerations and clarification of moisture resistance, *Journal of membrane science,* **189**(2), 179-191.

Niu, J. and Zhang, L., 2002. Potential energy savings for conditioning fresh air with a membrane-based energy recovery ventilator, *ASHRAE Transactions,* **108**(1), 54-63

Park, M.S., Howell, J.R., Vliet, G.C. and Peterson, J., 1994. Numerical and experimental results for coupled heat and mass transfer between a desiccant film and air in cross-flow, *International Journal of Heat and Mass Transfer,* **37**(Suppl. 1), 395–402.

Robertson, J.M., 1965. *Hydrodynamics in theory and application*. Prentice-Hall, inc./Englewood Cliffs, N.J.

Seyed Ahmadi, M., 2008. *Modeling the Transient Behavior of a Run-around Heat and Moisture Exchanger System*, M.Sc Thesis, Department of Mechanical Engineering, University of Saskatchewan, Saskatoon, Saskatchewan

Simonson, C.J. and Besant, R.W., 1997a. Heat and moisture transfer in desiccant coated rotary energy exchangers: Part I - Numerical model. *HVAC & R research,* **3**(4), 325-350.

Simonson, C. J. and Besant, R.W., 1997b, Heat and moisture transfer in desiccant coated rotary energy exchangers: Part II - Validation and sensitivity studies, *HVAC & R Research*, **3**(4), 35 1-368.

Simonson, C.J. and Besant, R.W., 1999a. Energy wheel effectiveness: Part I - development of dimensionless groups, *International journal of heat and mass transfer,* **42**(12), 2161-2170.

Simonson, C.J. and Besant R.W., 1999b. Energy wheel effectiveness: Part II-correlations. *International Journal of Heat and Mass Transfer* **42**, 2171_2185

Simonson, C.J., Shang, W. and Besant, R.W., 2000. Part-load performance of energy wheels: Part I - Wheel speed control, ASHRAE Trans., 106(1), 286-300

Simonson, C.J. 1998. *Heat and Moisture Transfer in Energy Wheels*, Ph.D. Thesis, Department of Mechanical Engineering, University of Saskatchewan, Saskatoon, Saskatchewan

Wargocki, P., Bako´-Biro´, Z., Clausen, G. and Fanger, P.O., 2002. Air quality in a simulated office environment as a result of reducing pollution sources and increasing ventilation. *Energy and Buildings* **34**, 775–783

White, F.M., 2003. *Fluid mechanics*, McGraw-Hill, Boston

Zaytsev, I.D. and Aseyev, G.G., 1992. *Properties of Aqueous Solutions of Electrolytes*, CRC Press, Inc.

Zeng, Y.Y., Besant, R.W. and Rezkallah, K.S., 1992. The effect of temperature-dependent properties on the performance of run-around heat recovery systems using aqueous-glycol coupling fluids. *ASHRAE Transactions* **98**(l), 551-562.

Zeng, Y.Y., Besant, R.W. and Rezkallah, K.S., 1992. The performance of a run-around system using a two-phase, gas-liquid coupling fluid. *ASHRAE Transactions* **98**(l),563-573.

Zeng, Y.Y., 1990. A study of the performance of run-around heat recovery system using aqueous glycol/air as the coupling fluid, M.Sc thesis. The University of Saskatchewan, Saskatoon, SK, Canada.

Zhang, L.Z. and Jiang, Y., 1999. Heat and mass transfer in a membrane-based energy recovery ventilator, *Journal of Membrane Science* **163**, 29-38.

Zhang, Y., Jiang, J., Zhang, L. Z., Deng, Y. and Jin, Z., 2000. Analysis of thermal performance and energy savings of membrane based heat recovery ventilator, *Energy* **25,** 515–527

Zhang, L.Z. and Niu, J.L., 2002. Effectiveness correlations for heat and moisture transfer processes in an enthalpy exchanger with membrane cores, *Journal of Heat Transfer,* **124**(5), 922-929.

Appendix A

Development of Governing Equations for Numerical Model

To develop the governing equations for the heat and moisture exchanger, the calculation domain representing a heat and moisture exchanger channel is divided into infinitesimal control volumes. The control volume and the coordinate system shown in Figure A.1

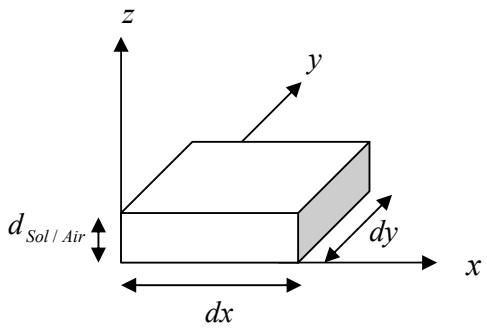

Figure A.1 *The coordinate system and the control volume of the exchanger*

A.1 Mass Transfer Equation

A.1.1 Air Side

To develop mass transfer equation in air side a separated infinitesimal control volume in the air side of the heat exchanger, as shown in Figure A.2, is investigated. Couple of assumptions are used in driving the equations such as steady state conditions and no mass diffusion in x and y directions. Therefore, the mass transfer equation can be developed.

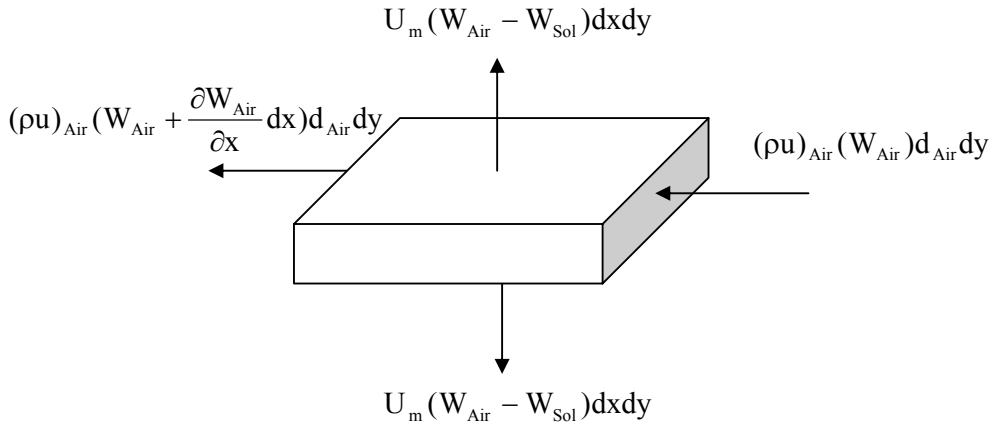

Figure A.2 *Mass transfer in an infinitesimal Control volume of the air flow*

According to the principle of conservation of mass, the inlet and outlet water vapor mass flow rates must be in balance therefore:

$$(\rho u)_{Air}(W_{Air})d_{Air}dy = 2U_m(W_{Air} - W_{Sol})dxdy + (\rho u)_{Air}(W_{Air} + \frac{\partial W_{Air}}{\partial x}dx)d_{Air}dy \quad \text{(A-1)}$$

which can be simplified to:

$$2U_m(W_{Air} - W_{Sol}) = -(\rho d)_{Air}(u_{Air}\frac{\partial W_{Air}}{\partial x}) \quad \text{(A-2)}$$

The air mass flow rate in each air channel is:

$$m_{Air} = \rho_{Air} u_{Air} d_{Air} y_0 \quad \text{(A-3)}$$

Substituting the mass flow rate of air in equation (A-2):

$$\frac{2U_m y_0}{m_{Air}}(W_{Air} - W_{Sol}) = -\frac{\partial W_{Air}}{\partial x} \quad \text{(A-4)}$$

where U_m is overall mass transfer coefficient

$$U_m = \left[\frac{1}{h_{m,Air}} + \frac{\delta}{k_m}\right]^{-1} \quad \text{(A-5)}$$

W_{Air} is the humidity ratio of air which is the ratio of the mass of water vapor in air to the mass of dry air and is a function of relative humidity and temperature of the air:

$$W_{Air} = \frac{\text{mass}H_2O}{\text{mass}Air} = f(\phi_{Air}, T_{Air}) \tag{A-6}$$

and W_{Sol} is the equilibrium humidity ratio of the salt solution which is a function of temperature and salt concentration of the solution.

$$W_{Sol} = f(X_{Sol}, T_{Sol}) \tag{A-7}$$

A.1.2 Liquid Side

A separated infinitesimal control volume in the liquid side of the heat exchanger is shown in Figure A.3. Using the same procedure and same assumptions for air side the mass transfer equation in liquid side is developed.

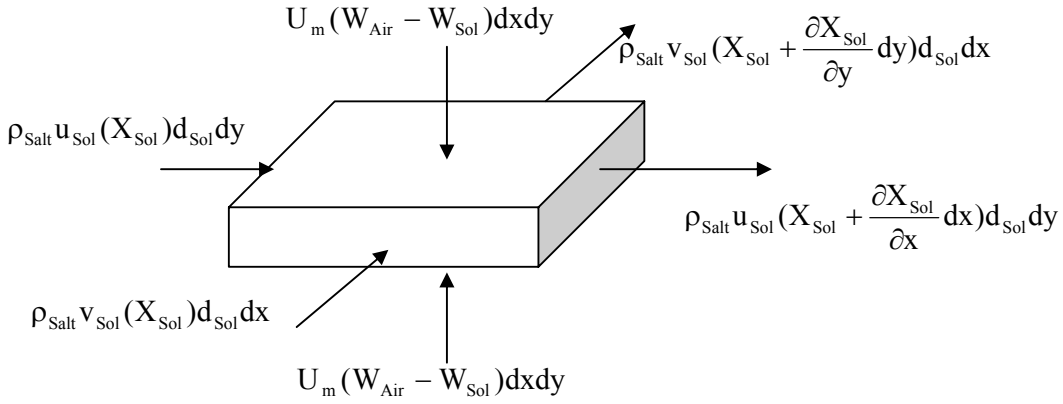

Figure A.3 *mass transfer in an infinitesimal control volume of the liquid flow*

Conservation of mass of water:

$$\begin{aligned}&\rho_{Salt} v_{Sol}(X_{Sol})d_{Sol}dx + \rho_{Salt} u_{Sol}(X_{Sol})d_{Sol}dy + 2U_m(W_{Air} - W_{Sol})dxdy = \\ &\rho_{Salt} v_{Sol}(X_{Sol} + \frac{\partial X_{Sol}}{\partial y} dy)d_{Sol}dx + \rho_{Salt} u_{Sol}(X_{Sol} + \frac{\partial X_{Sol}}{\partial x} dx)d_{Sol}dy\end{aligned} \tag{A-8}$$

which can be simplified to:

$$2U_m(W_{Air} - W_{Sol}) = \rho_{Salt} d_{Sol}(u_{Sol} \frac{\partial X_{Sol}}{\partial x} + v_{Sol} \frac{\partial X_{Sol}}{\partial y}) \tag{A-9}$$

where X_{Sol} is water mass fraction of salt solution and is the ratio of the mass of water in salt solution to the mass of pure salt:

$$X_{Sol} = \frac{Mass H_2O}{Mass Pure Salt} \tag{A-10}$$

A.2 Heat Transfer Equation

A.2.1 Air Side

Energy transfer in an infinitesimal control volume in air side is shown in Figure A.4.

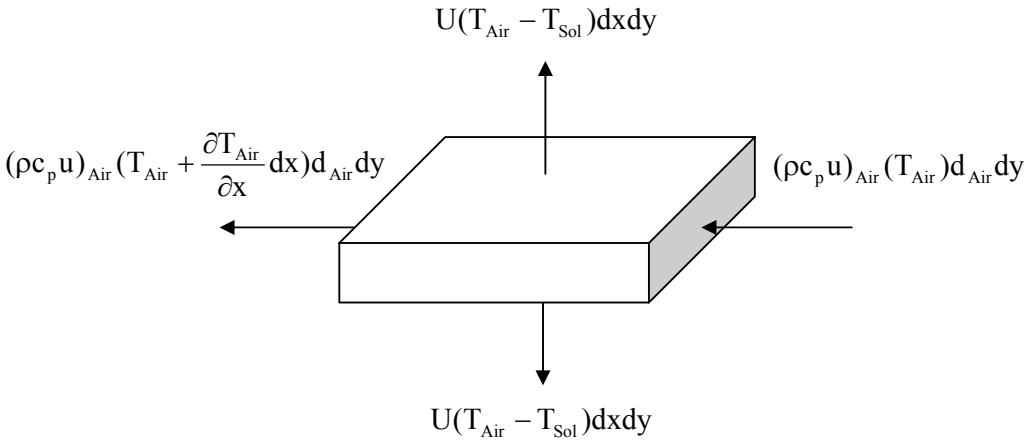

Figure A.4 *Heat transfer in an infinitesimal control volume of the air flow*

The heat gain and loss in this control volume must be in balance, according to conservation of energy

$$(\rho c_p u)_{Air}(T_{Air})d_{Air}dy = 2U(T_{Air} - T_{Sol})dxdy + (\rho c_p u)_{Air}(T_{Air} + \frac{\partial T_{Air}}{\partial x}dx)d_{Air}dy \tag{A-11}$$

which can be simplified to:

$$2U(T_{Air} - T_{Sol}) = -(\rho c_p d)_{Air}(u_{Air}\frac{\partial T_{Air}}{\partial x}) \tag{A-12}$$

The heat capacity rate of air in each channel is

$$C_{Air} = m_{Air} c_{P,Air} \tag{A-13}$$

Using the heat capacity rate of air in a single channel in equation (A-12):

$$\frac{2Uy_0}{C_{Air}}\left(T_{Air} - T_{Sol}\right) = -\frac{\partial T_{Air}}{\partial x} \tag{A-14}$$

Where U is overall heat transfer coefficient:

$$U = \left[\frac{1}{h_{Sol}} + \frac{\delta}{k} + \frac{1}{h_{Air}}\right]^{-1} \tag{A-15}$$

A.2.1 Liquid Side

The energy equation in liquid side can be developed by following a similar analysis as presented in previous sections. It is also assumed that water phase change occurs only in liquid channels. Therefore, another term which is accounting for water phase change is considered in energy equation on the liquid side. A control volume on the liquid side is shown in Figure A.5.

Based on conservation of energy:

$$\begin{aligned}&(\rho c_p u)_{Sol}(T_{Sol})d_{Sol}dy + (\rho c_p v)_{Sol}(T_{Sol})d_{Sol}dx + 2U(T_{Air} - T_{Sol})dxdy + 2U_m h_{fg}(W_{Air} - W_{Sol})dxdy = \\ &(\rho c_p u)_{Sol}(T_{Sol} + \frac{\partial T_{Sol}}{\partial x}dx)d_{Sol}dy + (\rho c_p v)_{Sol}(T_{Sol} + \frac{\partial T_{Sol}}{\partial y}dy)d_{Sol}dx\end{aligned} \tag{A-16}$$

which can be simplified to:

$$2U(T_{Air} - T_{Sol}) + 2U_m h_{fg}(W_{Air} - W_{Sol}) = (\rho c_p d)_{Sol}(u_{Sol}\frac{\partial T_{Sol}}{\partial x} + v_{Sol}\frac{\partial T_{Sol}}{\partial y}) \tag{A-17}$$

where $2U_m h_{fg}\left(W_{Air} - W_{Sol}\right)$ is the energy of phase change.

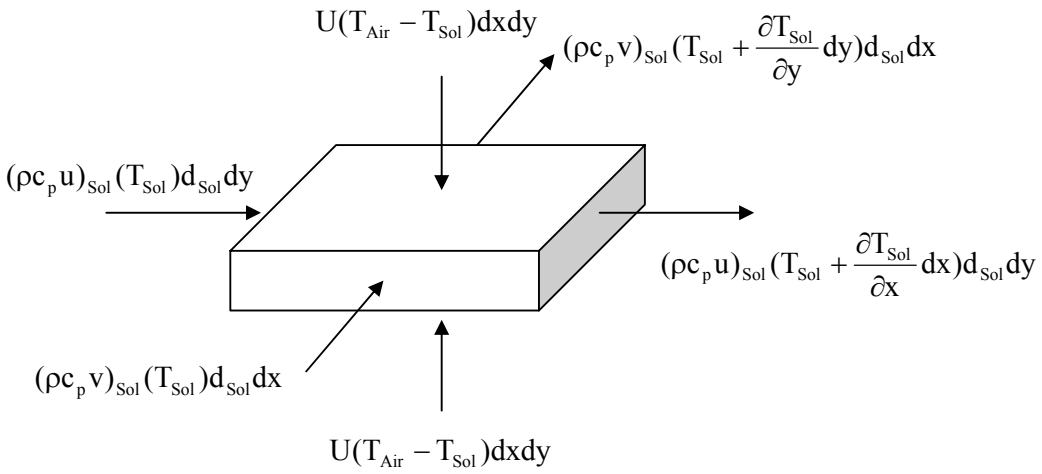

Figure A.5 *Heat transfer in an infinitesimal control volume of the liquid flow*

A.3 Discretization of the governing equations

The governing equations developed in the preceding sections are discretized in this section. The finite difference method is used in this study to solve coupled heat and mass transfer equations in the air and liquid sides. Backward differencing scheme is applied to solve the coupled heat and mass transfer equations and central scheme is used to solve Laplace equation to determine liquid flow distribution numerically. The discretized equations are listed below:

Liquid flow distribution:

From equation (2.3)

$$\frac{\psi^{i+1,j} - 2\psi^{i,j} + \psi^{i-1,j}}{(\Delta x)^2} + \frac{\psi^{i,j+1} - 2\psi^{i,j} + \psi^{i,j-1}}{(\Delta y)^2} = 0 \qquad \text{(A-18)}$$

Air side:

From equation (A-4)

$$\left(\frac{2U_m y_0 \Delta x}{m_{Air}} - 1\right) W_{Air}^{i,j} - \left(\frac{2U_m y_0 \Delta x}{m_{Air}}\right) W_{Sol}^{i,j} + W_{Air}^{i+1,j} = 0 \qquad \text{(A-19)}$$

and equation (A-14)

$$\left(\frac{2Uy_0\Delta x}{C_{Air}}-1\right)T_{Air}^{i,j}-\left(\frac{2Uy_0\Delta x}{C_{Air}}\right)T_{Sol}^{i,j}+T_{Air}^{i+1,j}=0 \tag{A-20}$$

Liquid side:

From equation (A-9)

$$\left(\frac{u_{Sol}^{i,j}}{\Delta x}+\frac{v_{Sol}^{i,j}}{\Delta y}\right)X_{Sol}^{i,j}-\left(\frac{u_{Sol}^{i,j}}{\Delta x}\right)X_{Sol}^{i-1,j}-\left(\frac{v_{Sol}^{i,j}}{\Delta y}\right)X_{Sol}^{i,j-1}-\frac{2U_m}{\rho_{Salt}d_{Sol}}\left(W_{Air}^{i,j}-W_{Sol}^{i,j}\right)=0 \tag{A-21}$$

and equation (A-17)

$$\left(\frac{u_{Sol}^{i,j}}{\Delta x}+\frac{v_{Sol}^{i,j}}{\Delta y}\right)T_{Sol}^{i,j}-\left(\frac{u_{Sol}^{i,j}}{\Delta x}\right)T_{Sol}^{i-1,j}-\left(\frac{v_{Sol}^{i,j}}{\Delta y}\right)T_{Sol}^{i,j-1}-\frac{2U}{\rho_{Salt}c_{P,Sol}d_{Sol}}\left(T_{Air}^{i,j}-T_{Sol}^{i,j}\right) \tag{A-22}$$
$$-\frac{2U_m h_{fg}}{\rho_{Salt}c_{P,Sol}d_{Sol}}\left(W_{Air}^{i,j}-W_{Sol}^{i,j}\right)=0$$

Appendix B

Properties of Magnesium Chloride Solutions

In this appendix the properties of the salt solutions required in the numerical model are presented. The experimental correlations are used to determine the solution properties in different temperature and salt concentrations. The properties include: specific heat capacity, density, viscosity, and thermal conductivity.

B.1 Density

To calculate the density of a multi-component solution, modified Ezrokhi equation can be used (Zaytsev and Aseyev 1992):

$$\log(\rho_{sol} / \rho_w) = \sum_i (A_i c_i) \tag{B-1}$$

where ρ_{sol} is the density of multi component solution in kg/m^3, ρ_w is the density of water in kg/m^3, A_i are empirical coefficients and c_i is the mass fraction of the component i in kilograms of the substance per kilogram of solution.

The density of water (kg/m^3) is approximated by the following equation (Zaytsev and Aseyev 1992):

$$\rho_w = 1000 - 0.062 \cdot t - 0.00355 t^2 \qquad (0 \le t \le 100^\circ C) \tag{B-2}$$

The coefficients A_i in equation (B-1) are calculated from the following empirical equation

$$A_i = b_{0i} + b_{1i} \cdot t + b_{2i} \cdot t^2 \tag{B-3}$$

where the b_{ni} coefficients are given in (Zaytsev and Aseyev 1992).

B.2 Specific heat capacity

The specific heat capacity of solutions is calculated using the following correlation (Zaytsev and Aseyev 1992):

$$c_{p_{sol}} = c_{p_w} + \sum_i (B_{1i} + B_{2i} c'_i + B_{3i} t + B_{4i} t^2) c_i \qquad \text{(B-4)}$$

where $c_{p_{sol}}$ is the heat capacity of a multi-component solution is J/(kg.K), c_{p_w} is the heat capacity of water in J/(kg.K), B_{ni} are coefficients, c'_i is the mass content of component i in a binary isopiestic solution in kilograms of the substance per kilogram of solution, and c_i is the mass content of the component i in a multi-component solution in kilograms of the substance per kilogram of the solution. The c'_i value is calculated by the following correlation:

$$c'_i = E_i^{-1} \cdot \sum_j E_j c_j \qquad \text{(B-5)}$$

where E_i coefficients are given in (Zaytsev and Aseyev 1992).

The specific heat capacity [J/(kg.K)] of pure water is calculated by the following correlation (Zaytsev and Aseyev 1992):

$$c_{p_w} = 134225.4(T/100)^{-6.5} + 3490 \cdot (T/100)^{0.14} \qquad (0 \le t \le 100^\circ C) \qquad \text{(B-6)}$$

B.3 Thermal Conductivity

For calculating the thermal conductivity of solutions the following correlation can be used (Zaytsev and Aseyev 1992):

$$k_{sol} = k_w \cdot \left[1 - \sum_i (\beta_i c_i)\right] \qquad \text{(B-7)}$$

where k_{sol} is the thermal conductivity of the solution in W/(m.K), k_w is the thermal conductivity of water in W/(m.K), β_i are empirical coefficients, and c_i is the mass fraction of the component in kilograms of the substance per kilogram of solution.

Thermal conductivity of water is calculated by a following correlation (Zaytsev and Aseyev 1992):

$$k_w = 0.5545 + 0.00246 \cdot t - 0.00001184 \cdot t^2 \quad (0 \le t \le 100^\circ C) \qquad \text{(B-8)}$$

B.4 Viscosity

Dynamic viscosity coefficients can be calculated using the modified Ezrokhi equation (Zaytsev and Aseyev, 1992):

$$\log\left(\mu_{Sol}/\mu_{w}\right) = \sum_{i} D_{i} c_{i} \qquad \text{(B-9)}$$

where μ_{Sol} is the viscosity of a multi-component solution in $Pa \cdot s$; μ_{w} is the viscosity of water in $Pa \cdot s$; D_i are coefficients; and c_i is the mass fraction of the component in the solution.

The viscosity of water can be determined from the Slott formula (Zaytsev and Aseyev, 1992):

$$\mu_{w} = 0.59849\left(43.252 + t\right)^{-1.5423} \qquad (0 \le t \le 100^{o}C) \qquad \text{(B-10)}$$

The D_i coefficients in (B-9) are calculated using the empirical equation (Zaytsev and Aseyev, 1992):

$$D_{i} = d_{0i} + d_{1i}.t + d_{2i}.t^{2} \qquad \text{(B-11)}$$

Appendix C

The Numerical Algorithm and Computer Program

The algorithm of the numerical mpodel is shown in Figure C.1 and the computer program in PGI visual FORTRAN is presented in following pages.

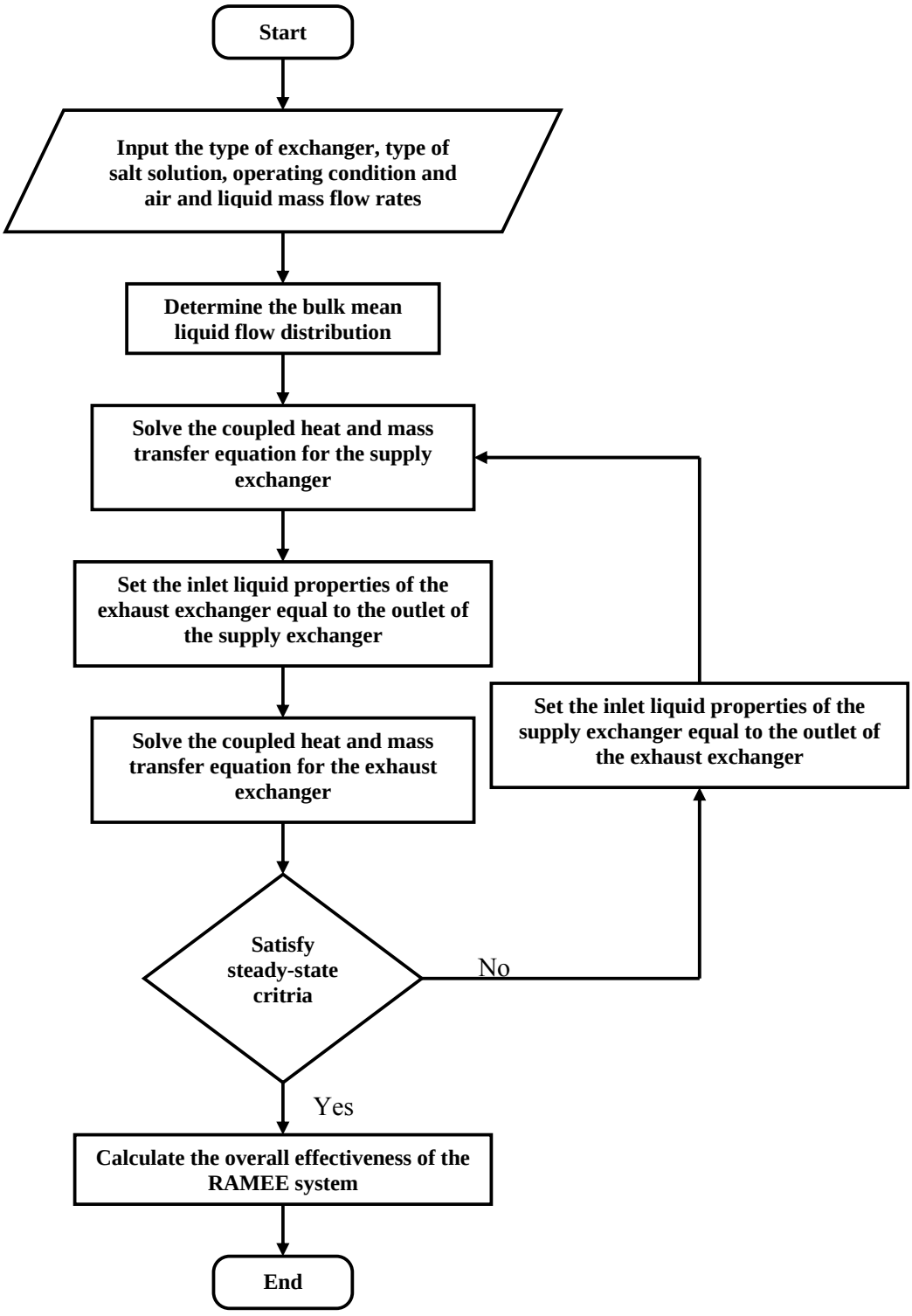

Figure C.1 *Algorithm of the numerical code to simulate the RAMEE system*

```
Numerical code to simulate the RAMEE system with two counter-flow, counter/cross flow and
Cross-flow exchangers under steady state condition

By: Alireza Vali (2007-2008)

Program RAMEE

!================================Parameters Definition==============================

integer::i,j
integer,parameter::m=201
integer,parameter::n=201

real(8),parameter::h_fg=2501300
integer::Con,SH
integer::SS
real(8)::Mw,Ms
real(8)::Ahta,Kai,Beta
real(8)::As,Bs,Cs,Ds,Es
real(8)::b1,b2,b3,b4
real(8)::d1,d2,d3
real(8)::D_sw
real(8)::de1,de2,de3
real(8)::Salt_density
real(8)::Mol_Co

integer::CCa,CCs,residual_S,residual_E
integer::HE_T,OP,me_cc
real(8),dimension(m,n)::DU,DV

real(8),dimension(m,n)::T_Air_S,T_Sol_S
real(8),dimension(m,n)::T_Air_E,T_Sol_E
real(8),dimension(m,n)::C_Sol_S,C_Air_S,Cp_Sol_S
real(8),dimension(m,n)::C_Sol_E,C_Air_E,Cp_Sol_E
real(8)::T_Air_in_S,T_Sol_in_S,X_Sol_in_S,W_Air_in_S,W_Sol_in_S
real(8)::T_Air_in_E,T_Sol_in_E,X_Sol_in_E,W_Air_in_E,W_Sol_in_E

real(8)::delta_x,delta_y
real(8)::M_Air,M_Sol,M_Salt

real(8)::eff_S,NTU_mMax_S,NTU_Max_S,E_S,C_r_S,Cm_r_S
real(8)::eff_E,NTU_mMax_E,NTU_Max_E,E_E,C_r_E,Cm_r_E

real(8)::d_S,d_A,d_M,error_S,error_E
real(8)::x_0,y_0,z_0,x_I
real(8),dimension(m,n)::X_sol_S,W_Air_S,W_Sol_S
real(8),dimension(m,n)::X_sol_E,W_Air_E,W_Sol_E
real(8),dimension(m,n)::x,y

real(8),dimension(m,n)::NTU_Sol_S,NTU_Air_S
real(8),dimension(m,n)::NTU_Sol_E,NTU_Air_E

real(8),dimension(m,n)::NTU_mSol_S,NTU_mAir_S,U_m_S
real(8),dimension(m,n)::NTU_mSol_E,NTU_mAir_E,U_m_E
```

```
real(8)::dT_Sol_S,dX_Sol_S,dT_Sol_E,dX_Sol_E

real(8)::T_Sol_Out_S,C_Sol_Out_S,X_Sol_Out_S
real(8)::T_Sol_Out_E,C_Sol_Out_E,X_Sol_Out_E

real(8)::T_Air_Out_S,W_Air_Out_S,C_Air_Out_S
real(8)::T_Air_Out_E,W_Air_Out_E,C_Air_Out_E

real(8)::Ca_Sol_S,Ca_Air_S,C_Air_in_S
real(8)::Ca_Sol_E,Ca_Air_E,C_Air_in_E

real(8)::Q_C_S,Q_H_S
real(8)::Q_C_E,Q_H_E
real(8)::J_Sol_S,J_Sol_E,J_Air
real(8)::Channel_Num,h_Air

real(8)::M_sol_in_S,M_sol_in_E

real(8)::C_Air_in_S,C_Air_in_E,C_Air_Min
real(8)::eff_sensible,eff_latent,eff_Total

real(8)::C_Sol_in_S,C_Sol_in_E
real(8)::M_s,Density_Sol,t0,tf

real(8)::Sensible_Effs_S,Latent_Effs_S,Total_Effs_S,error_mass_S,C_r_s_S
real(8)::Sensible_Effs_E,Latent_Effs_E,Total_Effs_E,error_mass_E,C_r_s_E
real(8)::eff_t,HH,Total_Eff

real(8)::E_H,E_C,Channel_Num,Cr_Show,NTU_Show
real(8),dimension(m,n)::h_Sol_S,C_Salt_S,C_Air_S,U_h_S
real(8),dimension(m,n)::h_Sol_E,C_Salt_E,C_Air_E,U_h_E

integer::counter


!=========================main body of the program=======================

Call cpu_time (t0)

! Selecting the type of heat excahnger (e.g. counter-flow, counter/cross flow or cross-flow
exchanger),Type
! of salt solution (e.g. LiBr, LiCr or MgCl2) and operating conditions (e.g. AHRI summer or Winter).

Call Input(HE_T,SS,OP)

! Heat exchanger size (x_0=length, y_0=height, z_0=width and x_I=inlet and outlet headers Length)

Call HE_Size(HE_T,x_0,y_0,z_0,x_I)

! d_M=Membrane thichness d_A=Air channel size and d_S=Liquid channel size

Call Thickness(d_M,d_A,d_S)

! Different properties and correlation constants for the salt solution
```

```
Call
Salt_Solution(SS,Mw,Ms,Ahta,Kai,As,Bs,Cs,Ds,Es,b1,b2,b3,b4,d1,d2,d3,D_sw,Beta,de1,de2,de3,Sal
t_density,Mol_Co)

Call Grid_Size(m,n,delta_x,delta_y)

Call
Initial_Values(OP,T_Air_in_S,T_Sol_in_S,X_Sol_in_S,W_Air_in_S,T_Air_in_E,T_Sol_in_E,X_Sol
_in_E,W_Air_in_E)

Call Sol_Density(SS,T_Sol_in_S,X_Sol_in_S,Density_Sol)

Call Mass_input(d_M,d_A,d_s,M_Air,M_Salt,z_0,Density_Sol,X_Sol_in_S,Channel_Num)

do j=1,n
   do i=1,m
                    x(i,j)=(i-1)*x_0*delta_x
                    y(i,j)=(j-1)*y_0*delta_y
         end do
end do

! Determining the bulk mean liquid flow distribution

Call
Velocity(HE_T,SS,m,n,d_S,M_Salt,x_0,y_0,x_I,DU,DV,delta_x,delta_y,T_Sol_in_S,X_Sol_in_S,x,
y)

Call C_Air_Inlet(M_Air,W_Air_in_S,W_Air_in_E,C_Air_in_S,C_Air_in_E)

Call
Tem_Con(T_Air_in_S,T_Sol_in_S,X_Sol_in_S,W_Air_in_S,T_Air_S,T_Sol_S,X_Sol_S,W_Air_S,
m,n)

Call
Tem_Con(T_Air_in_E,T_Sol_in_E,X_Sol_in_E,W_Air_in_E,T_Air_E,T_Sol_E,X_Sol_E,W_Air_E,
m,n)

me_cc=0
counter=0

!**************Calculating Haet and Moisture Transfer in the RAMEE System***************

do while(me_cc==0)

counter=counter+1

!================ ==========Supply Exchanger==============================

M_Sol_in_S=M_Salt*(1.+X_Sol_in_S)

Call Csol_in(SS,T_Sol_in_S,X_Sol_in_S,C_Sol_in_S,M_Sol_in_S)

residual_S=0
```

```
do while (residual_S==0)

do j=1,n

CCs=0

Call
NTU_S(SS,d_M,d_A,d_S,NTU_Sol_S,X_Sol_S,T_Sol_S,M_Sol_in_S,m,n,x_0,y_0,z_0,h_Sol_S,h_
Air,j,C_Sol_S,Cp_Sol_S,U_h_S)

Call
NTU_mS(d_M,h_Air,Cp_Sol_S,h_Sol_S,M_Sol_in_S,m,n,x_0,y_0,W_Air_in_S,X_Sol_in_S,NTU_
mSol_S,U_m_S,j,D_sw)

Call
GSs_solver(SS,m,n,x_I,x_0,y_0,d_S,DV,DU,NTU_Sol_S,NTU_mSol_S,U_m_S,T_Sol_S,T_Air_S,
M_Sol_in_S,T_Sol_in_S,T_Air_in_S,X_Sol_in_S,X_Sol_S,W_Air_S,W_Sol_S,delta_x,delta_x,U_h
_S,Cp_Sol_S,C_Sol_S,CCs,j)

end do

do j=1,n
CCa=0

Call
NTU_A(SS,d_M,d_A,d_S,NTU_Air_S,W_Air_S,T_Air_S,T_Sol_S,X_Sol_S,M_Air,m,n,x_0,y_0,z_
0,j,C_Air_S)

Call
NTU_mA(d_M,h_Air,Cp_Sol_S,h_Sol_S,M_Air,m,n,x_0,y_0,W_Air_in_S,X_Sol_in_S,NTU_mAir
_S,j,D_sw)

Call
GSa_solver(m,n,NTU_Air_S,NTU_mAir_S,T_Sol_S,T_Air_S,W_Sol_S,W_Air_S,T_Sol_in_S,T_Ai
r_in_S,delta_x,CCa,j)

end do

Call
Res_Finding(m,n,x_I,x_0,d_S,y_0,T_Sol_in_S,X_Sol_in_S,DV,DU,T_Air_S,T_Sol_S,W_Air_S,X_
Sol_S,U_h_S,Cp_Sol_S,NTU_Sol_S,NTU_Air_S,NTU_mSol_S,NTU_mAir_S,delta_x,delta_y,U_m
_S,residual_S,C_Sol_S,W_Sol_S)

end do

! Calculating the air and liquid properties at the outlet of the supply exchanger

Call
Sol_Out(SS,x_0,x_I,delta_x,M_Sol_in_S,T_Sol_S,C_Sol_S,X_Sol_S,m,n,T_Sol_Out_S,C_Sol_Out
_S,X_Sol_Out_S,M_Salt)

Call Air_Out(M_Air,T_Air_S,W_Air_S,C_Air_S,m,n,T_Air_Out_S,W_Air_Out_S,C_Air_Out_S)

! Computing the sensible energy, latent energy and total energy rate transfered in the supply
exchanger
```

```
Call
energy(SH,T_Air_in_S,T_Sol_in_S,T_Air_Out_S,T_Sol_Out_S,C_Air_Out_S,C_Sol_Out_S,X_Sol_
in_S,X_Sol_Out_S,M_Sol_in_S,Q_H_S,Q_C_S, error_S,M_Air,C_Sol_in_S,C_Air_in_S)

! Setting the inlet properties of the exhaust exchanger equal to outlet properties of the supply
exchanger
! to couple two exchangers in a closed loop

T_Sol_in_E=T_Sol_Out_S
X_Sol_in_E=X_Sol_Out_S


!==============================Exhaust Exchanger==============================

M_Sol_in_E=M_Salt*(1.+X_Sol_in_E)

Call SH_Inlet(m,n,delta_X,x_I,x_0,T_Sol_E,T_Sol_in_E,X_Sol_in_E,X_Sol_E)

Call Csol_in(SS,T_Sol_in_E,X_Sol_in_E,C_Sol_in_E,M_Sol_in_E)

residual_E=0

do while (residual_E==0)

do j=1,n
CCs=0

Call
NTU_S(SS,d_M,d_A,d_S,NTU_Sol_E,X_Sol_E,T_Sol_E,M_Sol_in_E,m,n,x_0,y_0,z_0,h_Sol_E,h_
Air,j,C_Sol_E,Cp_Sol_E,U_h_E)

Call
NTU_mS(d_M,h_Air,Cp_Sol_E,h_Sol_E,M_Sol_in_E,m,n,x_0,y_0,W_Air_in_E,X_Sol_in_E,NTU_
mSol_E,U_m_E,j,D_sw)

Call
GSs_solver(SS,m,n,x_I,x_0,y_0,d_S,DV,DU,NTU_Sol_E,NTU_mSol_E,U_m_E,T_Sol_E,T_Air_E,
M_Sol_in_E,T_Sol_in_E,T_Air_in_E,X_Sol_in_E,X_Sol_E,W_Air_E,W_Sol_E,delta_x,delta_y,U_
h_E,Cp_Sol_E,C_Sol_E,CCs,j)

end do

do j=1,n
CCa=0

Call
NTU_A(SS,d_M,d_A,d_S,NTU_Air_E,W_Air_E,T_Air_E,T_Sol_E,X_Sol_E,M_Air,m,n,x_0,y_0,z
_0,j,C_Air_E)

Call
NTU_mA(d_M,h_Air,Cp_Sol_E,h_Sol_E,M_Air,m,n,x_0,y_0,W_Air_in_E,X_Sol_in_E,NTU_mAir
_E,j,D_sw)
```

```
Call
GSa_solver(m,n,NTU_Air_E,NTU_mAir_E,T_Sol_E,T_Air_E,W_Sol_E,W_Air_E,T_Sol_in_E,T_
Air_in_E,delta_x,CCa,j)

end do

Call
Res_Finding(m,n,x_I,x_0,d_S,y_0,T_Sol_in_E,X_Sol_in_E,DV,DU,T_Air_E,T_Sol_E,W_Air_E,X_
Sol_E,U_h_E,Cp_Sol_E,NTU_Sol_E,NTU_Air_E,NTU_mSol_E,NTU_mAir_E,delta_x,delta_y,U_
m_E,residual_E,C_Sol_E,W_Sol_E)

end do


Call
Sol_Out(SS,x_0,x_I,delta_x,M_Sol_in_E,T_Sol_E,C_Sol_E,X_Sol_E,m,n,T_Sol_Out_E,C_Sol_Out
_E,X_Sol_Out_E,M_Salt)

Call Air_Out(M_Air,T_Air_E,W_Air_E,C_Air_E,m,n,T_Air_Out_E,W_Air_Out_E,C_Air_Out_E)

Call
energy(SH,T_Air_in_E,T_Sol_in_E,T_Air_Out_E,T_Sol_Out_E,C_Air_Out_E,C_Sol_Out_E,X_Sol
_in_E,X_Sol_Out_E,M_Sol_in_E,Q_H_E,Q_C_E, error_E,M_Air,C_Sol_in_E,C_Air_in_E)

! Checking the steady state convergance criteria

Call
balance_check(J_Sol_E,J_Sol_S,M_Salt,X_sol_in_E,X_Sol_out_E,Q_H_E,Q_H_S,Q_C_S,Q_C_E,
me_cc,M_Air,W_Air_out_E,W_Air_in_E,X_sol_in_S,X_Sol_out_S,W_Air_Out_S,W_Air_in_S)


T_Sol_in_S=T_Sol_Out_E
X_Sol_in_S=X_Sol_Out_E

Call SH_Inlet(m,n,delta_X,x_I,x_0,T_Sol_S,T_Sol_in_S,X_Sol_in_S,X_Sol_S)

end do

Call Inlet_W_Sol(SS,m,n,X_Sol_in_S,T_Sol_in_S,W_Sol_in_S)
Call Inlet_W_Sol(SS,m,n,X_Sol_in_E,T_Sol_in_E,W_Sol_in_E)

print*
print*,"T_Sol_in_S",T_Sol_in_S
print*,"X_Sol_in_S",X_Sol_in_S
print*,"W_Sol_in_S",W_Sol_in_S
print*,"T_Sol_in_E",T_Sol_in_E
print*,"X_Sol_in_E",X_Sol_in_E
print*,"W_Sol_in_E",W_Sol_in_E
print*
print*,"T_Air_in_S",T_Air_in_S
print*,"T_Air_out_S",T_Air_out_S
print*,"W_Air_in_S",W_Air_in_S
print*,"W_Air_out_S",W_Air_out_S
print*,"T_Air_in_E",T_Air_in_E
print*,"T_Air_out_E",T_Air_out_E
```

```
print*,"W_Air_in_E",W_Air_in_E
print*,"W_Air_out_E",W_Air_out_E

! Calculating the sensible latent and total effectiveness of each exchanger

Call
effectivness(T_Air_in_S,T_Sol_in_S,T_Air_Out_S,T_Sol_Out_S,C_Air_Out_S,C_Sol_Out_S,eff_S)

Call
Latent_effectivness(SS,W_Air_in_S,W_Air_out_S,X_sol_in_S,T_Sol_in_S,T_Air_in_S,M_Sol_in_
S,M_Air,eff_S,M_Salt,X_Sol_Out_S, Latent_Effs_S,Total_Effs_S,error_mass_S)


Call
effectivness(T_Air_in_E,T_Sol_in_E,T_Air_Out_E,T_Sol_Out_E,C_Air_Out_E,C_Sol_Out_E,eff_
E)

Call
Latent_effectivness(SS,W_Air_in_E,W_Air_out_E,X_sol_in_E,T_Sol_in_E,T_Air_in_E,M_Sol_in_
E,M_Air,eff_E,M_Salt,X_Sol_Out_E, Latent_Effs_E,Total_Effs_E,error_mass_E)

! Determining the system NTU, Cr*, NTUm and mSalt/mAir

Call NTU_Maximum(NTU_Air_S,NTU_Sol_S,NTU_Max_S,m,n)
Call NTU_Maximum(NTU_Air_E,NTU_Sol_E,NTU_Max_E,m,n)

Call NTUm_Maximum(NTU_mAir_S,NTU_mSol_S,NTU_mMax_S,m,n)
Call NTUm_Maximum(NTU_mAir_E,NTU_mSol_E,NTU_mMax_E,m,n)

Call
Mass_Ratio(C_Air_in_S,C_Air_Out_S,C_Air_in_E,C_Air_Out_E,C_Sol_in_S,C_Sol_out_S,C_Sol_
in_E,C_Sol_Out_E,C_r_S,C_r_E,C_Air_min)

! Determining the overall sensible, Latent and total effectiveness of the RAMEE system

Call
Effectiveness(Channel_Num,C_Air_in_S,T_Air_in_S,M_Air,W_Air_in_S,h_fg,C_Air_in_E,W_Air_
in_E,T_Air_Out_S,W_Air_out_S,T_Air_in_E,M_Salt,X_Sol_Out_S,X_Sol_in_S,C_Air_out_S,eff_s
ensible,eff_latent,eff_Total,C_Air_min)

Call
Total_effectivness(SS,W_Air_in_S,W_Air_in_E,T_Air_in_S,T_Air_in_E,eff_Sensible,eff_Latent,To
tal_Eff)
Call cpu_time (tf)

! desplaying the results on screen

print*
print*,"Sensible_eff_Supply",eff_S
print*
print*,"Latent_Eff",Latent_Effs_S
print*
print*,"Total_Eff",Total_Effs_S
print*
print*,"error mass",error_mass_S
```

```
print*
print*,"Sensible_eff_Exhaust",eff_E
print*
print*,"Latent_Eff_Exhaust",Latent_Effs_E
print*
print*,"Total_Eff_Exhaust",Total_Effs_E
print*
print*,"error mass_Exhaust",error_mass_E
print*
print*
print*,"eff_sensible",eff_sensible
print*,"eff_latent",eff_latent
print*,"eff_total",eff_total
print*,"Total_Eff",Total_Eff
print*
print*,"NTU_Supply",NTU_Max_S
print*,"NTU_Exhaust",NTU_Max_E
print*
print*,"NTU_M_Supply",NTU_mMax_S
print*,"NTU_M_Exhaust",NTU_mMax_E
print*
print*,"C_r_S",C_r_S
print*,"C_r_E",C_r_E
print*
print*,"M_Salt/M_Air",M_Salt/M_Air
print*
print*,"HE_Type",HE_T
print*
print*,"Time (min)=",(tf-t0)/60
print*
print*,"Q_C_S",Q_C_S
print*,"Q_C_E",Q_C_E

! Recording the results in a text file

open (unit=2,file="RAMEE.dat")

write(2,200)NTU_Max_E,
C_r_E,eff_sensible,eff_latent,eff_total,T_Sol_out_S,T_Sol_out_E,X_Sol_out_S, &
X_Sol_out_E,W_Sol_in_E,W_Sol_in_S,T_Air_in_S,T_Air_out_S,T_Air_in_E,T_Air_out_E,W_Air
_in_S,W_Air_out_S,W_Air_in_E,W_Air_out_E

Close (2)

200 format(22f15.5)
Print*,"Enter A Number"
read*,Con

END PROGRAM RAMEE
```

Appendix D

Numerical Results of Liquid-to-Air Membrane Energy Exchanger (LAMEE)

D.1 Introduction

A liquid-to-air membrane energy exchanger (LAMEE) or single heat and moisture exchanger needs to be investigated because RAMEE system is made of two LAMEEs coupled in a closed loop. In this appendix the numerical model developed in Chapter 2 is used to investigate the design characteristics of a counter/cross flow flat-plate exchanger. The design dimensionless parameters, presented in Chapter 2, are used to study the performance of the exchanger in different operating conditions. However, the effectiveness definition is modified for a single heat and moisture exchanger.

The performance of a LAMEE can be investigated by use of three dimensionless groups: dimensionless heat transfer rate (sensible effectiveness), dimensionless moisture transfer rate (Latent effectiveness) and dimensionless energy transfer rate (total effectiveness).

The sensible effectiveness of a LAMEE is:

$$\varepsilon_s = \frac{C_{Air}\left(T_{Air,in} - T_{Air,out}\right)}{C_{min}\left(T_{Air,in} - T_{Sol,in}\right)} \tag{D-1}$$

where

$$C_{min} = \min\left(C_{Air}, C_{Sol}\right) \tag{D-2}$$

Inlet and outlet conditions are shown in Figure D.1

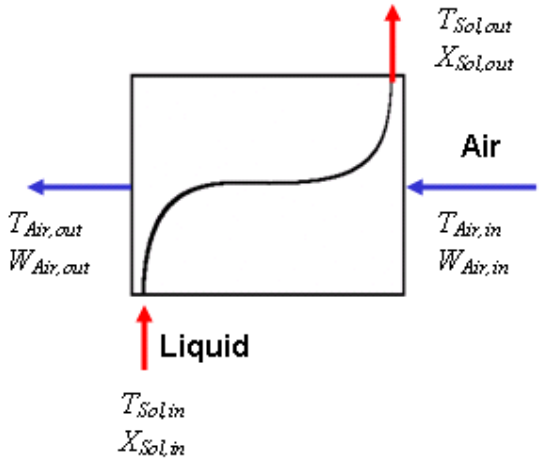

Figure D.1 *Schematic diagram of a counter/cross flow heat and moisture exchanger*

The latent effectiveness of the LAMEE is the ratio of actual moister transfer to the maximum possible moisture transfer.

$$\varepsilon_l = \frac{m_{Air}\left(W_{Air,in} - W_{Air,out}\right)}{\text{Maximum Possible Moisture Transfer}} \tag{D-3}$$

The maximum possible moisture transfer can be calculated with:

$$\text{Maximum Possible Moisture Transfer} = m_{Air}\left(W_{Air,in} - W_{Sol,in}\right) \tag{D-4}$$

(Simonson and Besant 1998) presented a correlation to estimate the total effectiveness by use of the sensible effectiveness and the latent effectiveness, the total effectiveness of the single exchanger can be calculated with following correlation:

$$\varepsilon_t = \frac{\varepsilon_s + \varepsilon_l H^*}{1 + H^*} \tag{D-5}$$

Where H^* is the operating condition factor:

$$H^* \approx 2500\frac{\Delta W}{\Delta T} \tag{D-6}$$

ΔW is the difference of the inlet air and inlet salt solution humidity ratios:

$$\Delta W = W_{Air,in} - W_{Sol,in} \tag{D-7}$$

and ΔT is the temperature difference of the inlet air and inlet salt solution:

$$\Delta T = T_{Air,in} - T_{Sol,in} \tag{D-8}$$

D.2 Temperature and Water Content Distribution in a LAMEE

Due to the phase change, the coupled heat and mass transfer equations must be solved in order to determine the temperature and moisture content at any point (x,y) in a single heat and moisture exchanger. Considering the assumption that the phase change energy is delivered to liquid desiccant, the sensible heat flux from the liquid to the air must be in balance with summation of the sensible heat flux from the air to the liquid and phase change heat rate. The balance of the heat transferred in the exchanger at any point (x,y) is:

$$(\rho c_p d)_{Air}(u_{Air}\frac{\partial T_{Air}}{\partial x}) + m_v h_{fg} = (\rho c_p d)_{Sol}(u_{Sol}\frac{\partial T_{Sol}}{\partial x} + v_{Sol}\frac{\partial T_{Sol}}{\partial y}) \tag{D-9}$$

As it can be seen in equation (D-9), the phase change heat affects the gradients of temperature on the air and the liquid side and affects the temperature distribution in heat and moisture exchanger. The phase change term, $m_v h_{fg}$, depends on the moisture transfer rate which is caused by the deference of the partial vapor pressure between the liquid and the air. The vapor pressure itself depends on the temperature of the fluids. Therefore, both the heat and mass transfer equations must be solved simultaneously to have an accurate solution and the phase change affects both heat and moisture transfer in an exchanger.

To have a better understanding of the effect of the phase change, the temperature and moisture content distributions of the air and the salt solution in a counter/cross flow exchanger are presented in following figures. In these figures, the temperature distributions when moisture transfer does not occur and also moisture content distributions without heat transfer are shown in both the air and the liquid side for comparison.

The temperature distributions when the inlet air is hot and humid, Table D.1, are presented in Figure D.2. The LAMEE parameters are described in Table 2.1 except the permeability of the membrane is 9.67×10^{-7} kg/ms. The mass flow rate of the air and the pure salt are 0.03 and 0.003, respectively and result NTU=10 and Cr*=0.5. Under the operating conditions listed in Table D.1, the air stream losses heat and moisture to the liquid desiccant. Therefore, the moisture transfers in form of vapor from air to liquid desiccant. At the gas-liquid interface water vapor changes to liquid and release the phase change heat to liquid desiccant which is in thermal equilibrium with the air under steady state conditions. The phase change, finally, increases the temperature of the salt solution and the air stream.

Table D.1. *Summer operating conditions of the single heat and moisture exchanger used for temperature and moisture content distributions (hot and humid air)*

Inlet temperature of the air stream ($T_{Air,in}$)	306.15 K (33°C)
Inlet humidity ratio of the air stream ($W_{Air,in}$)	17.5 g/kg (58%)
Inlet temperature of the salt solution ($T_{Sol,in}$)	287.15 K (14°C)
Inlet concentration of the salt solution ($X_{Sol,in}$)	2 kg/kg (33%)

Even thought the heat and moisture transfer is from the hot and humid air to liquid desiccant, when the liquid desiccant mass flow rate is small compared to air mass flow rate, there is a region where the liquid is heating the air due to the phase change heat. According to Figures D.2 (b) and D.2 (d), the temperature of the air and the liquid desiccant can be higher than the air inlet temperature. However, this phenomenon does not happen without the moisture transfer Figures D.2 (a) and D.2 (c). When the liquid flow rate is low, the phase change heat value can be greater than the heat transfer between the air and liquid in some region. This means the phase change energy heats the liquid to a temperature even higher than the air temperature. Therefore, the liquid is actually heating the air at this part of the exchanger regardless the air and liquid inlet conditions.

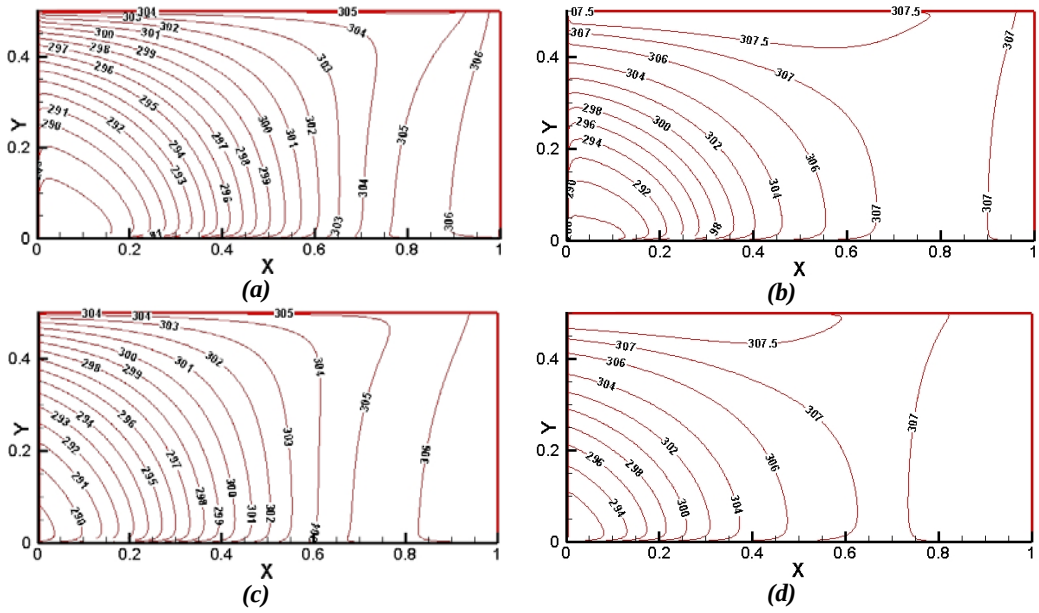

Figure D.2 *Temperature distributions in a counter/cross flow exchanger for air side (a) without moisture transfer and (b) with moisture transfer, and for the salt solution (c) without moisture transfer and (d) with moisture transfer (summer condition)*

Comparing the temperature distributions on the air and liquid sides with and without moisture transfer, it can be seen that with moisture transfer the temperature changes faster because of the phase change heat.

The moisture content distributions on the air and liquid sides in a counter/cross flow exchanger are illustrated in Figure D.3. Comparison of Figures D.3 (a) and D.3 (b) or Figures D.3 (c) and D.3 (d) shows that with heat transfer, both the shape and the magnitudes of constant moisture content lines of the air and the liquid desiccant differ significantly from distribution of moisture content without heat transfer. If the liquid-gas separating surface is assumed to be insulated, the partial vapor pressure just changes with changing of the concentration of the water in the fluids. However, with heat transfer, the partial vapor pressure changes with both the temperature and moisture content of the fluids.

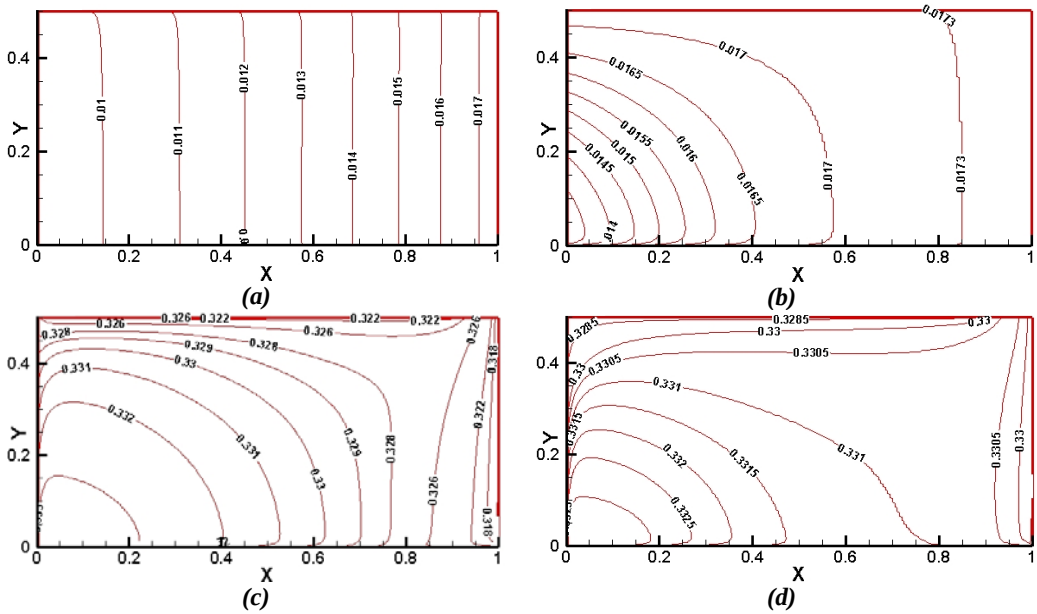

Figure D.3 *Humidity ratio distributions in a counter/cross flow exchanger for air side (a) without heat transfer and (b) with heat transfer, and salt concentration distributions for the salt solution (c) without heat transfer and (d) with heat transfer (summer condition)*

As another instance, the temperature distributions, when the inlet air is cold and dry, are presented in Figure D.4. The air and pure salt mass flow rates are 0.03 and 0.0015 respectively which give NTU=10 and Cr*=0.5. In this case, operating conditions are listed in Table D.2, the air stream gains moisture and heat from the liquid desiccant. Therefore, at the gas-liquid interface water changes to vapor and gains the phase change heat from the liquid desiccant.

Table D.2 *Winter operating conditions of the single heat and moisture exchanger used for temperature and moisture content distributions (Cold and dry air)*

Inlet temperature of the air stream ($T_{Air,in}$)	274.85 K (1.7^{o}C)
Inlet humidity ratio of the air stream ($W_{Air,in}$)	3.5 g/kg (75%)
Inlet temperature of the salt solution ($T_{Sol,in}$)	293.15 K (20^{o}C)
Inlet concentration of the salt solution ($X_{Sol,in}$)	4.25 kg/kg (19%)

From Figure D.4, it can be seen that with moisture transfer the temperatures of the salt solution and the air vary faster due to the phase change in the area of x<0.6, so at the region of x>0.6 the temperatures change slower.

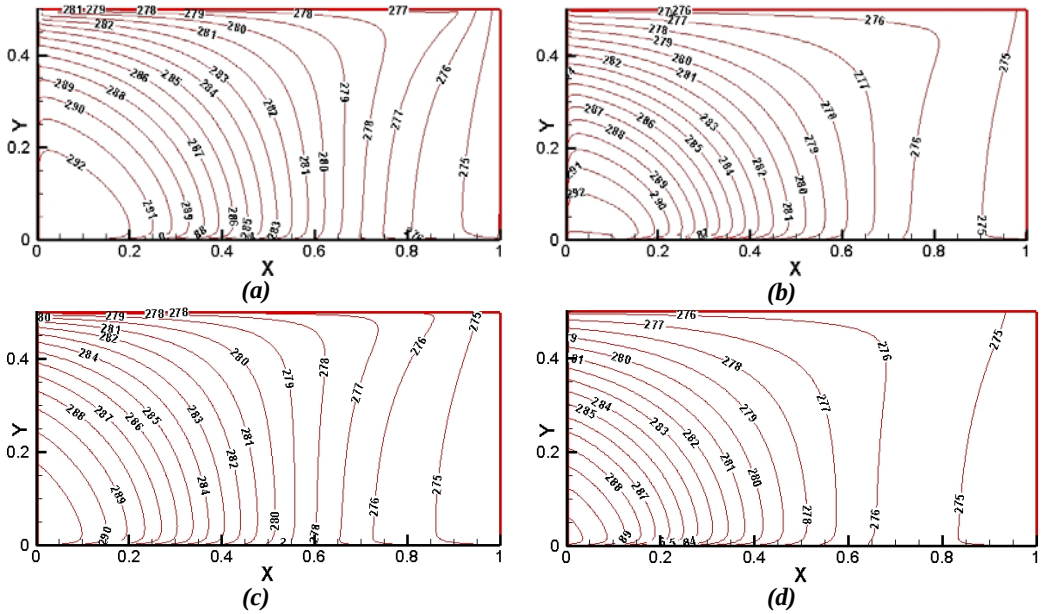

Figure D.4 *Temperature distributions in a counter/cross flow exchanger for air side (a) without moisture transfer and (b) with moisture transfer, and for the salt solution (c) without moisture transfer and (d) with moisture transfer (winter condition)*

Figure D.5 presented the moisture content distributions on the air and liquid sides for winter operating condition (Table D.2). As it is illustrated, the moisture transfers from liquid to air but because of the phase change heat the temperature of the salt solution decreases fast and the vapor pressure of the salt decreases to even lower than the vapor pressure of the air and the moisture transfer occurs in reverse direction from the air to liquid. As shown in Figure D.5, the magnitude and the shape of the constant moisture content lines are different for cases of with and without heat transfer.

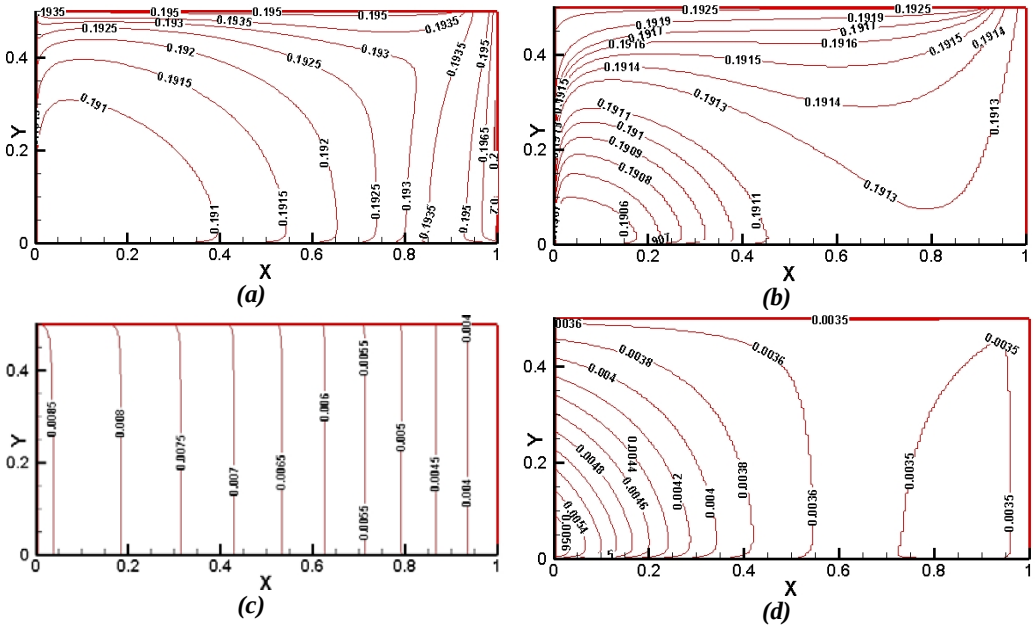

Figure D.5 *Humidity ratio distributions in a counter/cross flow exchanger for air side (a) without heat transfer and (b) with heat transfer, and salt concentration distributions for the salt solution (c) without heat transfer and (d) with heat transfer (winter condition)*

The results presented in this section demonstrate the great impact of phase change on the performance of the heat and moisture exchanger. As shown, the heat or moisture transfer maybe occurs in an unexpected direction as a result of the phase change.

D.3 Effect of Dimensionless Groups

In this section, the effects of the dimensionless parameters, defined in Chapter 2, on the performance of a counter/cross flow LAMEE with the parameters given in Table 2.1 are investigated. Besides, the effectiveness of the exchangers with the same design but different liquid-air flow configurations, cross-flow, counter-flow and counter/cross flow is compared and finally the performance of the counter/cross flow exchanger under different operating conditions is studied. The

operating conditions used in this section are listed in Table D.3. The inlet air is hot and humid so the heat and moisture transfer from the air to the desiccant solution.

Table D.3 *Summer operating conditions of the single heat and moisture exchanger used for sensitivity study (hot and humid air)*

Inlet temperature of the air stream ($T_{Air,in}$)	308.15 K (35^{o}C)
Inlet humidity ratio of the air stream ($W_{Air,in}$)	17.5 g/kg
Inlet temperature of the salt solution ($T_{Sol,in}$)	297.15 K (24^{o}C)
Inlet concentration of the salt solution ($X_{Sol,in}$)	2 kg/kg (33%)

D.3.1 Entrance Ratio

As presented in Chapter 2 the entrance ratio defined as the ratio of the length of inlet and outlet headers to the length of the LAMEE (x_i/x_0), affects the performance of the counter/cross flow exchanger. The sensible, latent and total effectivenesses of a counter/cross flow exchanger with entrance ratio are presented in Figure D.6. Besides the effectivenesses of a counter-flow and a cross-flow exchanger with the same design are shown in Figure D.6 for comparison. The effects of changing x_i/x_0 on the performance of the LAMEE are fairly similar to those presented and explained for the RAMEE system in Chapter 5.

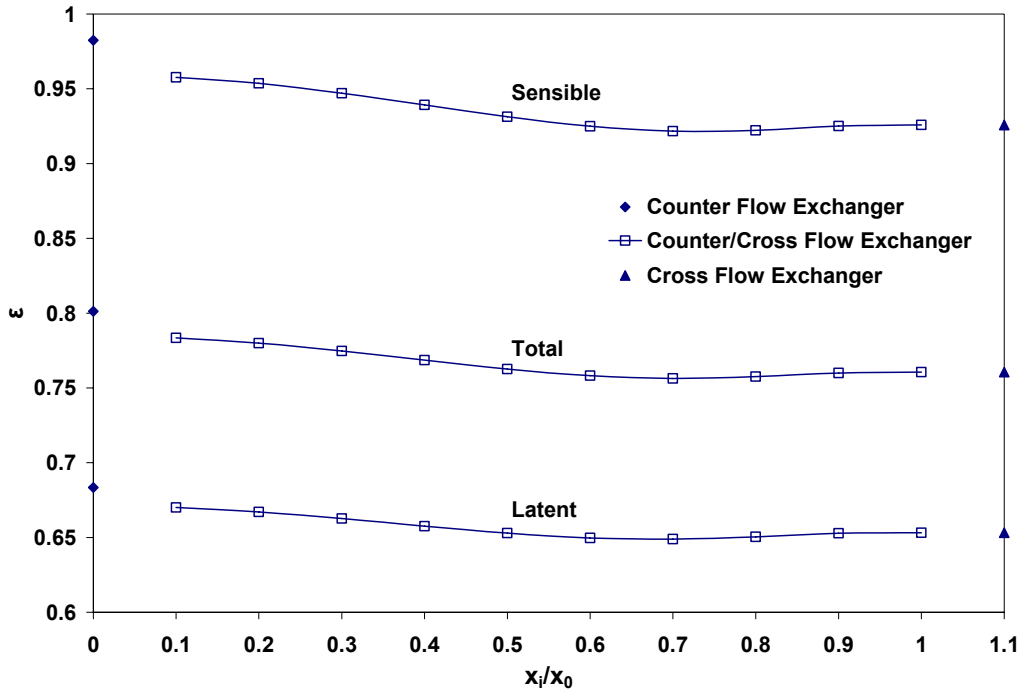

Figure D.6 *Sensible, latent and total effectiveness of a counter/cross flow LAMEE as a function of the size of the inlet header (entrance ratio, x_i/x_0) for NTU=10, Cr*=5 and y_0/x_0=0.5. The effectivenesses of pure cross-flow and pure counter-flow exchangers are included for comparison.*

D.3.2 Aspect Ratio

The aspect ratio affects the effectiveness of a counter/cross flow heat and moisture as presented in Figure D.7. The explanation is like that presented in Chapter 5 for the RAMEE system.

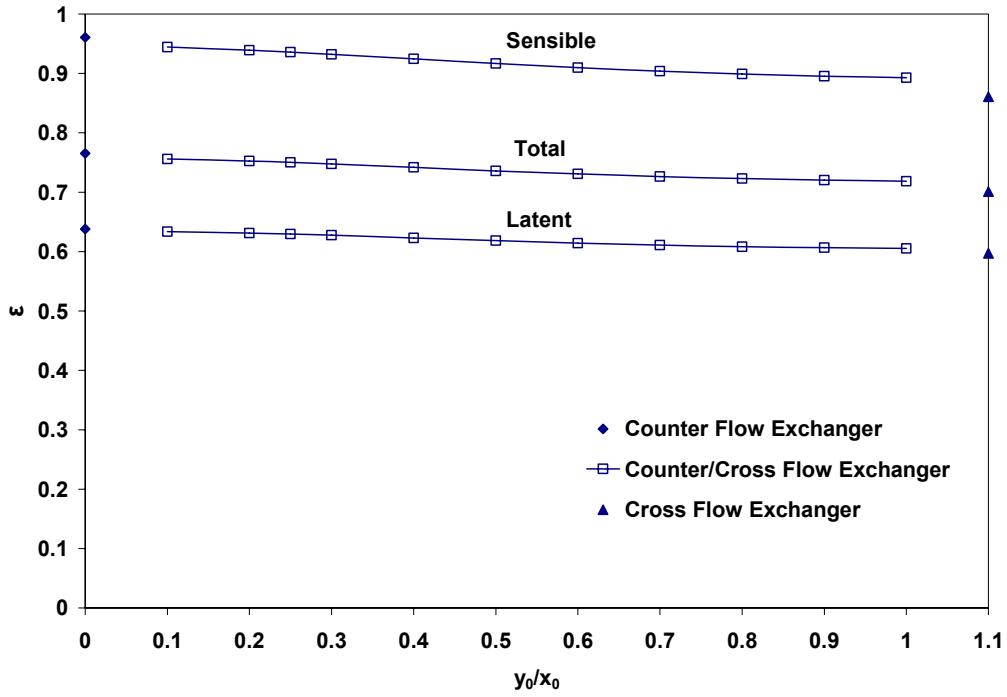

Figure D.7 *Sensible, latent and total effectiveness of a counter/cross flow LAMEE as a function of the aspect ratio (height to length) for NTU=10, Cr*=3 and x_i/x_0=0.1. The effectivenesses of pure cross and pure counter-flow exchangers are included for comparison.*

D.3.3 NTU and Cr*

The sensible, latent and total effectiveness of the counter/cross flow exchanger, as a function of Cr* (C_{Sol}/C_{Air}) for different NTU values, are illustrated in Figure D.8. Like that observed for a heat exchanger the sensible effectiveness of the heat and moisture exchanger decreases with Cr* when $C_{Sol}<C_{Air}$. The minimum sensible effectiveness occurs when the air and liquid desiccant heat capacity rates are equal (Cr*=1) then the sensible effectiveness increases with Cr*. This is similar to the response of heat exchangers to increasing the Cr* presented in Chapter 3 and those reported in the literature (Fan et al. 2006)

Due to the phase change, the sensible effectiveness of the heat and moisture exchanger changes with NTU differently compared to the heat exchanger. When Cr*>2, the sensible effectiveness of the heat and moisture exchanger increases with NTU which is like the heat exchanger effectiveness. However, as it can be seen in Figure D.8(a), the sensible effectiveness of the counter/cross flow heat and moisture exchanger for small Cr* increases with NTU till it peaks a maximum (in NTU≈5 in this example), and then it decreases with increasing NTU which is unexpected.

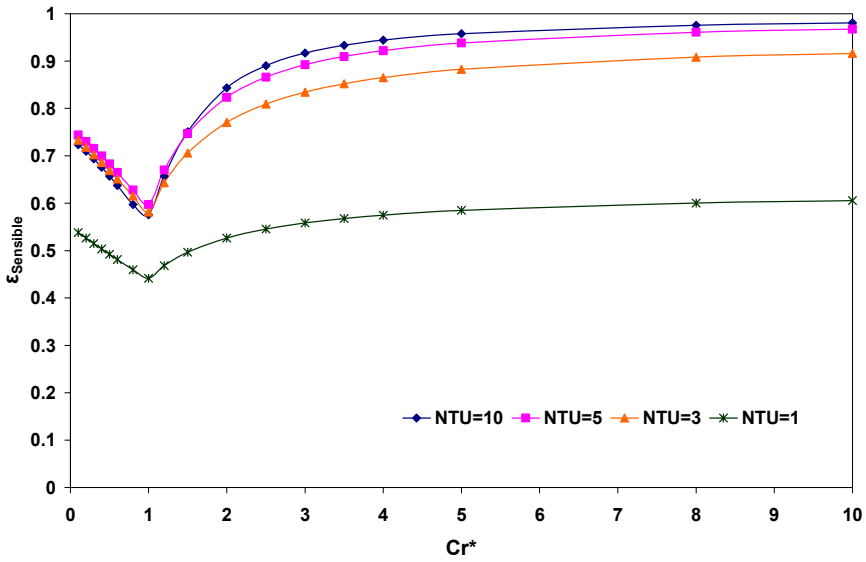

(a)

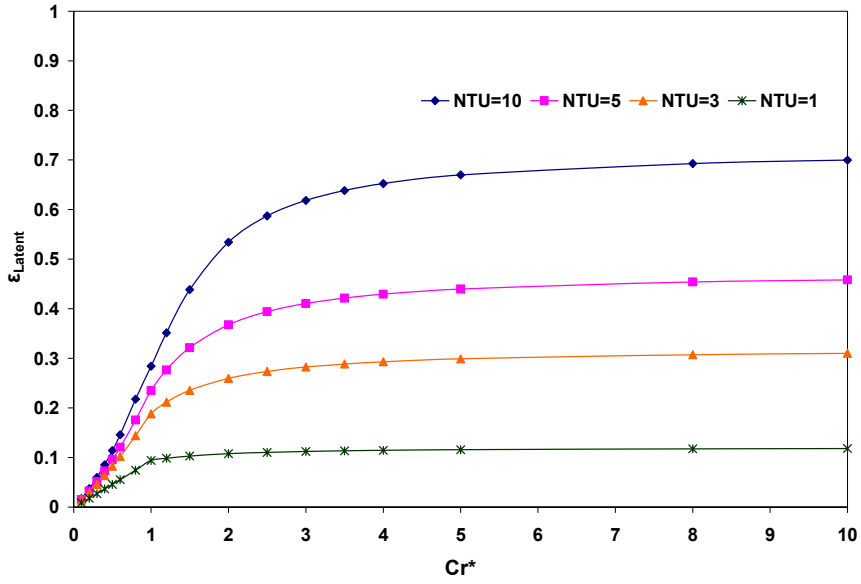

(b)

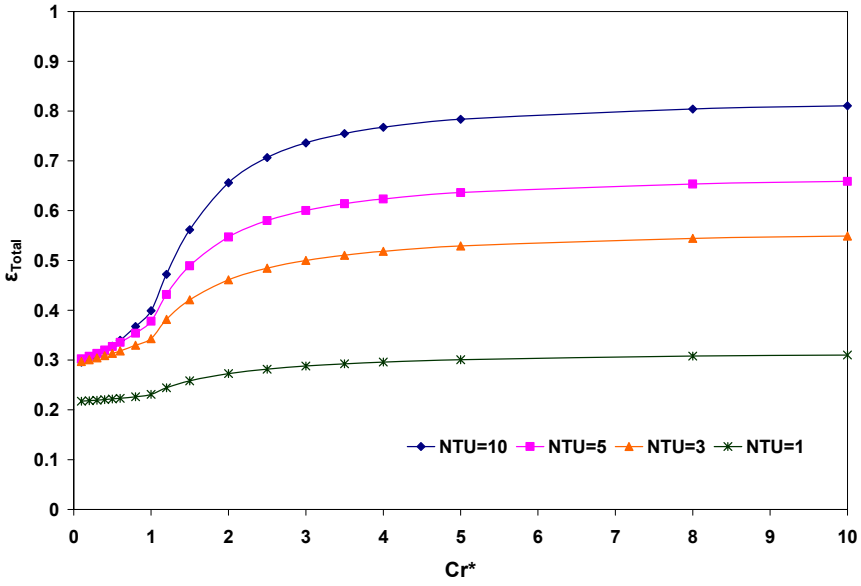

(c)

Figure D.8 *(a) sensible, (b) latent and (c) total effectiveness of a counter/cross flow exchanger as a function of Cr* and for different NTU values* $y_0/x_0=0.5$ *and* $x_i/x_0=0.1$

When the Cr* is small, it means the heat capacity rate of the desiccant solution is smaller than the air heat capacity ratio. Therefore, in high NTU the

temperature of the liquid desiccant changes dramatically due to great heat flux from the air side to liquid side. Besides, in this case the liquid dehumidifies the air and the phase change release heat in liquid side, so the heat of phase change accelerates the liquid temperature rise. As a result, the liquid temperature reaches the air temperature very fast. The phase change heats the liquid to a temperature even higher than the air temperature, and the heat flux direction is reversed. That is, the liquid heats the air and the air temperature increases which is against sensible effectiveness and leads to a decrease in the sensible effectiveness with NTU in small Cr*. On the other hand, when the NTU is less than a certain value (NTU≈5 in this example) because the heat flux from the air to the liquid desiccant decreases the liquid temperature dose not reach the air temperature and this phenomenon does not happen. Thus, the temperature of the air deceases though the exchanger and the sensible effectiveness trend dose not affected by phase change.

It can be seen in Figures D.8 (b) and (c) that the latent and total effectiveness are increasing with NTU and Cr*. The effectivenesses change with Cr* quite slightly for Cr*>5 and as NTU increases effectivenesses become more sensitive to the change of Cr*.

D.3.4 NTU_m and m*

In addition to the heat transfer dimensionless parameters (NTU and Cr*), the effectiveness of a heat and moisture exchanger is also a function of the number of mass transfer units (NTU_m) and the mass flow rate ratio (m*). Figure D.9 show the variation of the sensible, latent and total effectiveness with m*. As it can be seen,

the same trends are illustrated in Figures D.9 (a), (b) and (c) for $\varepsilon_{sensible}$, ε_{latent} and ε_{total} respectively. The effectivenesses increases as m* increases however when m*>1 the values of effectiveness is almost constant particularly when the NTU_m value is large.

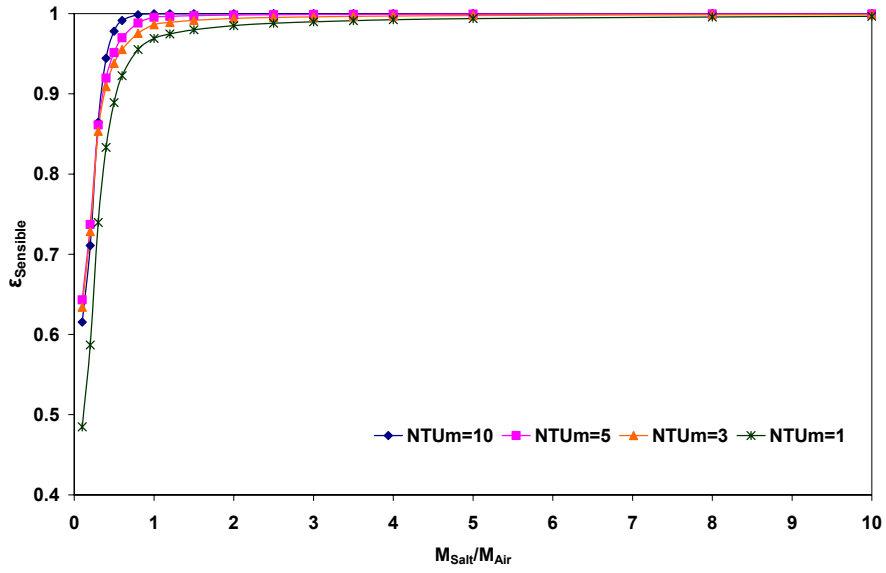

(a)

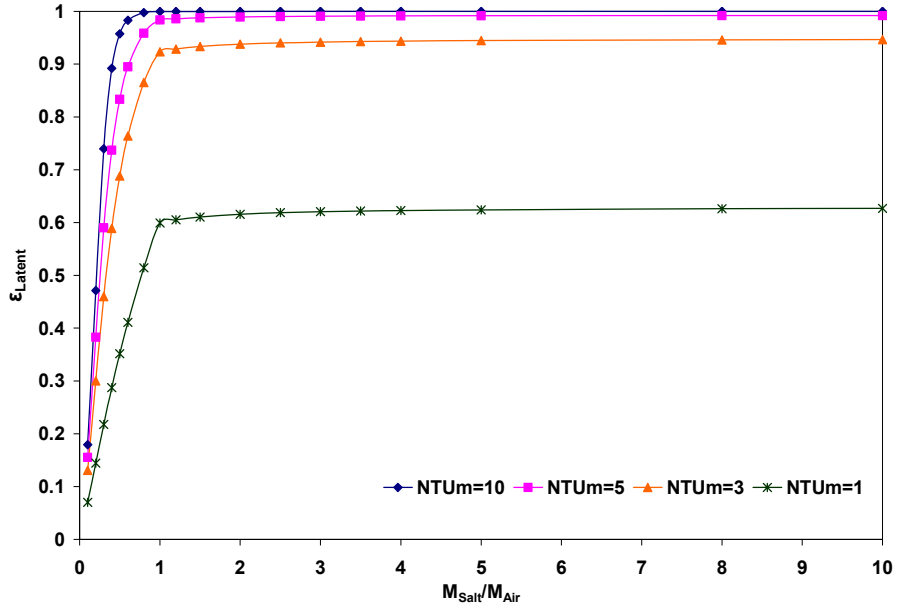

(b)

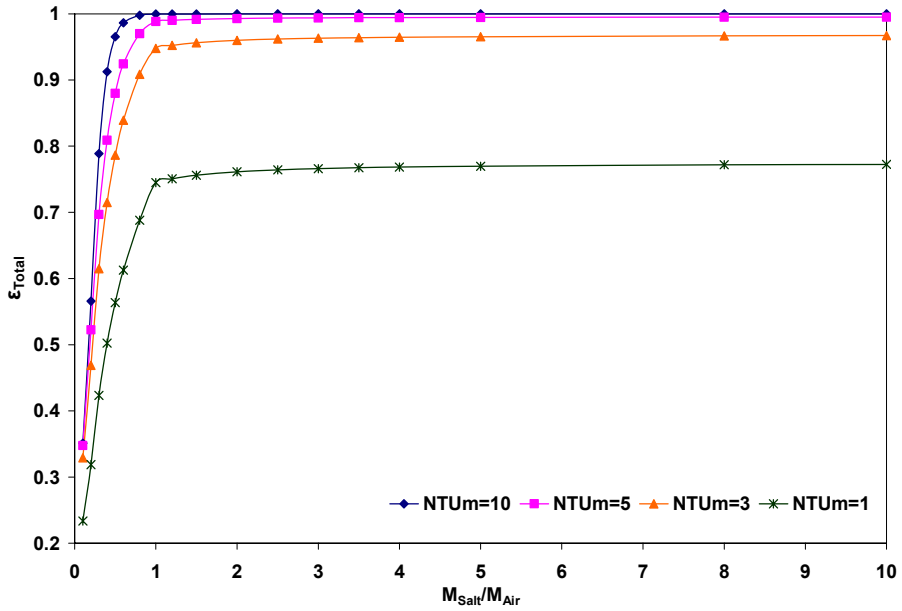

(c)

Figure D.9 *(a) sensible, (b) latent and (c) total effectiveness of a counter/cross flow exchanger as a function of* $\dot{m}_{Salt}/\dot{m}_{Air}$ *and for different* NTU_m *values* $y_0/x_0=0.5$ *and* $x_i/x_0=0.1$

D.3.5 Flow Arrangement

It is expected that the effectiveness of a counter/cross flow LAMEE falls between the effectiveness of a pure cross-flow exchanger and a pure counter-flow LAMEE with the same dimensionless parameters (NTU, Cr*, NTU_m, m*) and under the same operating conditions.

A comparison of the total effectiveness of three LAMEEs each with different flow configuration (pure cross-flow, pure counter-flow and counter/cross flow) is shown in Figure D.10. As indicated previously, depending on the geometry of the exchanger (aspect ratio y_0/x_0 and entrance ratio x_i/x_0) the effectiveness of the counter/cross flow LAMEE can be high like counter-flow or low like cross-flow LAMEE. In this specific case which the aspect ratio and the entrance ratio of counter/cross flow exchanger are 0.5 and 0.1 respectively, the $\varepsilon_{counter/cross}$ is almost in the middle.

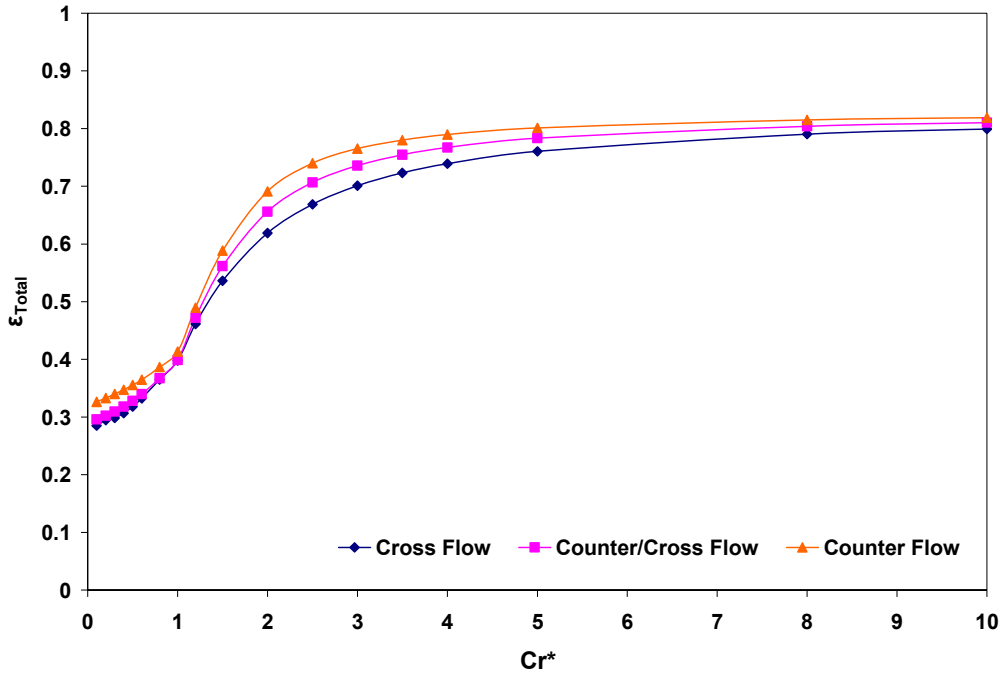

Figure D.10 *Total effectiveness of a heat and moisture exchanger with pure cross-flow, pure counter-flow and counter/cross flow arrangements as a function of Cr* when NTU=10. The exchanger with a combination of cross and counter-flow has an entrance ratio (x_i/x_0) of 0.1 and an aspect ratio (y_0/x_0) of 0.5.*

D.3.6 Operating Conditions

The last parameter affects the performance of a heat and moisture exchanger is the operating conditions. In this section, the sensitivity of the effectiveness of a counter/cross flow LAMEE to the operating conditions is investigated. The operating conditions of summer (hot and humid air) and winter (cold and dry air) are listed in Tables D.3 and D.4. The performance of the system under two different operating conditions is presented in Figure D.11.

Table D.4 *The winter operating conditions of the single heat and moisture exchanger used for sensitivity study (cold and dry air)*

Inlet temperature of the air stream ($T_{Air,in}$)	274.85 K (1.7°C)
Inlet humidity ratio of the air stream ($W_{Air,in}$)	3.5 g/kg
Inlet temperature of the salt solution ($T_{Sol,in}$)	297.15 K (24°C)
Inlet concentration of the salt solution ($X_{Sol,in}$)	4.25 kg/kg (19%)

As it can be seen in Figure D.11, the exchanger has the same response to increasing Cr* in both summer and winter. The sensible effectiveness of the exchanger is nearly the same for Cr*>5 but the latent effectiveness is still quite different for the summer and winter conditions.

The sensitivity of the LAMEE effectiveness to each inlet conditions is presented in following figures. In following figures the summer operating conditions are used unless that inlet property changes in each case. The effectivenesses are shown for two cases: NTU=10, Cr*=0.4 and NTU=10, Cr*=5. Even though Cr* is likely to be greater than one, the analysis of the performance of the exchanger in Cr*<1 can be beneficial for part load operating conditions.

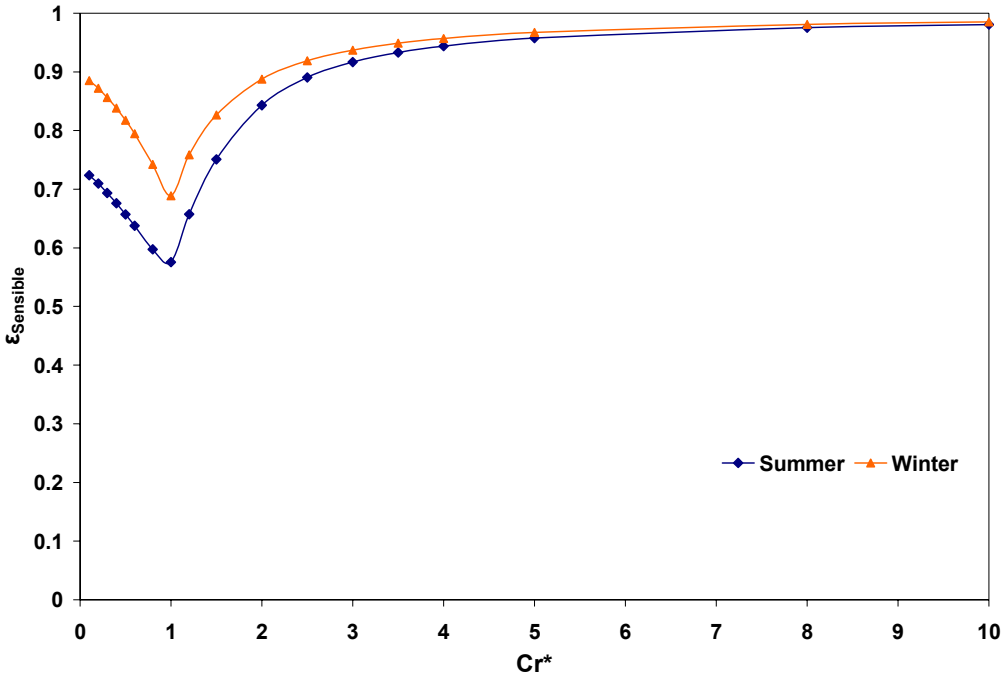

(a)

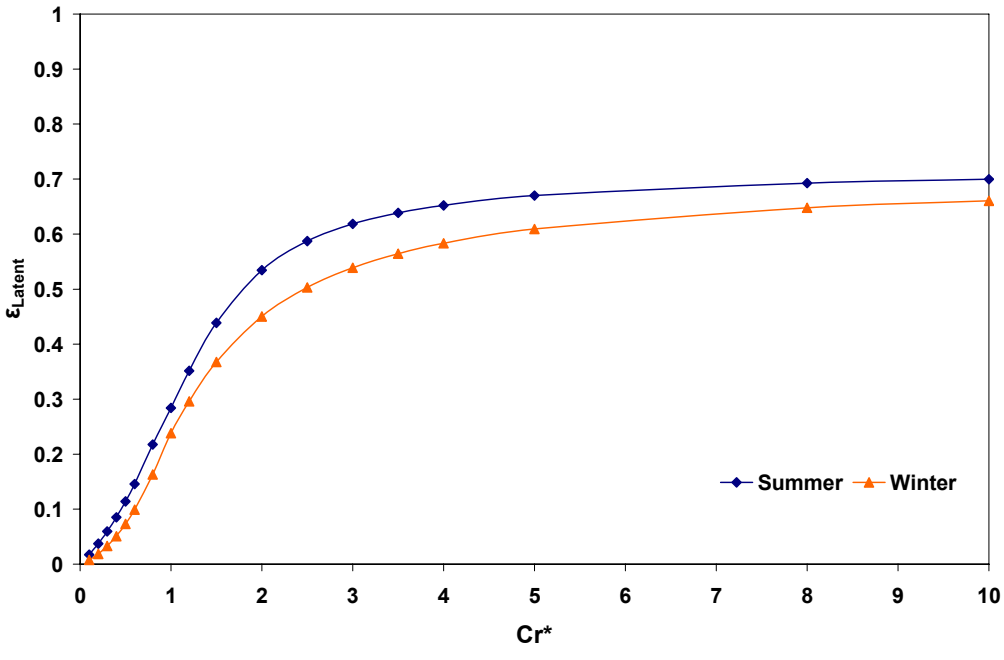

(b)

Figure D.11 *(a) sensible and (b) latent effectiveness of a counter/cross flow exchanger under different operating conditions. NTU=10* $x_i/x_0=0.1$ *and* $y_0/x_0=0.5$

In Figure D.12 the sensitivity of the effectivenesses of a counter/cross flow heat and moisture exchanger to changing the inlet air temperature is indicated. The effectivenesses, as shown in Figure D.12 (a), are more sensitive to inlet air temperature when Cr*=0.4 the total effectiveness increases about 20% with 10°C air temperature rise. However, they are less sensitive to air temperature in Cr*=5 (Figure D.12 (b)). Increasing the air temperature results in an increase in the sensible effectiveness since the temperature difference between the air and liquid increases. On the other hand, the air temperature rise causes a decrease of the latent effectiveness maybe because in higher temperature the phase change rate decreases (phase change releases energy in this example).

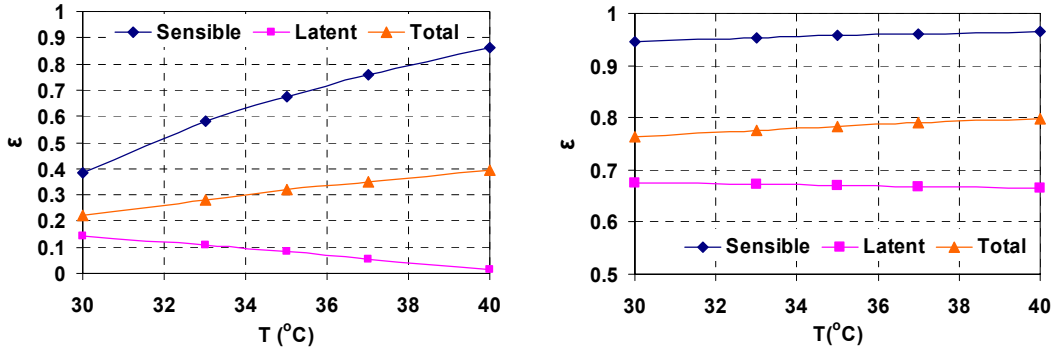

Figure D.12 *Variation in the effectiveness with inlet air temperature: NTU=10, x_i/x_0=0.1, y_0/x_0=0.5 and (a) Cr*=0.4, (b) Cr*=5*

The variation of the effectivenesses with the liquid desiccant temperature is illustrated in Figure D.13. As it can be seen in Figure D.13 (a), changing the solution temperature has minor effect on the values of the effectiveness in Cr*=0.4 compared to the air temperature (Figure D.13 (a)). The total effectiveness decreases up to 5% when solution temperature increases by 10°C.

In this case, both the sensible and latent effectivenesses decrease with increasing the solution temperature. The sensible effectiveness decreases due to the reduction in the air-liquid temperature difference. The latent effectiveness decreases as the phase change rate reduced in higher temperature.

From Figure D.12 (b) and D.13 (b) it can be concluded when Cr*=5 the effectiveness of the heat and moisture exchanger is not so sensitive to inlet air and liquid desiccant temperature, 5% effectiveness change as a result of 10°C temperature change.

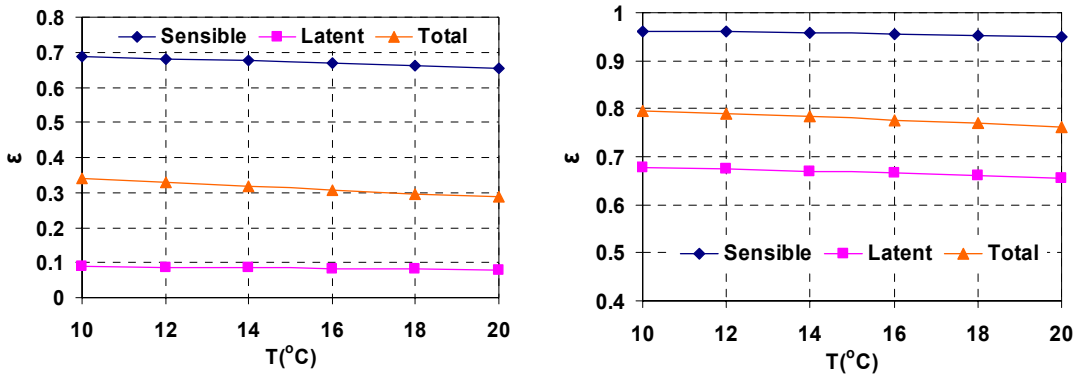

Figure D.13 *Variation in the effectiveness with inlet liquid desiccant temperature: NTU=10, x_i/x_0=0.1, y_0/x_0=0.5 and (a) Cr*=0.4, (b) Cr*=5*

The effect of the inlet air humidity ratio on the performance of the heat and moisture exchanger is presented in Figure D.14. An increase in the inlet air humidity ratio decreased the sensible effectiveness but increases the latent effectiveness. Increasing the inlet air humidity ratio means increasing the vapor pressure that leads to higher rate of moisture transfer, so the latent effectiveness increases. In higher air humidity ratio the moisture transfer release more energy in liquid desiccant and

heats the coolant which cause a decrease of sensible effectiveness with increasing the inlet air humidity ratio.

The performance of the exchanger varies significantly with the air humidity ratio for Cr*=0.4 because for Cr*<1 the heat of phase change plays an important role. As shown in Figure D.14 (a) if the inlet air humidity ratio is less than a specific value, (about 14 g/kg in this case) the moisture transfers in unlike direction which can cause a negative value as latent effectiveness and due to the heat of phase change a sensible effectiveness even greater than 1.

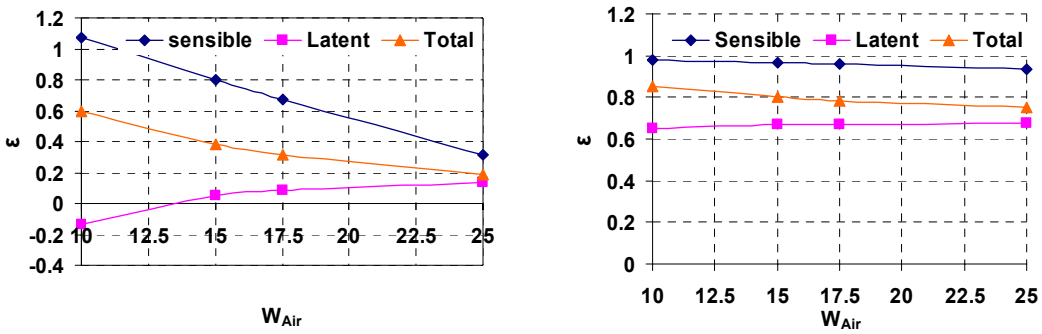

Figure D.14 *Variation in the effectiveness with inlet air humidity ratio: NTU=10, x_i/x_0=0.1, y_0/x_0=0.5 and (a) Cr*=0.4, (b) Cr*=5*

Eventually, the response of the exchanger to changing the inlet solution salt concentration is shown in Figure D.15. Like mentioned for the effect of the inlet air humidity ratio the effectivenesses are more sensitive for Cr*=0.4. As salt concentration increases, the partial water vapor pressure of the liquid solution decreases. As a result, the solution gains more moisture from air, and latent effectiveness increases. On the other hand the heat released from moisture transfer heats the liquid desiccant and reduced the sensible effectiveness.

Figure D.15 shows that for low salt concentration the moisture transfer can occur in reverse direction. It can be lead to a negative latent effectiveness and a high sensible effctiveness.

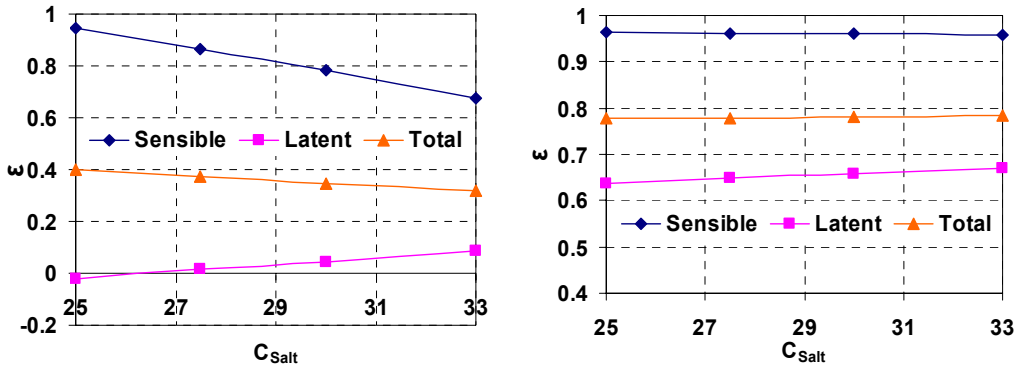

(a) ***(b)***

Figure D.15 *Variation in the effectiveness with inlet solution salt concentration: NTU=10, x_i/x_0=0.1, y_0/x_0=0.5 and (a) Cr*=0.4, (b) Cr*=5*

At Cr*=5, the inlet air humidity ratio and inlet salt concentration of the liquid desiccant do not dramatically affect the effectiveness of a heat and moisture exchanger.